Modeling the effect of intercalative particle binding on the overstretching transition of double-stranded DNA

Schakenraad, K.K.

Award date:
2014

Technische Universiteit
Eindhoven
University of Technology

Department of Applied Physics
Theory of Polymers and Soft Matter

Modeling the effect of intercalative particle binding on the overstretching transition of double-stranded DNA

Koen K. Schakenraad

October 2014

Under supervision of:

dr. C. Storm
prof. dr. ir. Paul van der Schoot

Abstract

DNA is best known from the perspective of genetics, but its mechanical properties are also an interesting and important field of study. These mechanical properties play an important role in cellular processes such as replication and transcription. To characterize the mechanics of DNA, physicists measure force-extension curves of individual double-stranded DNA molecules. They observe that the DNA molecule cooperatively overstretches to a length 1.7 times longer than B-DNA at a well-defined force of about 65 pN: the overstretching transition. To visualize these DNA mechanics, fluorescent molecules are bound to the DNA via the process of intercalation. However, these intercalators are known to perturb the DNA structure and thus change the features of the force-extension curve. In particular, the overstretching transition is found experimentally to shift to higher forces than 65 pN, as a function of intercalator concentration. In this work, we develop multi-state freely jointed chain models to gain an understanding of the physical principles behind the effect of intercalative particle binding on the overstretching transition of double-stranded DNA. We show that a freely jointed chain like model with three possible segment lengths reproduces experimental force-extension curves, and that this model captures the physical principles behind the effect of intercalation on the force-extension curve. The three segment lengths represent B-DNA, overstretched DNA, and intercalated DNA. Moreover, our model agrees quantitatively with the experimentally found linear dependence of the overstretching force on the intercalator concentration. Finally, our theory predicts a further elongation to twice the length of B-DNA, induced by intercalative binding at every base pair, in the force-regime beyond the overstretching transition.

Contents

Chapter 1

Introduction

Deoxyribonucleic acid probably is the most important molecule for the existence of life. This molecule, better known as DNA, is the carrier of the genetic code that is passed on from generation to generation and therefore it is the main character in the story of evolution. DNA is essential for many processes in the human cell. For example, during cell division all 46 DNA molecules are copied and transferred into the daughter cell. For protein production, DNA is used as a template for messenger RNA molecules in a process called transcription. Cellular processes such as replication and transcription are essential for a human being, and a proper understanding of those processes is therefore very important from a biological perspective [1].

During processes like replication and transcription, the DNA molecule must expose its genetic information by local unwinding [1]. To enable this unwinding, enzymes must exert mechanical stress on the DNA molecule. The response to external forces is called the mechanical behavior of the DNA molecule. Due to its important role in certain vital cellular processes, the mechanical behavior of DNA has drawn increased attention of biophysicists in recent decades. For reviews of pioneering work in this field, see Strick *et al.* [2], Bustamante *et al.* [3, 4], and Kumar and Mishra [5] and references therein.

1.1. Mechanical properties of DNA

The mechanical properties of DNA are investigated by relating forces or torques exerted on DNA to the response of that DNA. This is done both with bulk DNA [6–8] and with single DNA molecules [9–13]. In the research of the past decades a wide range of such forces and torques has been used on single DNA molecules. For example, DNA can be twisted [9], bend [10, 11], or stretched [12, 13]. The focus of this work is on the latter: the stretching of an individual double-stranded DNA molecule. That is, we focus on the relation between a stretching force and the resulting extension of the molecule, obtaining a so called force-extension relation.

Much scientific work has already been done on the force-extension relation of DNA molecules. Experiments have been performed on single-stranded DNA (ssDNA) (for a review, see [5]) and double-stranded DNA (dsDNA) [2]. The techniques that are used in these experiments are described in section 2.2.1. A lot of work has also been done on the theoretical side of the problem. The simplest model available for obtaining the force-extension relation of a polymer (like DNA) is the freely jointed chain (FJC) model [14, 15]. The FJC or Kuhn model treats the polymer as a chain of rigid, non-deformable segments (Kuhn segments) joined by perfectly flexible hinges. In other words, the FJC does not resist bending between the Kuhn segments.

Real polymers, however, do resist bending. A model that takes this into account is the wormlike chain (WLC) [16–18]. The WLC treats the polymer as a continuum elastic body with a bend stiffness. A WLC can be characterized by its *persistence length*, the characteristic length scale associated with the loss of directional correlation. However, this treatment of a polymer as a continuum elastic rod is only valid as long as the persistence length is much longer than the

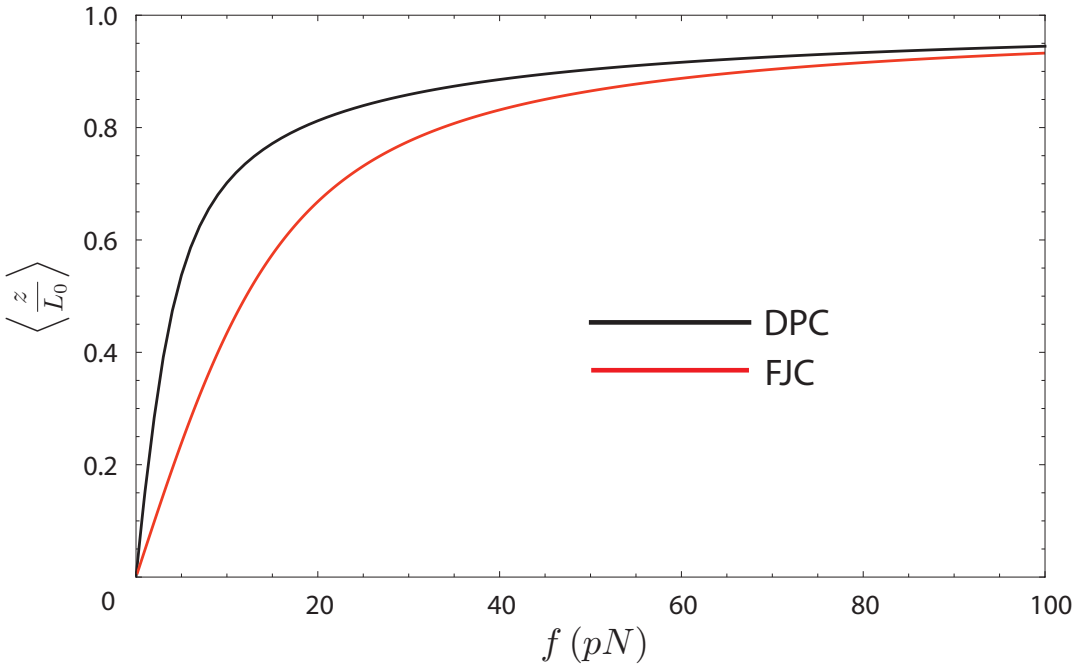

Figure 1.1: Theoretical force-extension curves of the freely jointed chain (FJC, red) and discrete persistent chain (DPC, black): the expectation value (thermal average) of the normalized extension is plotted as a function of the stretching force. The normalized extension is obtained by dividing the shortest distance between the end points, z, by the total length of the chain L_0. The plots use realistic parameters for ssDNA [15]: 0.6 nm as the length of a Kuhn segment for both the FJC and the DPC and a persistence length of 1.15 nm for the DPC. The discrete persistent chain is easier to stretch than the freely jointed chain because the DPC resists bending, while the FJC does not.

physical monomer length. When this constraint is not met, the lack of discreteness in the WLC is a serious defect in the theory. In 2003, Storm and Nelson [15] proposed a model that combines the best of two worlds: the discrete persistent chain (DPC) combines bend stiffness with discreteness by using the rigid segments of the FJC and adding an energy penalty proportional to the square of the angle between two adjacent segments. Figure 1.1 shows theoretical curves corresponding to the freely jointed chain (red) and the discrete persistent chain (black). For both curves a segments size of 0.6 nm has been used, and the discrete persistent chain has a persistence length of 1.15 nm. Those numbers are characteristic for ssDNA [15]. The curves show the expectation value of the *normalized extension*, $\left\langle \frac{z}{L_0} \right\rangle$ as a function of the stretching force f. The normalized extension is obtained by dividing the shortest distance between the end points, z, by the total length of the chain L_0. The notation $\langle\ \rangle$ shows that a thermal average is calculated. The figure shows that the discrete persistent chain is easier to stretch than the freely jointed chain. This can be understood by realizing that the discrete persistent chain is effectively a freely jointed chain that resists bending, and therefore favors stretching more than the freely jointed chain does. The force-extension relation of the freely jointed chain is discussed in more detail in section 3.1.

The overstretching transition

The force-extension curve of double-stranded DNA looks quite different from that of single-stranded DNA (figure 1.1). In 1996 Cluzel *et al.* [12] and Smith *et al.* [13] observed that at a force of about 65 pN the end-to-end length of the dsDNA molecule suddenly increased by a factor of 1.7. They assigned this sudden elongation to the unwinding of the double helix (section 2.1). As far as we know there is no consensus in the scientific community on the nature

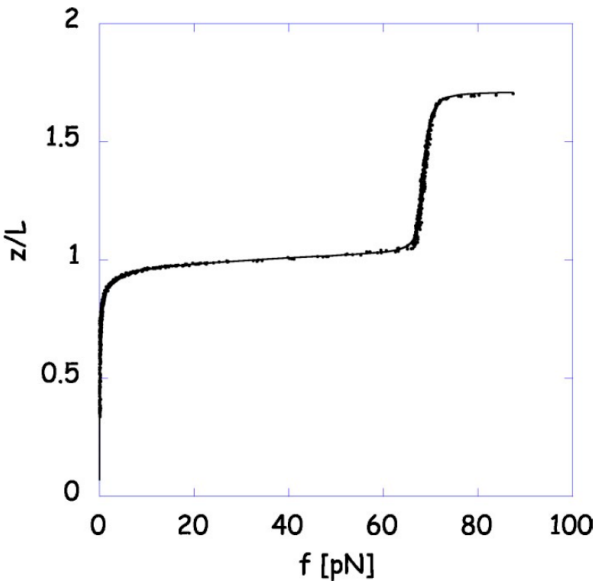

Figure 1.2: A force-extension curve of dsDNA: the normalized end-to-end length of the DNA (z/L) is plotted as a function of stretching force f. Around 65 pN the curve shows a cooperative overstretching transition from B-DNA to a state of DNA that is 70% longer, which we call "overstretched DNA". Image taken from [15].

of this unfolded state of DNA at the time of writing this thesis. Some [12, 13, 15, 19] claim that the the unfolded state is a novel form of non-helical double-stranded DNA, which they call S-DNA. Others [20–24] claim that the result of the unwinding is a pair of two detached single-stranded DNA molecules. Recently it was reported that it depends on the experimental conditions whether S-DNA or ssDNA is formed [25–27]. Regardless of this debate, the result is an unwound state of DNA which 70% longer than the standard, helical, ground-state of DNA, which is called B-DNA. The cooperative transition from B-DNA to this new state is now called the *overstretching transition*. The work in this thesis is not concerned with the distinction between S-DNA and ssDNA, so to avoid controversy the state of DNA at forces higher than the overstretching transition is called the 'overstretched state' in the remainder of this thesis. Section 2.1 gives more background information about the structures of dsDNA that are relevant for this thesis. Finally, we note that the overstretching transition only occurs if the dsDNA is free to rotate, and therefore to untwist, while being stretched [28]. What happens when the dsDNA is torsionally constrained is beyond the scope of this thesis, and can be found in the work of Allemand *et al.* [29] and Leger *et al.* [30].

Storm and Nelson [15] extended their discrete persistent chain (DPC) model, introduced above, by allowing each Kuhn segment to be in one of two possible states. The segments can either be in their ground state, corresponding to B-DNA, or they can be in an excited state, corresponding to overstretched DNA. A segment in the excited state is 70% longer than one in the ground state. This leads to the Ising-DPC model, which is a model for the force-extension curve of dsDNA including the overstretching transition. Figure 1.2 is an example of force-extension data (dots) of dsDNA together with a fit of the Ising-DPC model to this data (solid line) [15]. The plot clearly shows the overstretching transition at a force of about 65 pN.

1.2. Intercalators

Experiments and theory on force-extension curves of dsDNA as presented in section 1.1 are useful to gain more understanding of the elastic behavior of dsDNA, and therefore help in obtaining more insight in biological mechanisms such as DNA replication and transcription. However, they

only give a mesoscopic image: they show the elastic response of an entire DNA molecule to an externally applied force. They do not provide any information on local microscopic processes along the DNA molecule. If one wants to gain a better understanding of replication or transcription, obtaining this microscopic information is essential.

For this reason scientists want to be able to actually see the DNA molecules they are investigating. This is not straightforward since the typical diameter of a DNA strand is about 2 nm [31] and can therefore not be seen with an optical microscope. Morikawa *et al.* [32] were the first to succeed in directly observing a single DNA molecule under the microscope by using fluorescent molecules. Their method was later improved by Matsumoto and co-workers [33]. These molecules bind to the DNA molecule and are designed in such a way that they fluoresce much brighter in the bound state than in the unbound state [34]. For this reason these particles are called a fluorescent dye. The result is a DNA-dye complex that fluoresces upon illumination and which can be observed under the microscope. Using this method, Bianco and co-workers [35] were able to directly visualize the unwinding of a double-stranded DNA molecule by the enzyme helicase.

While the work of Bianco *et al.* shows the great potential of the use of fluorescent dyes, there is also a major drawback to this use. This drawback is the fact that the dye particles actually bind to the DNA molecule. It is not hard to imagine that a particle that attaches to a DNA molecule also modifies the properties of this very DNA molecule. The consequence of this simple statement is that the data obtained from experiments performed with fluorescent dyes might have been different if the dyes were not used. But those experiments might not be executable without the use of dyes. As an example, the helicase activity in the work of Bianco *et al.* [35] might have been different in the absence of dye molecules, but the activity can not be observed in the absence of those same dye molecules. It is for this reason that the role of fluorescent dyes on the mechanical behavior of DNA has drawn increased attention in the past decade [36, 37].

Fluorescent dyes are not the only particles that can bind to DNA to form a particle-DNA complex. Many cellular processes involve protein binding to DNA, such as gene expression, physical chromosome organizations, DNA replication and genetic recombination [38–41]. The interaction of small molecules with dsDNA molecules has also been investigated for the purpose of rational drug design for cancer therapy [42–44] or the development of other specific and efficient drugs [45]. All these examples illustrate the wide scope of DNA-particle interactions and the relevance of studying the mechanisms behind them. In this study we focus on one particular type of particle binding to DNA, being that of intercalation [46, 47]. In this binding mode small molecules insert their planar aromatic moiety between two adjacent base pairs of the double-stranded DNA molecule. These small molecules are called intercalators. The mechanism of dsDNA intercalation is illustrated schematically in figure 1.3. The figure shows the intercalation of ethidium as an example. It shows how the intercalator is inserted between two adjacent base pairs of a dsDNA molecule, disrupting the local DNA structure. From this schematical picture of the binding mechanism, we can understand why intercalation modifies the properties of dsDNA. The particles do not simply attach to the outside of the molecule backbone. Instead, they penetrate into the helical structure and change the local conformation of the dsDNA molecule. We discuss the binding mechanism of intercalation and its influence on the DNA conformation in more detail in section 2.1.

The small molecules in the examples of drug design given above [21, 42, 45, 48] are intercalators, as well as many fluorescent dyes that are used to visualize DNA during experiments. Examples of work on intercalating fluorescent dyes include, but are not limited to, references [32–35, 48–54]. The wide scope of applications, as discussed here, shows that the scientific relevance of the perturbing effect of intercalation on dsDNA can not only be found in fluorescence experiments, but also in rational drug design. Moreover, it is not unthinkable that the perturb-

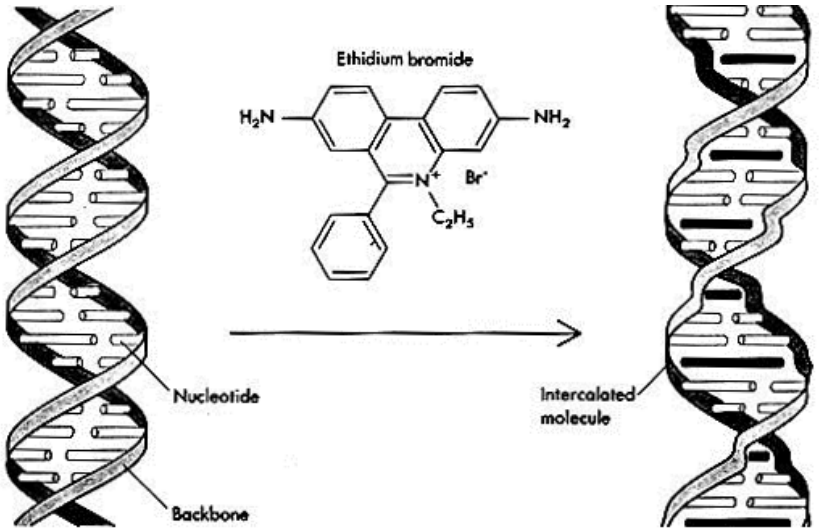

Figure 1.3: The mechanism of intercalation shown schematically. The intercalating molecule, which is ethidium in this case, is inserted between two adjacent base pairs of a dsDNA molecule. This disrupts the local DNA conformation, and therefore modifies the mechanical properties of the dsDNA molecule. Image taken from [55].

ing effect of intercalation might play a role in cellular processes involving dsDNA, such as those discussed in the introduction of this thesis.

Force-extension curves and intercalators

The influence of intercalating molecules on the mechanical behavior of DNA can be studied by investigating force-extension curves, which were already briefly discussed in section 1.1. Several experimental studies have been performed on the shape of the force-extension curve of dsDNA as a function of intercalator concentration [21, 48, 54]. Figure 1.4 shows two examples of those studies. Both studies have measured several force-extension curves for varying concentrations of particles. The curves are equilibrium curves; they are measured on time scales that allow the system to equilibrate. Figure 1.4a shows data from the master thesis of Roel Roijmans [54] where the fluorescent dye SYTOX Orange is used as intercalator. Figure 1.4b shows data from Vladescu *et al.* [21], who used ethidium particles as intercalators. In both curves we swapped the x-axis and the y-axis with respect to the figures in the original references [21, 54], where the force is plotted as a function of extension. This is a matter of convention. Theoreticians generally tend to plot the extension as a function of force, while experimentalists tend to do it the other way around. In this thesis we use the theoretical convention and plot the extension as a function of force. Also note that figure 1.4a gives the extension of the entire dsDNA molecule on the y-axis, while figure 1.4b gives the extension per base pair. The experimental techniques used to obtain these curves are discussed in section 2.2.1.

Both figures show clear evidence for the perturbing effect of intercalator binding on the force-extension curve of dsDNA. In particular the curves with relatively high concentrations show completely different qualitative behavior than the zero-concentration curves. Remarkable effects are the intercalator-induced shift of the overstretching transition, the jump in DNA extension that marks the transition from B-DNA to overstretched DNA, towards higher forces in figure 1.4b and the eventual complete disappearance of the cooperative overstretching transition in both figures. These effects are discussed and analyzed more extensively in section 2.2.2. To our knowledge, there is no theoretical understanding of these effects yet. In this thesis we develop an analytic theory that models the interaction between dsDNA and intercalating particles, and that explains the perturbing effect of intercalators on the force-extension curve of dsDNA.

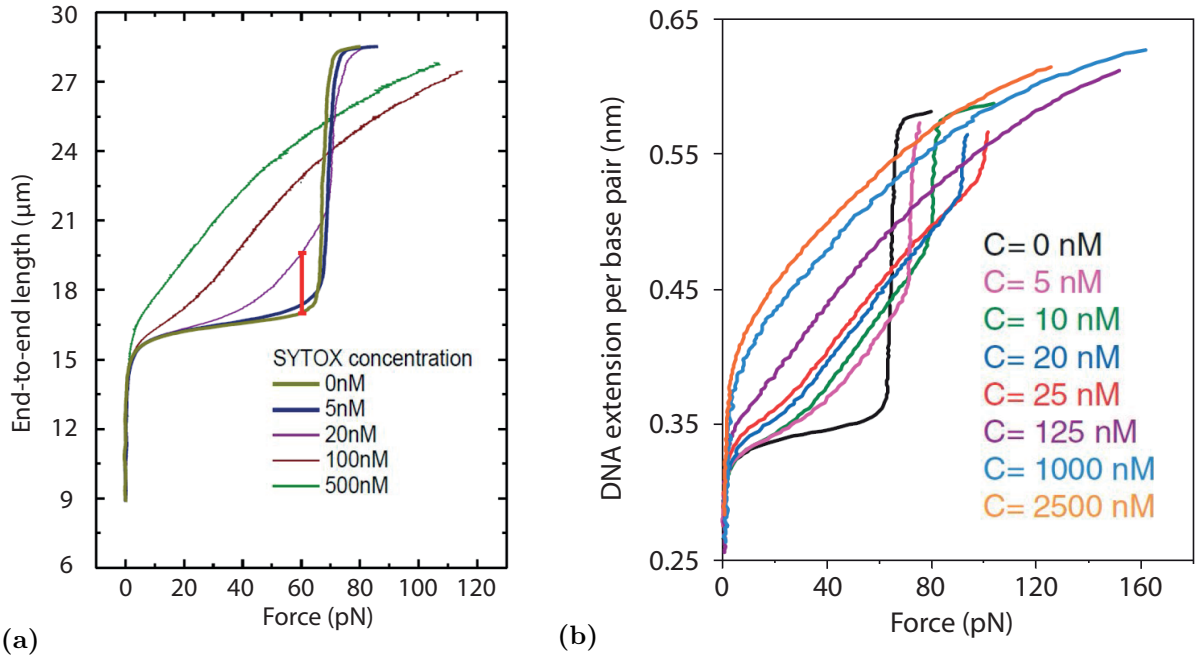

(a) (b)

Figure 1.4: Experimental data that shows the effect of intercalating particles on the force-extension curves of double-stranded DNA. The intercalators are SYTOX Orange (figure a) and ethidium (figure b). Both figures show several force-extension curves with different intercalator concentrations. The high-concentration curves show completely different qualitative behavior than the zero-concentration curves. Striking features of the high-concentration curves are the intercalator-induced shift of the overstretching force towards higher forces in (b) and the eventual complete disappearance of the overstretching transition in both (a) and (b). Note that (a) gives the extension of the entire dsDNA molecule, while (b) gives the extension per base pair. The axes are swapped with respect to the original references. Figures modified from the master thesis of Roel Roijmans [54] (a) and from Vladescu *et. al.* [21] (b).

Prior theoretical work on dsDNA intercalation

We are not the first to do theoretical modeling on the effect of intercalators on the force-extension curves of dsDNA. Plenty of polymer models that describe the interplay between dsDNA and intercalators or other binding particles have been reported in literature [38, 56–61]. For example, Lam and Zhen [38] used a discrete persistent chain (DPC) model in which they allowed particles to bind to the Kuhn segments of the chain. They modelled the influence of interacting particles to the bending regidity of dsDNA by assigning different local persistent lengths to bound and unbound Kuhn segments. As another example, Zhang and Marko [56] used Maxwell relations to predict the fraction of bound proteins as a function of applied force or torque.

1.3. Aim of this study

We named several theoretical studies that investigated the effect of particles on the force-extension curves of dsDNA in the previous section. However, none of those studies [38, 56–61] looked into the overstretching transition of dsDNA. All theoretical studies on this subject known to us perform calculations on the influence of bound particles on the force-extension curve of DNA at forces *smaller* than the overstretching force. The resulting models can therefore not explain all features of the data in figure 1.4. Because these studies do not model the overstretching transition, they cannot predict or explain an intercalator-induced shift in the overstretching force or the complete disappearance of the cooperative overstretching transition. It is the aim of

this thesis to develop an elastic model of dsDNA-intercalator complexes that does explain these effects.

The studies mentioned above show that the influence of intercalation on the force-extension curve of dsDNA is fairly well understood in the low-force regime. That is, this influence is well understood for forces smaller than the overstretching transition. Therefore, we focus our study on the high-force regime of the force-extension curve; we focus our study on the location and magnitude of the overstretching transition, which clearly depend on intercalator concentration according to figure 1.4b. The nature of these dependencies is not properly understood yet, so our main goal is to understand what physical principles cause the influence of intercalators on the overstretching transition. We use analytical theory to gain more understanding of these physical principles. In doing this we focus on the equilibrium properties of the dsDNA-intercalator system. The dynamics of the interactions are beyond the scope of this thesis.

To summarize the above and conclude, we present the aim of this thesis:

Research aim: We want to understand the physical principles behind the effect of intercalative particle binding on the location and magnitude of the overstretching transition of double-stranded DNA.

1.4. Outline of this thesis

We continue this thesis in chapter 2 with biological and experimental background knowledge that is relevant for our work. We first give a biochemical background of the double-stranded DNA molecule and the interaction of dsDNA with intercalating particles in section 2.1. In section 2.2.1 we discuss the experimental methods that are used for obtaining force-extension curves, and we finish the chapter with an analysis of the force-extension results obtained with these methods. We conclude this analysis with a list of five observed effects of intercalating particles on the overstretching transition of dsDNA. The rest of this thesis is dedicated to explaining those five effects.

In chapter 3 we present our first elastic model of double-stranded DNA, the 2-state Kuhn model. We start by reviewing the freely jointed chain (FJC) model, in section 3.1, which is the basis for our more advanced models. Then we present the 2-state Kuhn model in section 3.2, and we calculate the theoretical force-extension relation according to the 2-state Kuhn model. This force-extension relation is analyzed mathematically in section 3.3, and we compare the results of the model with experimental data in section 3.4. We finish chapter 3 by concluding that the 2-state Kuhn model is unable to explain the effects listed at the end of chapter 2.

Therefore we develop a more advanced elastic model of dsDNA in chapter 4: the 3-state Kuhn model. This model is an extension of the 2-state Kuhn model, and takes particle binding into account. We motivate the modeling choices in section 4.1, after which we present the model in section 4.2. In sections 4.3 and 4.4 we analyze the 3-state Kuhn model mathematically. This allows us to come back to our research aim in section 4.5, where we explain the physical principles behind the influence of intercalators on the overstretching transition of dsDNA. In section 4.6 we quantify this influence, and in section 4.7 we predict the force-extension curve of a dsDNA-intercalator complex in a force-regime beyond the overstretching transition.

We finish this thesis with a brief summary of the most important conclusions of this work in chapter 5, after which we give several suggestions for future research and briefly discuss the technological relevance of our work. Finally, we give a list of references to literature, a table with all used symbols, and appendices A and B.

We realize that this thesis might be read by two different types of readers. Some readers might read this thesis because they are theoretically interested in our methods and work, while others

might read this thesis from a more practical point of view and might be mainly interested in our results. We have sought to make this thesis interesting for both types of readers. Therefore, we marked some sections in chapters 3 and 4 with an asterisk. These sections are related to derivations of our results, or to mathematical analyses that go deeper than most analyses. Sections marked with an asterisk give a deeper understanding of our model, but this thesis can be read without them. We leave it to the reader whether or not to read these sections.

Chapter 2

Experiments on DNA

In this chapter we address biological and experimental background knowledge that is required to understand the theoretical modeling that is done in chapters 3 and 4. In section 2.1 we give a biochemical background of the double-stranded DNA molecule and the interaction of dsDNA with intercalating particles. Section 2.2 considers the experimental methods used for obtaining force-extension curves and gives an analysis of the results obtained with these methods.

2.1. DNA

The helical structure of the double-stranded DNA molecule as we know it today was first suggested by Watson and Crick in 1953 [62], using key data from Rosalind Franklin and Maurice Wilkins [63]. Two right-handed helical chains are coiled around the same axis. Those two chains are connected to each other by chemical bonds, which can schematically be seen as steps on a helical ladder. DNA in this state is called B-DNA. A schematic image of B-DNA is given in figure 2.1a [62]. This B-DNA has a diameter of 2 nm [31]. On a more detailed level the dsDNA structure looks like figure 2.1b [54], which shows the chemical details of the dsDNA structure. Figure 2.1b is in fact a zoom-in of figure 2.1a on 4 steps of the ladder, where the helicity has been omitted from the figure for clarity. Colors have been used to label the different chemical groups in the molecule.

The phosphate-deoxyribose backbones of the dsDNA molecule can be seen on the left and on the right in figure 2.1b. This backbone is a linear structure that consists of alternating sugar (2-deoxyribose) (orange in figure 2.1b) and phosphate (yellow) groups [64]. The two backbones of the molecules are connected by so called nucleobases, which form base pairs. Each base is connected to the sugar group of one of the two backbones, and two bases on different backbones bind by hydrogen bonds. These nucleobases come in four types: adenine (green), thymine (purple), guanine (blue) and cytosine (red). They always pair in the way shown in the figure: adenine to thymine and guanine to cytosine. Relating this chemical structure in figure 2.1b to the schematical image of 2.1a, the phosphate-deoxyribose backbones form the helical chains that define the 'molecular ladder' and the base pairs are represented by the ladder steps. The distance between these ladder steps is 0.34 nm [62] and the ladder makes one complete turn every 10.5 ladder steps (base pairs) [31]. Or, alternatively put, B-DNA has a twist of 100.8 °/nm [31]. Finally, the arrows in figure 2.1a and the 5' and 3' notations in figure 2.1b indicate that the two backbones are oriented antiparallel. The experiments studied in this thesis (figure 1.4 [21, 54]) were performed with bacteriophage lambda DNA, which is dsDNA that contains about 48.500 base pairs [31].

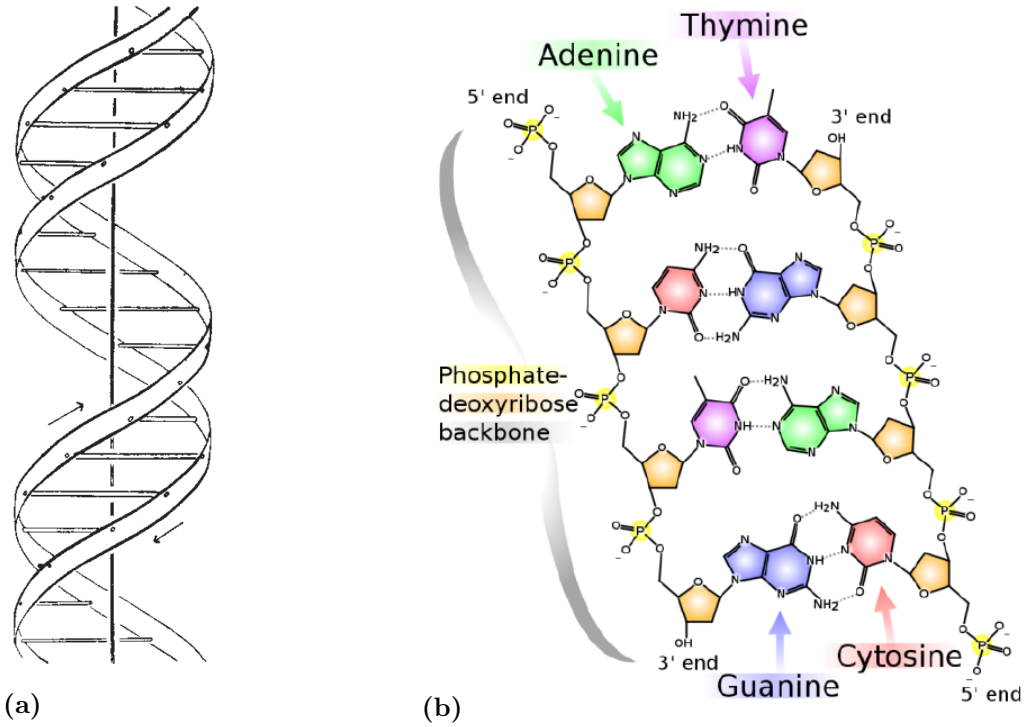

Figure 2.1: Schematical images of double-stranded DNA. (a) The double helical structure of DNA that was first proposed by Watson and Crick [62]. (b) A zoom in on the chemical details of the structure in figure (a). The structure is formed by two phosphate-deoxyribose backbones, which are interconnected by pairs of nucleobases. Four different nucleobases can be found in DNA, being adenine, thymine, guanine and cytosine. Adenine always binds thymine and guanine always binds cytosine. The colors are used to label the different chemical groups. Images taken from [62] (a) and [54] (b).

Overstretched DNA

When DNA is overstretched by an external force (section 1.1) the picture of figure 2.1 changes. The double helix unwinds [12, 13], leading to a different structure of DNA. As mentioned already in section 1.1 there has been debate on the nature of overstretched DNA since the discovering of the overstretching transition. Recent work [25–27] has shown that, depending on the experimental conditions, two different forms of overstretched DNA occur. S-DNA is a novel form of double-stranded DNA that has the same chemical structure as B-DNA, but with greatly reduced helicity of the backbones [30]. Leger *et al.* [30] estimated a number of 37.5 base pairs per turn, corresponding to 22 nm per turn. In comparison, B-DNA has a helicity of 3.6 nm per turn [31]. In other words, figure 2.1b is valid for S-DNA, but figure 2.1a should be replaced by a ladder that rotates much slower than the ladder shown. The other possibility is the formation of two strands of single-stranded DNA: in addition to unwinding of the helical structure, the hydrogen bonds between the nucleobases are broken, leaving the two backbones unconnected. In the ladder picture this is equivalent to a ladder where all steps have been broken. Regardless of the molecular details, overstretched DNA is longer than B-DNA by a factor 1.7, leading to a distance between base pairs of 0.58 nm [12, 13].

DNA intercalation

When particles bind to DNA via intercalation, they alter the local structure of the DNA molecule in a different way than overstretching does. Lerman [46] was the first to report about the binding mechanism of intercalation. He reported that a planar molecule or a planar part of a molecule

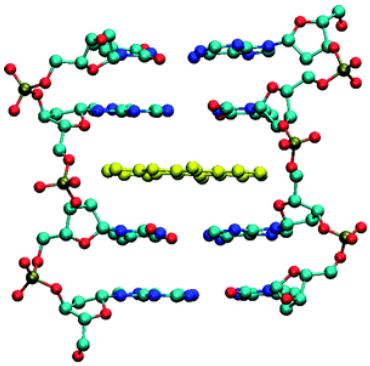

Figure 2.2: A schematic image of ethidium (yellow), intercalated between two adjacent base pairs of dsDNA. The space required for the intercalation is provided by a local untwisting of the dsDNA helix and an extension of the backbone. This leads to an increased distance between adjacent base pairs from 0.34 nm to 0.68 nm [66–68]. Image taken from [65].

is inserted between normally neighboring base pairs in a plane perpendicular to the helical axis. This mechanism was already briefly discussed in section 1.2. There we showed a schematical image of this process (figure 1.3) to illustrate how the binding of an intercalator disrupts the local dsDNA structure, and therefore changes the mechanical properties of the dsDNA. Here we zoom in on that picture and see how the local structure is affected on the scale of a base pair. Figure 2.2 [65] shows a schematic image of ethidium (yellow) intercalated between two adjacent base pairs in a dsDNA molecule. The space required for this intercalator is provided by an extension of the backbone and a local untwisting of the helix, which leads to an increase of the distance between adjacent base pairs from 0.34 nm to 0.68 nm [66–68]. This doubling of the distance between adjacent baseapairs can be seen in figure 2.2.

We remark that the intercalators described here are a special case of DNA intercalators. We described how a planar molecule is inserted between normally neighboring base pairs. Such intercalators are called mono-intercalators. However, there also exists molecules that insert multiple planar groups in between base pairs simultaneously. For example, a molecule that inserts two planar groups, each at different positions along the DNA molecule, is called a bis-intercalator [69, 70]. However, the experimental data that we are working with (figure 1.4) was obtained with ethidium (figure 1.4b) and SYTOX Orange (figure 1.4a) as intercalators. Ethidium is well-known to be a mono-intercalator (as shown in figure 2.2), while SYTOX Orange was reported to be a mono-intercalator by Yan *et al.* [71]. For this reason, we focus on mono-intercalation in this work.

It was experimentally observed [72, 73] that a bound intercalator inhibits other intercalators to bind at adjacent binding sites on the DNA molecule. This is called the neighbor-exclusion principle [66]. Jain and Sobell [74, 75] and Vladescu *et al.* [20] reported that this exclusion principle is not caused by direct repulsion between intercalated molecules, but that it is a result of intercalator-induced structural changes in the dsDNA. An important consequence of the exclusion principle would be the fact that a saturated DNA molecule has only half its binding sites occupied. This is in accordance with the experimentally observed 1.5-fold elongation (instead of 2-fold) of the DNA molecule at saturation [76, 77].

However, Yan and Marko [57] predicted that at high stretching forces the maximum binding could be increased to one intercalating molecule per base pair. Indeed, Vladescu *et al.* [21] showed that at high stretching forces the overall contour length of saturated DNA (0.68 nm per base pair) was twice as long as for B-DNA (0.34 nm per base pair). Vladescu *et al.* [21] contributed this violation of the neighbor-exclusion principle to the fact that the exclusion is mediated by structural changes in the DNA backbone. Apparently the strong stretching forces promote these structural changes because they allow the force to do more work.

2.2. Experimental obervations

Now that we have seen the molecular structure of double-stranded DNA and the microscopic picture of DNA overstretching and DNA intercalation, we are ready to review the experiments that were briefly discussed in section 1.2. First the experimental methods used in force-extension measurements will be discussed, after which we will discuss the experimental results shown in figure 1.4 more extensively.

2.2.1. Experimental methods

This section is concerned with the experimental methods used to measure force-extension curves of dsDNA. While there are more possibilities, mainly magnetic tweezers [56, 57, 59, 60, 78, 79] and optical tweezers [28, 51–53, 80, 81] are frequently used for this purpose. Another example is the use of so called molecular combing [51, 82]. The data given in both figure 1.4a [54] and figure 1.4b [21] in chapter 1 were obtained with optical trapping, so we will focus on this technique here. For more information on magnetic tweezers we refer to the available literature [56, 57, 59, 60, 78, 79].

Optical trapping was first demonstrated by Ashkin *et al.* [83] in 1986. An optical trap uses a focussed laser beam to trap an object in a fixed or moving point in space. Optical traps are capable of stably trapping particles with sizes ranging from diameters much smaller than the wavelength of light (Rayleigh-size regime) to diameters much larger than the wavelength of light (ray optics regime) [84]. The size of many particles that are used in biophysical experiments are in the order of the wavelength of light and therefore they fall in between these two regimes [84]. A correct theoretical description of optical trapping in this intermediate regime is difficult, but Ashkin showed that ray optics can nevertheless be used to gain qualitative insight in the mechanism behind optical trapping [85]. Basically this mechanism comes down to the competition between two forces. The first force is called the *scattering force*. The scattering force is caused by the backscattering of photons on the target particle and this force pushes the particle down the optical axis. On the other hand there is the *intensity gradient force* which pulls the object in the direction of increasing laser intensity. In other words, the intensity gradient force pulls the particle towards the laser focus. When these forces balance each other, the target particle can be held at a stable position just downstream of the laser focus: the particle is optically trapped [84]. For a more extensive explanation of the optical trap we refer to the work of Ashkin [85].

The target particle for DNA force-extension experiments is a micron-scale polystyrene bead. A dsDNA molecule is attached to such a polystyrene bead at both ends in such a way that only only one DNA molecule binds to the beads [84]. The result is a system of two polystyrene beads connected by a DNA molecule. The beads are then optically trapped by a laser set-up, which controlles the position of both beads separately. When the laser focus moves, the associated polystyrene bead moves along. If the other bead is kept in place, this leads to a change in end-to-end length of the DNA molecule. The DNA resists this stretching by pulling on the polystyrene beads, leading to a slight movement of the beads out of their equilibrium position. This small shift can be observed by measuring the deflection of the laser light [86, 87]. From this measured deflection the force exerted by the DNA molecule on the polystyrene beads can be calculated, which is equal to the force of the beads on the DNA molecule. Since the laser deflection also contains information about the position of the beads, this method gives the relation between the end-to-end length of the DNA molecule and the force required to obtain it [51, 84]. The method is illustrated in figure 2.3, which shows two alternatives for the technique described here. In figure 2.3a [51] both polystyrene beads are controlled by an optical trap, while in figure 2.3b [28] one bead is controlled by an optical trap and the other bead is kept in place by a micropipette.

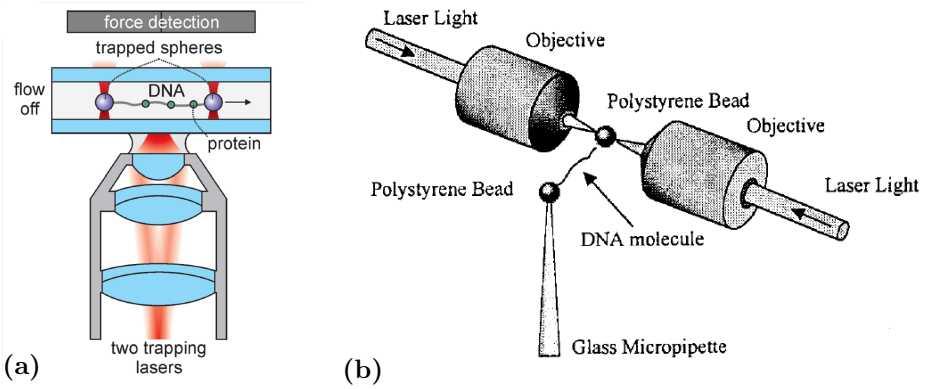

Figure 2.3: Schematic drawings of optical trapping techniques for the purpose of measuring force-extension curves of dsDNA. A DNA molecule is attached to a polystyrene bead at both ends. The position of the beads can be controlled by an optical set-up in which a laser is used to trap the polystyrene bead in the laser focus. When the laser focus moves, the bead moves along, leading to a change in the end-to-end length of the DNA molecule. The elastic force associated with this end-to-end length pulls the beads slightly out of its equilibrium position near laser focus, which is detected by analyzing the laser deflection. The force is then calculated from this deflection. This technique can be performed by controlling both polystyrene beads in an optical trap (a) or by using an optical trap for one bead and a micropipette to keep the other bead in place (b). Images taken from [51] (a) and [28] (b).

2.2.2. Experimental results

The optical trapping method described in section 2.2.1 was used to produce the data that was given in figure 1.4 [21, 54] in section 1.2. We briefly discussed the influence of intercalator concentration on the dsDNA force-extension curves in chapter 1 to explain the aim of this thesis. This aim is to understand the physical principles behind the influence of intercalative particle binding on the location and magnitude of the overstretching transition of double-stranded DNA (section 1.3). However, to understand what *causes* the intercalators to change the force-extension curve, we first need to determine *how* the force-extension curves are changed. In this section, we review the data of figure 1.4 and analyze the qualitative behavior of the force-extension curves as a function of the intercalator concentration. We use our observations in the development of theoretical models for dsDNA-intercalator systems in chapters 3 and 4. For ease of reading, we show the data again in figure 2.4. We focus mainly on the data in figure 2.4b, because ethidium (which is used in figure 2.4b, but not in figure 2.4a) is considered as the standard for dsDNA intercalation [21, 66, 88], and the ethidium-dsDNA binding mechanism has been extensively studied [89–91]. By studying the intercalation of ethidium we avoid complications due to exitations of other, non-intercalative, binding modes, which may interfere if more complicated intercalators are used. So by studying ethidium we make sure that the particle binding we study is intercalative in nature.

Figure 2.4 shows that the force-extension curve of dsDNA changes significantly upon intercalation, not only quantitatively but also qualitatively. The most evident change in the shape of the curves is the disappearance of the overstretching transition, the cooperative transition from B-DNA to overstretched DNA that is normally accompanied by an elongation of about 70%. Both figure 2.4a and figure 2.4b show that this decrease in cooperativity upon intercalation leads to an *increase* of end-to-end length at forces smaller than the original overstretching force and a *decrease* of end-to-end length at forces larger than the original overstretching force. This behavior might be indicative for a change from a cooperative overstretching transition to an anti-cooperative transition. Alternatively, there might be a third microscopic state involved if particles intercalate, that has a length in between that of B-DNA and overstretched DNA. If this third state becomes important when more particles are available for binding, this might explain the length *increase* at low forces and the length *decrease* at high forces. We know from section

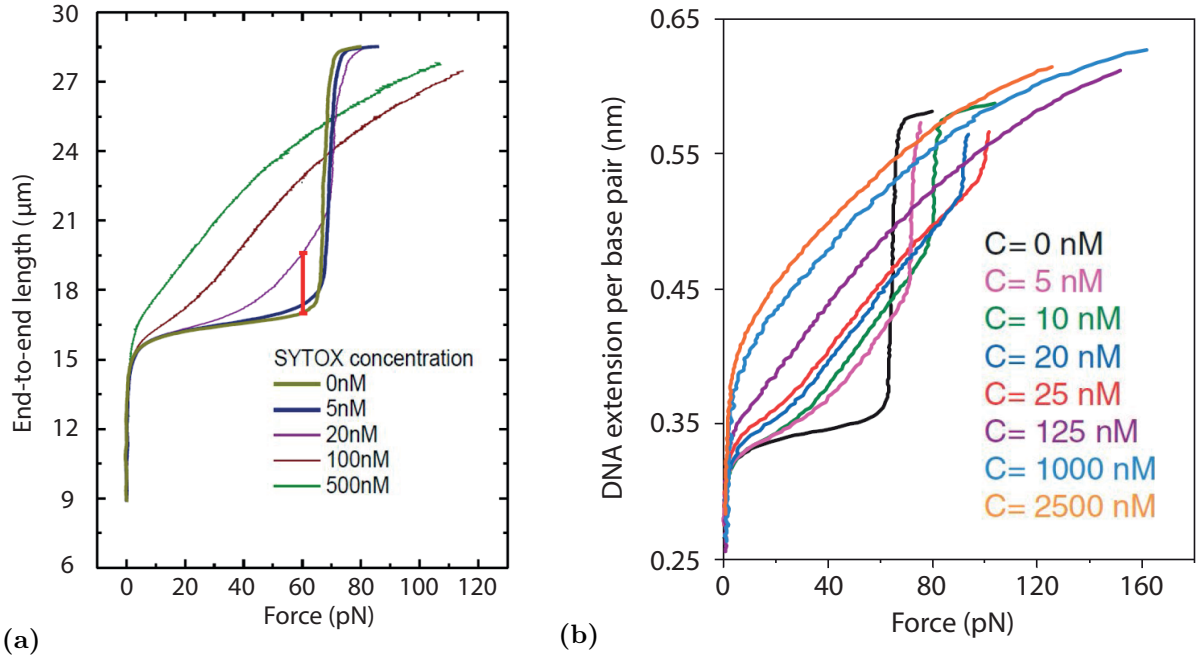

(a) (b)

Figure 2.4: This figure is identical to figure 1.4. It is repeated here for the ease of reading. The experimental data shows the effect of intercalating particles on the force-extension curves of double-stranded DNA. Both figures show several force-extension curves with different intercalator concentrations. The high-concentration curves show completely different qualitative behavior than the zero-concentration curves. Striking features of the high-concentration curves are the intercalator-induced shift of the overstretching force towards higher forces in (b) and the eventual complete disappearance of the overstretching transition in both (a) and (b). Note that (a) gives the extension of the entire dsDNA molecule, while (b) gives the extension per base pair. The axes are swapped with respect to the original references. Figures modified from the master thesis of Roel Roijmans [54] (a) and from Vladescu *et. al.* [21] (b).

2.1 that such a state indeed exists: if a particle intercalates between two DNA base pairs, it elongates the DNA locally by a factor of 2. However, section 2.1 also tells us that at moderate forces, a bound intercalator inhibits other intercalators to bind at adjacent binding sites on the DNA molecule. This leads to an effective maximum elongation upon intercalation of 1.5, which is indeed in between the length of B-DNA (not elongated) and overstretched DNA (elongated by a factor 1.7).

Another striking effect of the intercalating particles is the force-shift of the overstretching transition, which can be seen in figure 2.4b and which was already briefly discussed in sections 1.2 and 1.3. For nonzero concentrations the overstretching force initially increases with particle concentrations. At the same time the elongation upon overstretching decreases because the end-to-end length of intercalated DNA molecules is already significantly larger than 1 at forces smaller than the overstretching force (figure 2.4b). This large end-to-end length for forces smaller than the overstretching force is also an evident change of qualitative behavior, since the zero-concentration curve shows an approximately constant extension of about 1 before the overstretching transition. For even higher concentrations, the overstretching transition vanishes. This can be seen in figure 2.4a starting at a concentration of 100 nM and in figure 2.4b for concentrations of 125 nM and more. In these force-extension curves there is no sign of any cooperativity. A good theoretical model must be able to explain all observations discussed here.

In chapters 3 and 4 we develop such a model. In chapter 3 we develop a 2-state model (B-DNA and overstretched DNA) to investigate whether a change from cooperativity to anti-cooperativity might explain the change in qualitative behavior in figures 2.4a and 2.4b. We conclude that it does not (section 3.5). While this model might explain the disappearance of the cooperative overstretching transition, we will see that it cannot explain an intercalator-induced

shift of the overstretching force. Also, we will see that a 2-state model cannot explain why the end-to-end length of intercalated dsDNA is already significantly larger than 1 for forces lower than the overstretching force (figure 2.4b, concentrations 5-25 nM). Despite the fact that the 2-state model is not satisfying for our purposes we analyze it extensively. We will do this for three reasons; first, an understanding of why the 2-state model is insufficient for explaining the data in figure 2.4 helps understanding why the more advanced 3-state model, that is discussed in chapter 4, is designed the way it is. The second reason is the relative simplicity of the 2-state model. The 2-state model is an ideal model to explain the physical concepts that will also be relevant in the mathematically much more challenging 3-state model. And finally, in chapter 4 we will see that for reasonable parameter choices the 3-state model behaves like a combination of 2-state models.

In chapter 4 we show how the 2-state model can be extended by including a third molecular state, which is associated with a part of the dsDNA that is intercalated. We attribute a length to this state that is twice the length of B-DNA, in accordance with the knowledge about DNA intercalation from section 2.1. We see that the existence of this third state, in combination with cooperativity and anti-cooperativity, enables the model to explain all observations given earlier this section.

To summarize, our aim is to understand the physical principles that govern the influence of intercalative particle binding on the location and magnitude of the overstretching transition of double-stranded DNA. To obtain this understanding, we need to understand five intercalator-induced effects that we observe in figure 2.4:

- A force shift of the overstretching transition as a function of intercalator concentration.
- An end-to-end length that is significantly larger than 1 for forces smaller than the overstretching force.
- An end-to-end length increase at forces smaller than the original overstretching force.
- An end-to-end length decrease at forces larger than the original overstretching force.
- The disappearance of the overstretching transition for large concentrations.

A theoretical model that explains these five features of figure 2.4 is able to answer the main research question. We see in chapter 4 that our 3-state model is indeed capable of explaining all these features.

Chapter 3

The 2-state Kuhn model

In this chapter we present our first elastic model of double-stranded DNA, the 2-state Kuhn model. First we review the standard Kuhn model, which is commonly known as the freely jointed chain (FJC) model, in section 3.1. Then we present the 2-state Kuhn model in section 3.2, where we also calculate the 2-state force-extension relation. In section 3.3 we analyze this force-extension relation, followed by a comparison of the model with experimental data in section 3.4. We do not yet discuss the modeling of intercalative binding in this chapter; this is discussed in chapter 4. We finish the chapter by concluding that the 2-state Kuhn model is unable to answer our research questions.

3.1. The freely jointed chain

The freely jointed chain (FJC) or Kuhn model forms the starting point for both theoretical models that we discuss, in this chapter and in chapter 4. The freely jointed chain model is the simplest polymer model available for investigating force-extension relations. It treats the polymer as a chain of identical, rigid, non-deformable segments (Kuhn segments) joined by perfectly flexible hinges [14, 15]. Later in this thesis we introduce multi-state Kuhn models in which we allow each Kuhn segment to occupy two or three different states. We call them the 2-state and 3-state Kuhn models. For clarity, we refer to the standard Kuhn model as the freely jointed chain or the 1-state Kuhn model.

To describe a microstate of the FJC, we assign a unit vector $\hat{t}$ to each Kuhn segment. We label them such that $\hat{t}_i$ is the unit vector that points in the direction of the i^{th} segment, and θ_i is defined as the angle between $\hat{t}_i$ and the z-axis. The collection of all unit vectors $\{\hat{t}_i\}$, together with the length of a Kuhn segment l_0, fully describes the configuration of the freely jointed chain; l_0 is also called the *Kuhn length*. An example of such a FJC configuration is given in figure 3.1. The figure also shows the *end-to-end length* of the FJC, which is the shortest distance between the end points of the chain. The *contour length* is defined as the length along the chain, which is equal to Nl_0 for the 1-state Kuhn model, where N is the number of Kuhn segments. Obviously, the end-to-end length of a FJC is always smaller than or equal to its contour length. To calculate the force-extension relation, we apply a stretching force with magnitude f in the z-direction. The resulting calculation is presented in section 3.1.1, but before that we briefly address the question of why the freely jointed chain resists stretching.

A freely jointed chain is sometimes referred to as an *entropic spring*. The origin of this name is in the fact that all possible microstates of the freely jointed chain are energetically equivalent. After all, the Kuhn segments are all perfectly rigid and non-deformable, and all hinges are perfectly flexible. Nevertheless, the freely jointed chain does resist stretching. This is a consequence of entropy: more distinct microstates exist that belong to a specific end-to-end vector with short length than microstates that lead to a specific long end-to-end vector. Or, to put it differently,

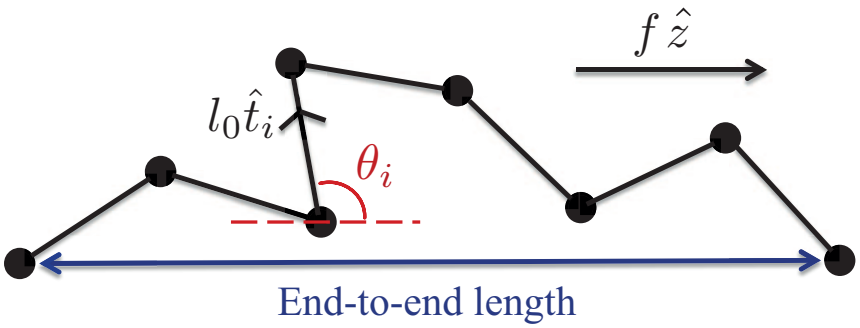

Figure 3.1: A possible configuration of a freely jointed chain (FJC). The rods display the Kuhn segments, while the circles represent infinitely flexible hinges that connect the Kuhn segments. A unit vector $\hat{t}_i$ is introduced such that it points in the direction of the i^{th} Kuhn segment. θ_i is the angle between $\hat{t}_i$ and the z-axis. The configuration of the freely jointed chain is fully described by the Kuhn length l_0 and the collection of all unit vectors $\{\hat{t}_i\}$. A force f is applied in the z-direction to calculate the force-extension relation. The result of this force is a certain distance between the end points of the chain, which is called the end-to-end length.

there is a loss of conformational entropy upon end-to-end length increase. Since all states are energetically equivalent, this decrease in conformational entropy causes an increase in total free energy. However, like every physical system the freely jointed chain is more likely to be in a state with low free energy than in a state with high free energy, and therefore it resists stretching. Hence the term *entropic spring*.

3.1.1. The force-extension curve of the freely jointed chain

Now that we understand why the FJC resists stretching, we can calculate quantitatively how. In other words, we can calculate the force-extension curve of the freely jointed chain. The starting point is the energy functional for the chain:

$$\frac{\varepsilon^{\mathrm{FJC}}[\{\hat{t}_i\}]}{k_B T} \;=\; -\frac{l_0}{k_B T}\sum_{i=1}^{N}\vec{f}\cdot\hat{t}_i \;=\; -\frac{f l_0}{k_B T}\sum_{i=1}^{N}\hat{t}_i\cdot\hat{z}, \tag{3.1}$$

where $\varepsilon^{\mathrm{FJC}}[\{\hat{t}_i\}]$ is the total energy of the freely jointed chain, which is normalized by the thermal energy $k_B T$. Here T is the temperature and k_B is Boltzmann's constant. Since all microstates are equivalent for the internal energy of the FJC, the only term arising on the right side of equation 3.1 is the work done by the chain, which is minus the work performed on the chain by the stretching force in the z-direction. Thus, the extension is determined by a competition between energy (the work done) and conformational entropy. Note that there is no energetic term in equation 3.1 associated with self-avoidance of the chain. We justify this simplification by pointing out that the probability of a chain under tension crossing itself is negligible.

The first step in the calculation involves the calculation of the partition function, Z. We describe the required steps here but we omit the actual mathematical operations. The theoretically interested reader can find the calculations in Appendix A.1.

$$Z \;=\; \sum_{\{\hat{t}_i\}}\exp\left(-\frac{\varepsilon^{\mathrm{FJC}}[\{\hat{t}_i\}]}{k_B T}\right). \tag{3.2}$$

The free energy F is now given by

$$F \;=\; -k_B T\,\ln(Z), \tag{3.3}$$

and the expectation value of the end-to-end length in the z direction is obtained from the free energy by differentiation to its conjugated variable. This is minus the force, $-f$:

$$\langle z \rangle \;=\; -\frac{\partial F}{\partial f}. \tag{3.4}$$

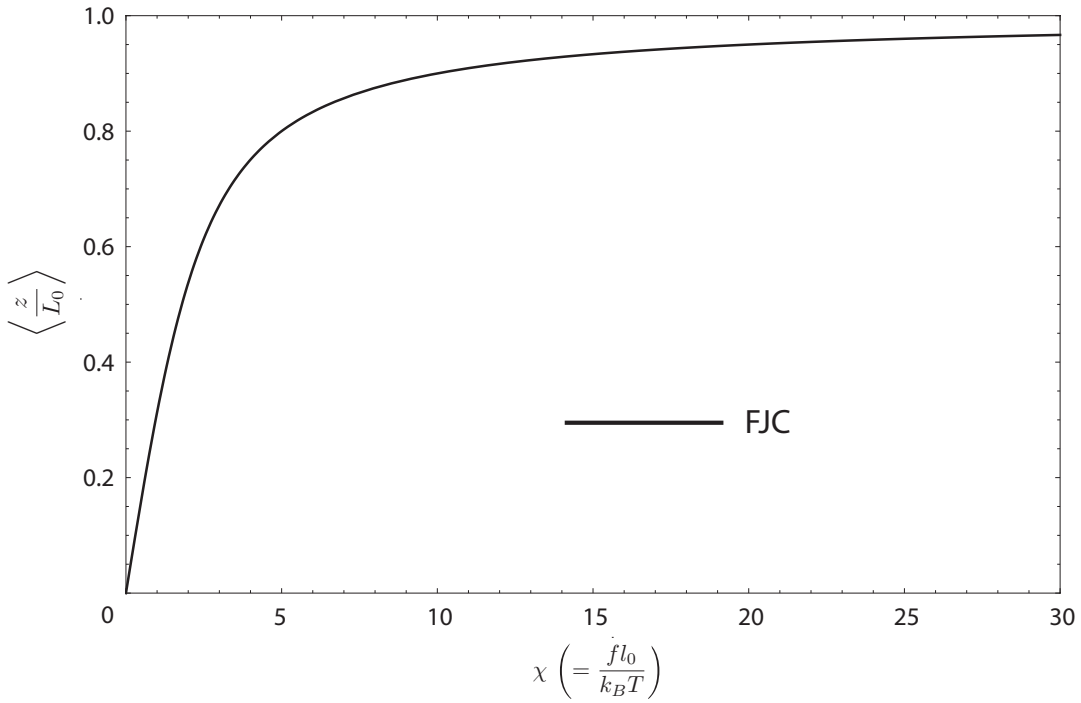

Figure 3.2: The dimensionless force-extension curve of the freely jointed chain or 1-state Kuhn model shows the expectation value of the dimensionless extension, $\left\langle \frac{z}{L_0} \right\rangle$, as function of the dimensionless force $\chi \equiv \frac{f l_0}{k_B T}$, according to equation 3.8. Here z is the end-to-end length in the z direction, L_0 is the contour length of the chain, l_0 is the Kuhn length, f is the stretching force, k_B is Boltzmann's constant, and T is the temperature. The curve is general for any FJC, and shows the competition between the work done by the stretching force (which favors a large end-to-end length z) and the maximization of conformational entropy (which favors a small end-to-end length z).

The expectation value in equation 3.4 denotes a thermal average. We are interested in the thermal average because we study the equilibrium properties of dsDNA systems in this thesis (section 1.3). The final result is the force-extension relation: the expectation value of the end-to-end length $\langle z \rangle$ as a function of the stretching force,

$$\langle z \rangle \;=\; N l_0 \left[\coth\left(\frac{f l_0}{k_B T} \right) - \frac{k_B T}{f l_0} \right], \tag{3.5}$$

where $\coth x \equiv \frac{1}{2}\left(\exp x + \exp(-x)\right)$ is the hyperbolic cotangent function. Note that the term $N l_0$ is just the contour length of the chain, which we call L_0. Dividing by the contour length gives the relative extension as function of force, which is given by the *Langevin function*:

$$\left\langle \frac{z}{L_0} \right\rangle \;=\; \mathcal{L}\left(\frac{f l_0}{k_B T} \right) \;=\; \coth\left(\frac{f l_0}{k_B T} \right) - \frac{k_B T}{f l_0}. \tag{3.6}$$

Finally, we define a dimensionless force χ,

$$\chi \;\equiv\; \frac{f l_0}{k_B T}, \tag{3.7}$$

which gives the dimensionless force-extension relation:

$$\left\langle \frac{z}{L_0} \right\rangle = \coth(\chi) - \frac{1}{\chi}. \tag{3.8}$$

The dimenionless force-extension relation is plotted in figure 3.2. Note that the plot represents any freely jointed chain, since it does not depend on the Kuhn length l_0 or the temperature T. Both are taken into account indirectly in the dimensionless force χ.

3.2. A 2-state Kuhn model for DNA

We now expand the 1-state Kuhn model from section 3.1 by allowing each Kuhn segment to occupy two different states. We first present the 2-state Kuhn model and discuss the molecular basis of the model. In other words, we discuss why we choose this model to describe a double-stranded DNA molecule. Subsection 3.2.3 deals with the calculations of the force-extension curve of the 2-state Kuhn model. The corresponding results are discussed in section 3.3.

The 1-state Kuhn model is used as the simplest model for the elastic behavior of single-stranded DNA, but a model for double-stranded DNA requires something more. At a stretching force of about 65 pN the dsDNA suddenly elongates by a factor of 1.7; this is known as the *overstretching transition*. In section 2.1 we gave the biological background of this transition: at forces lower than the overstretching force, the DNA is in the helical Watson-Crick [62] state that is called B-DNA. At forces higher than the overstretching force the DNA is in a different, non-helical state of DNA that we call overstretched DNA and that is 1.7 times longer than B-DNA. The 1-state Kuhn model does not contain these different states of DNA, and therefore it is not suitable for dsDNA at high forces.

This deficiency can be overcome by allowing two different states for each Kuhn-segment. The Kuhn segment can either represent B-DNA or it can represent overstretched DNA. A Kuhn segment that represents B-DNA has a length of l_0, while the length of an overstretched Kuhn segment is $1.7\,l_0$. To keep our model generally valid, we assign a length of $\gamma_1 l_0$ to an overstretched Kuhn segment, with γ_1 the *elongation factor* of the overstretched state with respect to B-DNA. We choose $l_0 = 0.34$ nm, the distance between two base pairs in B-DNA. This might seem contradictory with the fact that the Kuhn length of a freely jointed chain, that is optimal for fitting force-extension data, should be twice the persistence length of the actual polymer [15]. The persistence length of dsDNA is about 53 nm, more than 150 times the monomer length of 0.34 nm [15]. This suggests that the Kuhn length l_0 should be around 300 monomers in length. Instead, we choose l_0 to be one monomer length: the distance between two base pairs. We do this because we allow each monomer to overstretch independently from other monomers. If we would use a segment length of 300 monomers, then overstretching always has to occur with 300 monomers at the same time. That is very undesirable in our model, since this changes the features of the overstretching transition. Moreover, we use a similar argument in chapter 4, when we allow each base pair to bind an intercalator independently from neighboring base pairs. The downside of this approach is that the effective persistence length of our model is much smaller than the actual persistence length of dsDNA. Our choice for the segment length l_0 therefore leads to a difference in interpretation between the segment length and the Kuhn length. The Kuhn length is a characteristic length scale associated with the loss of directional correlation, while the segment length l_0 is the length of a single Kuhn segment in the chain. In a conventional freely jointed chain, the segment length and the Kuhn length are identical. However, in our model the chosen segment length $l_0 = 0.34$ nm is about 300 times smaller than the Kuhn length of dsDNA.

In addition to the length increase, we assign a free energy penalty ε_1 to a Kuhn segment in the overstretched state, which shows that B-DNA is the preferred state in the absence of any force.

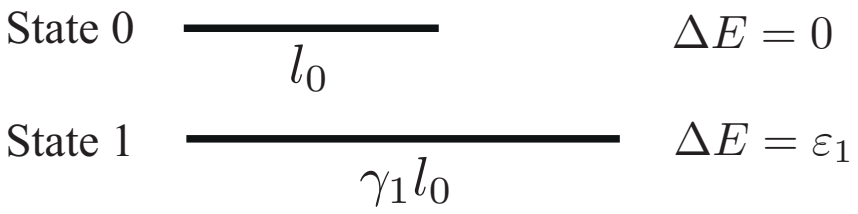

Figure 3.3: Two states of DNA in the 2-state Kuhn model. State 0 represents B-DNA and is the ground state of dsDNA with a segment length of l_0. State 1 represents overstretched DNA with a length of $\gamma_1 l_0$. A free energy penalty ε_1 is associated with the transition from state 0 to state 1.

We call B-DNA, which is the ground state of dsDNA, *state 0*. Overstretched DNA is referred to as *state 1*. We use the *state parameter* S_i to keep track of the state of the i^{th} Kuhn segment: $S_i = 0$ means the i^{th} Kuhn segment is B-DNA, while $S_i = 1$ is used for overstretched DNA. In a force-extension experiment, the value of the state parameter S_i is determined by a competition between the work done by the stretching force, which favors state 1 because it is the longer state, and the free energy penalty for state 1, ε_1, which favors state 0. At the overstretching transition these free energies balance each other. The model is summarized schematically in figure 3.3. We note that, in reality, it is not unthinkable that the values of these parameters (ε_1 and γ_1) depend on the type of nucleobase that they describe. However, we do not distinguish between different nucleobases, so our parameters can be considered as averages over all nucleobases in the DNA.

One more ingredient has to be added to the model to catch the essential features of the overstretching transition. From experimental data of the overstretching transition [12, 13] it is clear that the overstretching transition is cooperative in nature. In other words, as soon as the helix overstretches at some location along the DNA molecule, it is easier for neighboring base pairs to overstretch too. This is indicative of the existence of a free energy cost upon the creation of an 'interface' between B-DNA and overstretched DNA. At this 'interface' there is a small volume in the dsDNA molecule that has to adopt properties of both B-DNA and overstretched DNA. This intermediate state is energetically unfavorable, resulting in a free energy cost for such an 'interface'. The quotation marks indicate that we are not talking about an interface in the conventional sense, such as the interface that separates a liquid from a gas; with interface we refer to a small volume in dsDNA in between B-DNA and overstretched DNA. In terms of our model, such an interface exists between a Kuhn segment in state 0 and a Kuhn segment in state 1. We assign a free energy penalty to each such interface. We call this free energy penalty the *cooperativity parameter* and use the symbol λ for it. An example of a possible configuration of the 2-state Kuhn model is given in figure 3.4.

We note that, at this point, we have created a 2-state Kuhn model that is designed to explain the overstretching transition of dsDNA. In other words, the 2-state model is designed to explain the behavior of the force-extension curve of dsDNA in the absence of particle binding; we have not yet modeled intercalative binding. We introduce intercalators in our models in chapter 4. Before we do this, we first want to analyze and understand the 2-state Kuhn model for a couple of reasons. In doing so we show that the 2-state model is not capable of answering our research questions. This shows that the influence of intercalative binding cannot be attributed to a rescaling of parameters that dictate the force-extension curve in the absence of binding (ε_1, λ, γ_1). Instead, it shows that we need a more sophisticated model to take binding into account, which justifies the complexity of the 3-state Kuhn model that we introduce in chapter 4. Moreover, the relative simplicity of the 2-state model makes it suitable for explaining the physical concepts that will also be relevant in the mathematically much more challenging 3-state model. And finally, in chapter 4 we will see that for reasonable parameter choices the 3-state model largely behaves like a combination of three 2-state models. A proper understanding of the 2-state Kuhn model is therefore very useful for analyzing the 3-state model in chapter 4.

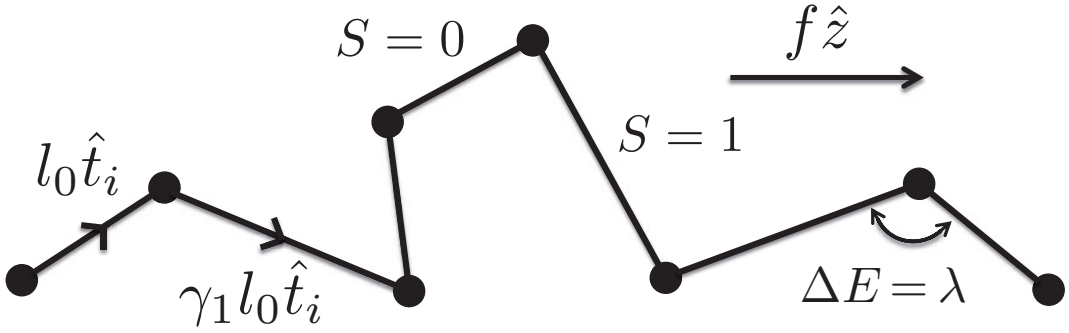

Figure 3.4: An example of a possible configuration of the 2-state Kuhn model. The example shows Kuhn segments in state 0 ($S = 0$), representing B-DNA, and Kuhn segments in state 1 ($S = 1$), representing overstretched DNA. Segments in state 1 are elongated with respect to state 0 with a factor γ_1, which is 1.7 for the overstretching transition of dsDNA. In addition to the free energy penalty for a Kuhn segment in state 1, as displayed in figure 3.3, there is a free energy penalty λ for an interface between two Kuhn segments in different states.

3.2.1. The absence of bend stiffness

This 2-state approach for modeling the overstretching transition of dsDNA is not new. As briefly mentioned in section 1.1 of the introduction, Storm and Nelson [15] used exactly that approach. They introduced the Ising-DPC model, which is an extension of their discrete persistent chain (DPC) model. In this Ising-DPC model they allowed each Kuhn segment to be in one of two possible states in exactly the same way as we allow our Kuhn segments to be in either state 0 or state 1 (figure 3.3). They also use a free energy penalty equivalent to ε_1 and a cooperativity parameter equivalent to λ. In other words, they expanded their DPC model in exactly the same way that we expanded the freely jointed chain model. Indeed, we could just as well have named our 2-state model the Ising-FJC model. Therefore, the only difference between our 2-state Kuhn model and their Ising-DPC model is exactly the same as the difference between the DPC model and the FJC model: the presence (DPC) versus absence (FJC) of bend stiffness. The Ising-DPC model penalizes bending between two Kuhn segments, and therefore the model contains a persistence length that is much larger than the actual monomer length. Our 2-state Kuhn model does not. Force-extension data shows that the persistence length of dsDNA is around 53 nm, more than 150 times the monomer length (0.34 nm) [15, 31].

The question arises why we neglect the bending stiffness of the dsDNA. The answer can be found in our main research question. We are interested in the influence of intercalative particle binding on the overstretching transition of dsDNA. Or, to put it differently, we are interested in the influence of intercalative particle binding on the high-force regime of the force-extension curve. The influence of bend stiffness or persistence length in the high-force regime is found in the way in which the stretching force diverges when the end-to-end length approaches the contour length: $f \sim (L_0 - z)^{-\alpha}$ [18]. The coefficient α is equal to 1 for a freely jointed chain model, while $\alpha = 2$ for the worm-like chain and the discrete persistent chain. However, we are mainly interested in the approximate length of the chain at a given force, rather than in the asymptotic behavior of this length. Existing data of the overstretching transition of dsDNA (figure 1.2) shows that a force which is large enough to overstretch B-DNA has already stretched it to an extent that the end-to-end length is approximately equal to the contour length. Due to the large stretching force, there is hardly any bending left in the molecular chain. Therefore the degree to which the chain resists bending, the bend stiffness, is not important for our purposes in the high-force regime.

While the significance of bend stiffness for this work is limited, including bend stiffness would greatly increase the complexity of our model. Introducing a bend resistance between the Kuhn segments effectively leads to an additional cooperativity parameter in the model: a correlation

between the unit vectors $\hat{t}_i$ and $\hat{t}_{i+1}$. This complicates calculations of the force-extension relation greatly. For the details of this calculation we refer to the work of Storm and Nelson [15], but the most important consequence of this additional cooperativity mechanism is that the model cannot be solved analytically and that a variational scheme is necessary to approximate the force-extension curve [15, 18]. Our 2-state model, however, can be solved analytically. We present the results in section 3.2.3. While not a trivial expression, we are able to gain more understanding about our system by systematically analyzing it. Moreover, calculating force-extension curves is much more straightforward for our analytical result than for the variatonal approach of the Ising-DPC model. In our view, this complication and extra effort is not worth the limited improvement of our model in the large-force regime, especially since we wish to focus on the complication due to the particle binding and the addition of a third molecular state in chapter 4. Recall that the aim of our work is to understand the essential physics involved in the influence of intercalators on the force-extension curve. To understand what are the leading physical principles that dictate this influence, we keep our model as simple as possible and only introduce parameters if we think they are essential for gaining this understanding. Finally, we note that the other frequently used polymer model that contains bend stiffness, the worm-like chain (section 1.1), is not suitable for our multi-state models because its lack of discreteness.

3.2.2. A course-grained model

We have come to the point where we have introduced the 2-state Kuhn model, and considered which parameters to take into account and which to neglect. In principle, we are now ready to start with the calculations of the force-extension curve. Before that, however, we need to ask ourselves one more question. This question concerns the difference in complexity between an actual DNA molecule and the complexity of a freely jointed chain or Kuhn model. In chapter 2, we showed the helical structure of dsDNA in figure 2.1a. More molecular details are shown in figure 2.1b, that shows the chemical structure of the phosphate-deoxyribose backbone and the paired nucleobases. A real dsDNA molecule is even more complex since interactions arise between non-neighboring atoms along the backbone when the molecule is formed into a helical structure. And yet we model this very dsDNA molecule by regarding it as a chain of perfectly rigid rods that are free to rotate with respect to each other. What justifies this great reduction of complexity?

The answer to this question lies in our approach of *coarse-graining*: we average over all microscopic details of the dsDNA and we use a small number of *effective parameters* that model the essential features of the molecule. Consider the 2-state model that we just introduced: we used four independent parameters for this model: l_0, γ_1, ε_1 and λ. Of these four parameters, l_0 (physical monomer length) and γ_1 (elongation of such a monomer upon overstretching) have a clear microscopic background. For the other two parameters, ε_1 and λ, there is no obvious microscopic picture: they are effective paremeters. Their origin might be in structural transition in the DNA itself or in interactions of the DNA with the surrounding solution. While ε_1 and λ might be interesting topics of study, we do not attempt to state anything about their nature, their origin or their microscopic background because that is not the aim of this study. Regardless of their origin, we do know from experimental data (section 1.1 [12, 13]) that microscopic interactions exist that effectively lead to a free energy penalty upon overstretching (ε_1) and a free energy penalty for an interface between a Kuhn segment in state 0 and a Kuhn segment in state 1 (λ). In other words, we present a coarse-grained model that we use to capture the essential features of the force-extension curve of dsDNA. The justification of doing so can be found in our results. Section 3.4.1 shows that our model indeed captures the essential features of dsDNA overstretching.

We now derive the force-extension curve for the 2-state Kuhn model. The reader that is mainly interested in our results can skip section 3.2.3 and continue reading in section 3.3.

3.2.3. Methods and calculations*

We use the same principles in the derivation of the force-extension relation of the 2-state Kuhn model that we used when deriving the force-extension relation of the 1-state Kuhn model in section 3.1.1. The difference is in the mathematics, which is more difficult due to the extra Kuhn state and the cooperativity between the two states.

We start again by formulating the energy functional of the chain:

$$\frac{\varepsilon^{2-\text{state}}[\{\hat{t}_i\},\{S_i\}]}{k_BT} = \sum_{i=1}^{N}\left[-\frac{fl_0\left[1+S_i\left(\gamma_1-1\right)\right]}{k_BT}\,\hat{t}_i\cdot\hat{z}+\varepsilon_1 S_i\right]+\sum_{i=1}^{N-1}\lambda(1-\delta_{S_i,S_{i+1}}). \tag{3.9}$$

The first term in the energy functional is the work done by the chain. Comparing with equation 3.1 for the 1-state Kuhn model, we notice that the length l_0 has been replaced by $l_0\left[1+S_i\left(\gamma_1-1\right)\right]$, which is equal to l_0 for $S_i=0$ and $\gamma_1 l_0$ for $S_i=1$. Recall that $S_i=0$ represents B-DNA and $S_i=1$ represents overstretched DNA. The second term in equation 3.9 gives the free energy penalty for overstretching and the final term displays the free energy penalty for interfaces between state 0 and state 1 segments (0/1-interfaces) in the chain. Here $\delta_{S_i,S_{i+1}}$ is the Kronecker delta, which is equal to 1 if $S_i=S_{i+1}$ and equal to 0 otherwise. Note that both ε_1 and λ are not divided by the thermal energy k_BT. This is because we define both ε_1 and λ as dimensionless free energies by normalizing them to k_BT. In other words, the unit-bearing free energy penalties are given by $k_BT\varepsilon_1$ and $k_BT\lambda$. As in the case of the 1-state Kuhn model, we neglect self avoidance in the energy functional.

From here on we take the same steps that we took for the 1-state Kuhn model in section 3.1.1, and again we only present the required steps but omit mathematical details. The complete derivation is presented in Appendix A.2. This derivation is an important part of our work, and we encourage the theoretically interested reader to study it. However, the rest of this thesis can be read without studying the derivation in Appendix A.2.

We first calculate the partition function, but now the summation over all possible microstates involves a summation over all sets $\{S_i\}$ as well as over all sets of unit vectors $\{\hat{t}_i\}$.

$$Z = \sum_{\{\hat{t}_i\}}\sum_{\{S_i\}}\exp\left(-\frac{\varepsilon^{2-\text{state}}[\{\hat{t}_i\},\{S_i\}]}{k_BT}\right). \tag{3.10}$$

Calculating this partition function is, however, much more difficult than calculating the partition function of the 1-state Kuhn model (Appendix A.1). In the case of the 1-state Kuhn model the partition function factorized (equation A.3), because all Kuhn segments behave independently. However, in the 2-state Kuhn model the cooperativity parameter λ causes an interaction between neighboring Kuhn segments, which prevents the partition function from factorizing. We employ a technique called the *transfer matrix method* [92] to calculate the non-factorized partition function. The details of the calculations can be found in Appendix A.2. In the final steps of the derivation we calculate the free energy and the expectation value of the end-to-end according to equations 3.3 and 3.4, repeated here for convenience,

$$F = -k_BT\,\ln(Z), \tag{3.11}$$

$$\langle z\rangle = -\frac{\partial F}{\partial f}. \tag{3.12}$$

The result of the calculations presented in Appendix A.2 in the infinite-chain limit reads

$$\lim_{N\to\infty}\left\langle\frac{z}{L_0}\right\rangle = \frac{1}{2}\left(-\frac{2}{\chi}+\coth(\chi)+\gamma_1\coth(\gamma_1\chi)\right) + \frac{\gamma_1\left[\cosh(\gamma_1\chi)+\exp(\varepsilon_1)\left(\cosh(\chi)-\gamma_1\coth(\gamma_1\chi)\sinh(\chi)\right)\right]-\coth(\chi)\sinh(\gamma_1\chi)}{2\sqrt{4\exp(\varepsilon_1)\gamma_1\sinh(\chi)\sinh(\gamma_1\chi)\exp(-2\lambda)+\left(-\exp(\varepsilon_1)\gamma_1\sinh(\chi)+\sinh(\gamma_1\chi)\right)^2}}. \tag{3.13}$$

Here the extension is again normalized on $L_0 = Nl_0$ and $\chi = \frac{fl_0}{k_BT}$ is a normalized force which was first defined in equation 3.7. L_0 is the contour length of the 1-state Kuhn model, but not necessarily the contour length of the 2-state Kuhn model. The latter varies because of the variable length of the Kuhn segments. Therefore, the normalized extension $\left\langle\frac{z}{L_0}\right\rangle$ has a maximum value of γ_1 instead of 1. Recall that $\gamma_1 = 1.7$ for the overstretching transition of dsDNA. $\sinh x \equiv \frac{1}{2}(\exp x - \exp(-x))$, $\cosh x \equiv \frac{1}{2}(\exp x + \exp(-x))$ and $\coth x \equiv \frac{\cosh x}{\sinh x}$ are the hyperbolic sine, cosine and cotangent respectively.

As can be seen from equation 3.13, we have used the thermodynamic limit, or ground-state approximation, ($N \to \infty$) in the derivation of the force-extension relation. This simplifies the calculations and, more importantly, greatly reduces the complexity of the expression for the extension as a function of force. This enables us to analyze the force-extension relation analytically in section 3.3. We justify this approximation by noting that the difference between the thermodynamic limit result and the exact result, for an arbitrary number of Kuhn segments N, is only significant at a very small number ($N \lesssim 50$) of segments (Appendix B). The experimental results that we study (figure 1.4 [21, 54]) were obtained by stretching bacteriophage lambda DNA that contains about 48.500 base pairs (section 2.1). Since every Kuhn segment models one base pair ($l_0 = 0.34nm$, section 3.2), this means that the thermodynamic limit is a very reasonable approximation to use in this thesis. Appendix B shows the exact result for arbitrary N graphically, compares this with the thermodynamic limit result, and justifies the statement that the thermodynamic limit is a decent approximation for $N \gtrsim 50$.

3.3. The force-extension curve of the 2-state Kuhn model

The reader who skipped section 3.2.3 should know that we defined ε_1 and λ to be dimensionless free energies by normalizing them to the thermal energy k_BT.

We presented the force-extension relation of the 2-state Kuhn model in equation 3.13. In this section we analyze this expression and explore how the behavior of the force-extension curve depends on the system parameters. We illustrate this analysis by showing the force-extension relation in graphical form. We start with an example of the non-cooperative case; we plot a dimensionless force-extension curve with $\lambda = 0$ in figure 3.5. The force-extension curve of the 1-state Kuhn model (freely jointed chain) is plotted as a reference. The values of ε_1 ($= 15$) and λ ($= 0$) are chosen because they produce a plot that clearly illustrates the features of the 2-state force-extension curve. They are not representative for dsDNA. The elongation factor γ_1 is 1.7. Section 3.4 relates the model to experimental data on dsDNA.

For small forces the 2-state force-extension curve in figure 3.5 is indistinguishable from the 1-state force-extension curve. The work done by such a low force is not enough to overcome the free energy penalty ε_1 and to excite a Kuhn segment from state 0 to state 1. At higher forces ($16 < \chi < 28$), however, some Kuhn segments are excited to state 1 and the force-extension curve starts deviating from the single-state case. This force regime shows a coexistence of Kuhn

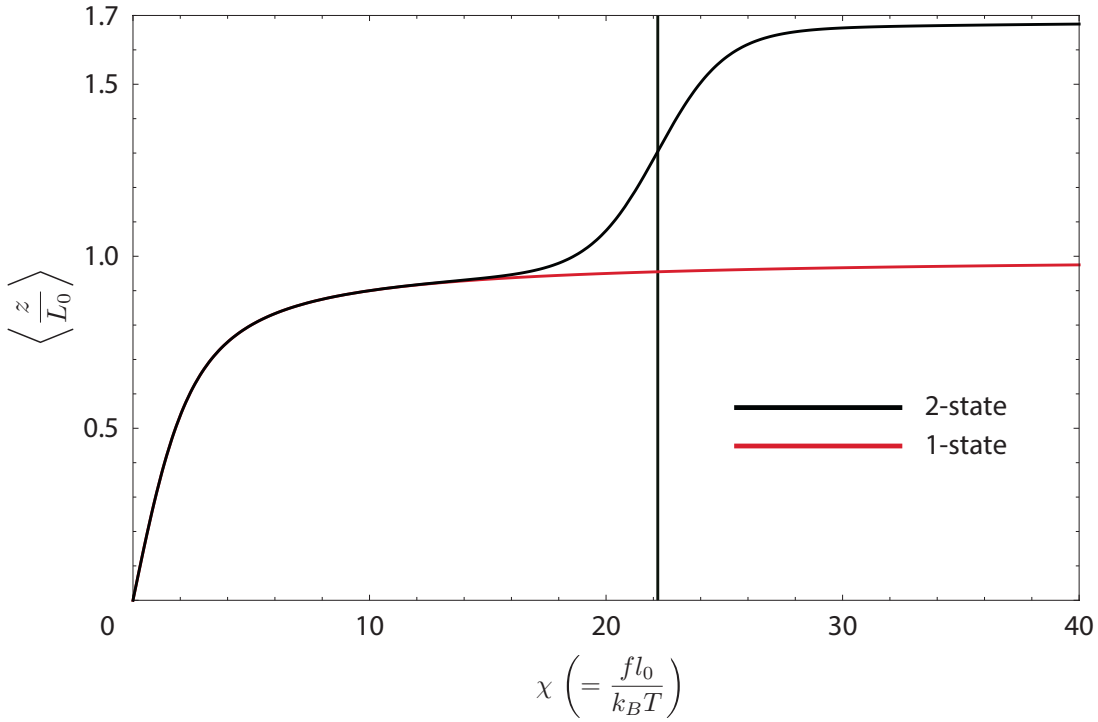

Figure 3.5: A dimensionless force-extension curve of the 2-state Kuhn model (black) with axes that are identical to those in figure 3.2. The force-extension curve of the 1-state Kuhn model (freely jointed chain) is plotted as a reference. For small forces ($\chi \lesssim 16$) the 2-state curve is indistinguishable from the single-state curve, and approximately all Kuhn segments are in state 0. At high forces ($\chi \gtrsim 28$), approximately all Kuhn segments are excited to state 1, with corresponding length $\gamma_1 l_0 = 1.7\, l_0$. The chain then behaves like a freely jointed chain with segment length $\gamma_1 l_0$ instead of l_0. At intermediate forces ($16 < \chi < 28$) Kuhn segments in states 0 and 1 coexist. We call this force regime the overstretching transition. The vertical line indicates the center of this overstretching transition, and the corresponding force is called the overstretching force (χ_{01}). The values of the system parameters, $\varepsilon_1\,(= 15)$ and $\lambda\,(= 0)$, are not representative for dsDNA, but they are chosen because they produce a plot that clearly illustrates the features of the 2-state force-extension curve.

segments in state 0 and Kuhn segments in state 1. At even higher forces ($\chi \gtrsim 28$), approximately all Kuhn segments are excited to state 1. The chain then behaves like a freely jointed chain again. The only difference is that in that case all Kuhn segments have a length of $\gamma_1 l_0$ instead of l_0. We call the force-regime that shows coexistence between state 0 and state 1 the *overstretching transition*. The center of this overstretching transition is marked with a vertical line in figure 3.5. This is the point on the curve where 50% of the Kuhn segments is in state 0 and the other 50% is in state 1. We call the corresponding force the *overstretching force*, and use the symbol χ_{01} for it. The subscript 01 indicates that this is the overstretching force of the transition between freely jointed chains with segments in state 0 and state 1 respectively. In chapter 4 we encouter transitions between other states than 0 and 1 as well.

We already understand the force-extension relation of the freely jointed chain; we studied it in section 3.1. The more interesting regime of the 2-state force-extension curve is the overstretching transition. The transition is characterized by two independent quantities: the position of the transition and the transition width. We analyze them in sections 3.3.1 and 3.3.2 respectively.

3.3.1. The position of the overstretching transition

We define the position of the overstretching transition as the overstretching force χ_{01}, that was defined above and given by the vertical line in figure 3.5. We calculate the overstretching force from equation 3.13 by using that half of the Kuhn segments is in state 0 and the other half

in state 1 at this force. This indicates that the end-to-end length is exactly in between the end-to-end lengths of freely jointed chains with short (l_0) and long ($\gamma_1 l_0$) segments. The average of these two end-to-end lengths is given by

$$\left\langle \frac{z}{L_0} \right\rangle_{\chi_{01}} = \frac{1}{2}\left(\coth(\chi) - \frac{1}{\chi} + \gamma_1 \coth(\gamma_1 \chi) - \frac{1}{\chi} \right). \tag{3.14}$$

The first two terms in equation 3.14 give the expression of the FJC with segment length l_0 (equation 3.8). The last two terms give the force-extension relation of an FJC with segment length $\gamma_1 l_0$ that is normalized on $L_0 = N l_0$.

Note that equation 3.14 gives the the first term in the 2-state force-extension relation (equation 3.13). In other words, the first term in equation 3.13 describes the average of a state 0 FJC and a state 1 FJC. The second term gives the deviation from this average. Equating the second term to 0 therefore gives the position of the overstretching force. The resulting equation can be reduced to equation 3.15. We omit the proof, but the interested reader can verify that the numerator of the second term reduces to 0 if equation 3.15 applies,

$$\sinh(\chi_{01}) = \frac{1}{\gamma_1} \exp(-\varepsilon_1) \sinh(\gamma_1 \chi_{01}). \tag{3.15}$$

Equation 3.15 does not have an exact solution. However, we can approximate the solution if we assume that the dimensionless force χ_{01} is large. That is, if $f l_0$ is large compared with $k_B T$ at the position of the overstretching transition. In that case the force has stretched the chain to an end-to-end length of approximately $N l_0$ before it overstretches. In other words, for forces approaching the overstretching force, all angles between Kuhn segments are close to zero and the mechanical energy dominates the thermal energy. In mathematical terms this condition implies that $\sinh(\chi_{01}) = \frac{\exp(\chi_{01}) - \exp(-\chi_{01})}{2} \approx \frac{\exp(\chi_{01})}{2}$, leading to

$$\exp(\chi_{01}) = \frac{1}{\gamma_1} \exp(-\varepsilon_1 + \gamma_1 \chi_{01}). \tag{3.16}$$

The solution of equation 3.16 gives

$$\chi_{01} = \frac{\varepsilon_1 + \log \gamma_1}{\gamma_1 - 1}, \tag{3.17}$$

which defines the position of the overstretching transition. For forces smaller than χ_{01}, a Kuhn segment is favored to be in state 0, because that state has the lowest free energy. In this case the free energy penalty for state 1 dominates the work done by the stretching force. If $\chi > \chi_{01}$, the work dominates over the free energy penalty and Kuhn segments are favored to be in state 1.

We make this more explicit by substituting the definition of the dimensionless force χ (equation 3.7) in equation 3.17 and rearranging terms. This yields for the unit-bearing overstretching force, f_{01},

$$f_{01} l_0 (\gamma_1 - 1) = k_B T \varepsilon_1 + k_B T \log \gamma_1. \tag{3.18}$$

The left hand side in equation 3.18 represents the work by the stretching force when a single Kuhn segment is elongated from a length of l_0 to a length of $\gamma_1 l_0$. The first term on the right hand side is the free energy penalty upon this elongation, as defined in section 3.2. Recall that ε_1 is defined as this free energy penalty normalized by $k_B T$ (section 3.2.3). The second term on the right hand side is a renormalization of the penalty ε_1. It has an entropic origin that is quite subtle; when a state 0 segment is elongated to a state 1 segment, the length increase is $l_0(\gamma_1 - 1)$. However, in reality a segment is never perfectly aligned with the z-direction (the direction of the force). So to obtain a length increase in the z-direction of $l_0(\gamma_1 - 1)$, the long segment needs

a greater degree of alignment with the force than the short segment. In other words, it has to reduce its polar angle θ. In our model, a reduction of the angle θ is a reduction of conformational entropy. That is a consequence of our choice to calculate the partition function by integrating over the angles ϕ and θ and not over Cartesian coordinates (Appendix A.2, equation A.12 and associated footnote). Therefore, to obtain the work on the left hand side of equation 3.18, an entropic penalty has to be imposed on state 1. We speculate that this entropic penalty is $k_BT \log \gamma_1$. In the end, however, this entropic term is not very relevant for our purposes. It is just a rescaling of a phenomenologic free energy ε_1. We can easily absorb the rescaling in ε_1 without the loss of generality. So the right hand side of equation 3.18 represents the free energy penalty upon elongation of a single Kuhn segment.

When $f > f_{01}$ the left hand of equation 3.18 is larger than the right and the work dominates the free energy penalty: state 1 is favored over state 0. When $f < f_{01}$ the right hand term is larger and the free energy penalty upon overstretching is larger than the energy reduction by the work: state 0 is favored over state 1.

Finally we note that the cooperativity parameter λ does not appear in equation 3.17; the position of the overstretching transition does not depend on the cooperativity of the transition. λ only influences the width of the transition.

3.3.2. The width of the overstretching transition

Figure 3.5 clearly shows that the overstretching transition is not infinitely sharp. It has a certain width. The 2-state force-extension curve of figure 3.5 is plotted again in figure 3.6. However, this plot shows two reference curves: a freely jointed chain with all segments in state 0 and a freely jointed chain with all segments in state 1. The overstretching transition is the region of the curve where the 2-state extension is in between those of the state 0 and state 1 freely jointed chains. This region is marked with the blue vertical lines. The black vertical line again indicates the position of the overstretching force (section 3.3.1).

Below we calculate the width of the overstretching transition and investigate the influence of the cooperativity parameter λ on this width. First, however, we answer the question of why the transition has a nonzero width. After all, we calculated the position of the overstretching force χ_{01} in the previous section. We stated that for $\chi < \chi_{01}$ state 0 is favored over state 1 and for $\chi > \chi_{01}$ it is the other way around. Why, then, are there already Kuhn segments in state 1 for $\chi < \chi_{01}$ and still Kuhn segments in state 0 for $\chi > \chi_{01}$?

The answer is entropy. Entropy favors a mixing of state 0 and state 1, since there a more possible microstates with a mix of states 0 and 1 than with only one of them. In the end, it is not the energy of the total chain, but the free energy $F = E - TS$ that is minimized. The smaller the energy difference between states 0 and 1 is, the larger the influence of the mixing entropy S_{mix} is. This causes a significant amount of Kuhn segments to be in the energetically unfavored state at forces close to the overstretching force.

Alternatively, the coexistence of states 0 and 1 can be understood by considering the probability distribution of the Kuhn segments, which is given by the Boltzmann distribution. This distribution gives the probability P_ν of a system to be in a certain microstate ν according to equation 3.19,

$$P_\nu \propto \exp\left(-\frac{E_\nu}{k_BT}\right), \tag{3.19}$$

where E_ν is the energy corresponding to microstate ν. Equation 3.19 shows that there is always a finite probability for a system to be in an energetically unfavored state. If we consider a single Kuhn segment as our system, this means that there is always a finite probability for the segment to be in state 1 even if state 0 has a lower energy. In fact, it is even very unlikely for *all* segments to be in the energetically *favored* state simultaneously; the expectation value for the fraction of

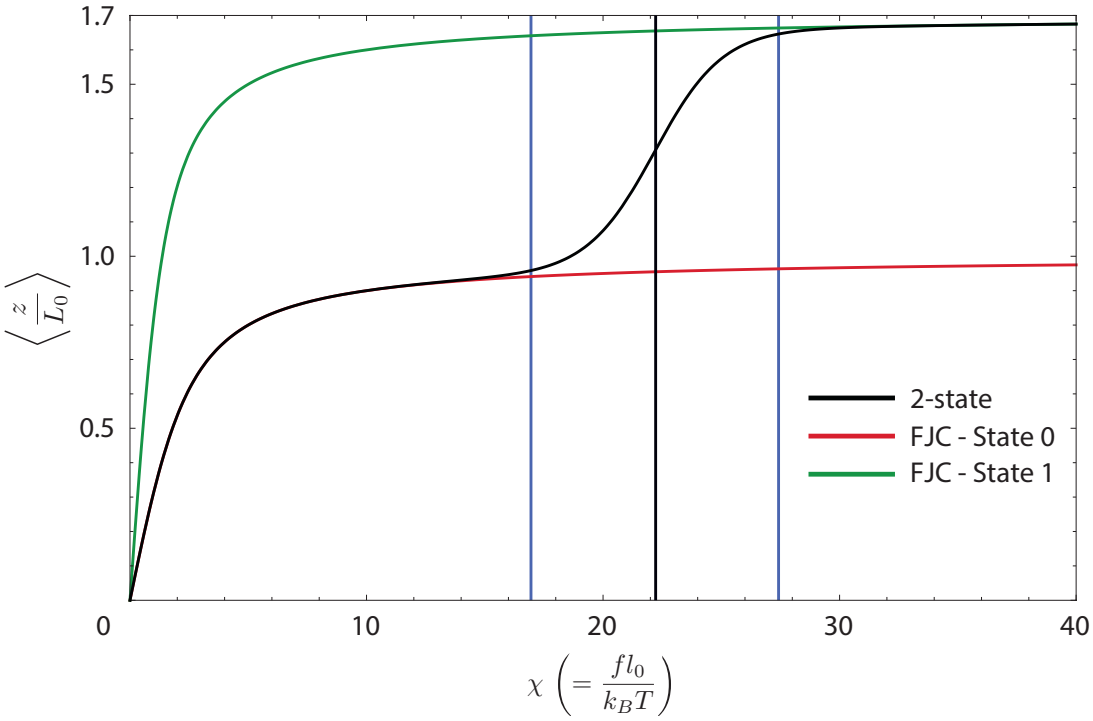

Figure 3.6: The 2-state force-extension curve (black) that was also shown in figure 3.5, with two reference curves: the state 0 FJC (red), with segment length l_0, and the state 1 FJC (green), with segment length $\gamma_1 l_0 = 1.7\, l_0$. The blue verticle lines mark the overstretching transition: the force regime where the extension is in between those of the two reference curves. The black vertical line displays the center of the overstretching transition: the overstretching force.

Kuhn segments in state 1, $P_{S_i=1}$, is given by

$$P_{S_i=1} = \frac{\exp\left(-\frac{\Delta E}{k_B T}\right)}{1 + \exp\left(-\frac{\Delta E}{k_B T}\right)}, \tag{3.20}$$

which is the well-known expression for the probability of the excited state in a two level system. Equation 3.20 can easily be derived from equation 3.19 by normalizing the total probability of the Kuhn segment to be in *any* state to 1. Here $\Delta E = E_1 - E_0$ is the free energy difference between states 1 and 0, which does not only include the free energy penalty $\varepsilon_1 + \ln \gamma_1$, but also the work done.

Equation 3.20 shows why the overstretching transition in figure 3.5 is not infinetely sharp. Close to the overstretching force the free energy difference ΔE is small and the probability for a Kuhn segment to be in state 1 is approximately $\frac{1}{2}$. For forces larger than the overstretch force, ΔE becomes negative and state 1 dominates the force-extension curve. Finally, we would like to remark that the explanation using the Boltzmann distribution, given here, and the explanation using mixing entropy, given above, are completely equivalent and describe the same physical principle.

In the following we calculate the width of the overstretching transition. This section can be skipped if desired. We advise the reader who does so to continue reading at the subheading 'The cooperativity parameter λ'.

Calculating the transition width*

Now that we know why the overstretching transition has a nonzero width, we are ready to calculate how large this width is, and how it depends on the parameters of the model. For this calculation we use the general force-extension relation of the 2-state Kuhn model (equation 3.13). Before we start the calculation, however, we need to define what we mean by width. The 2-state force-extension curve gets arbitrarely close to the state 0 and state 1 freely jointed chains for small and large forces respectively (figure 3.6), but it is never exactly equal to either of them. Thus, the definition of the transition width depends on how close we want the 2-state curve to approach complete saturation in one of the two Kuhn states. Our goal is, however, to find how the width depends on our system parameters rather than find a specific number for it. We introduce a parameter ϕ to define the transition width. We first present the equation from which we calculate the transition width, and use this equation to explain the meaning of ϕ. The equation is given by

$$\frac{\gamma_1\Big[\cosh(\gamma_1\chi)+\exp(\varepsilon_1)\Big(\cosh(\chi)-\gamma_1\coth(\gamma_1\chi)\sinh(\chi)\Big)\Big]-\coth(\chi)\sinh(\gamma_1\chi)}{2\sqrt{4\exp(\varepsilon_1)\gamma_1\sinh(\chi)\sinh(\gamma_1\chi)\exp(-2\lambda)+\Big(-\exp(\varepsilon_1)\gamma_1\sinh(\chi)+\sinh(\gamma_1\chi)\Big)^2}} = \frac{1}{2}\Big(\gamma_1\coth(\gamma_1\chi)-\coth(\chi)\Big)\phi. \quad (3.21)$$

The left hand side of equation 3.21 is equal to the second term in the 2-state force-extension relation (equation 3.13). Recall from section 3.3.1 that this term represents the deviation of the normalized extension, $\left\langle \frac{z}{L_0} \right\rangle$, from the normalized extension at the overstretching force, $\left\langle \frac{z}{L_0} \right\rangle_{\chi_{01}}$. The right hand side multiplies our new parameter ϕ with the difference between the extension of a chain saturated in state 1 and the extension at the overstretching force, $\left\langle \frac{z}{L_0} \right\rangle_{\chi_{01}}$. This leads to an interpretation of ϕ as a measure for the saturation of the chain in state 1. If $\phi = 1$ the chain is completely saturated and the extension is equal to that of a state 1 FJC. $\phi = -1$ represent the exact opposite: complete saturation in state 0. $\phi = 0$ represents a state with equal amounts of state 0 and state 1 and therefore defines the overstretching force. Indeed, if we substitute $\phi = 0$ in equation 3.21 we retrieve the equation that lead to the expression for the overstretching force in section 3.3.1.

The definition for the transition width depends on the degree of saturation that we define to bound the overstretching transition. In other words, the definition depends on our choice for ϕ. This choice is arbitrary; we can use any number between 0 and 1 for ϕ. Figure 3.7 illustrates the interpretation of ϕ; the figure adds three possible definitions of transition width W, together with the corresponding values of ϕ, to the force-extension curves of figure 3.6.

To calculate the width W we need to solve equation 3.21 for χ. We have been unable to solve this equation analytically. This is why we choose to make the same approximation that we made for deriving the overstretching force: $\chi >> 1$ (section 3.3.1). This simplifies the hyperbolic sine, cosine and cotangent and leads, after rearranging, to

$$\frac{(\gamma_1-1)\Big[\exp(\gamma_1\chi)-\gamma_1\exp(\varepsilon_1+\chi)\Big]}{2\sqrt{4\gamma_1\exp\Big[\varepsilon_1+(\gamma_1+1)\chi-2\lambda\Big]+\Big[-\gamma_1\exp(\chi+\varepsilon_1)+\exp(\gamma_1\chi)\Big]^2}} = \frac{1}{2}(\gamma_1-1)\phi. \quad (3.22)$$

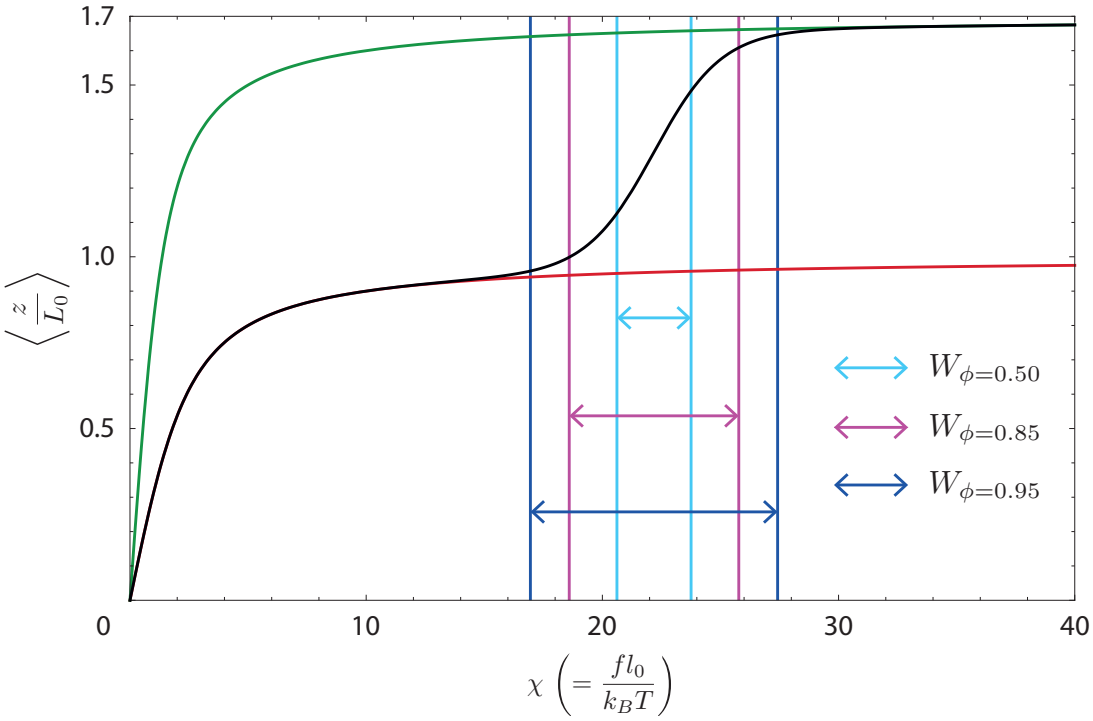

Figure 3.7: Three possible definitions of the transition width are added to force-extension curves of 3.6, to illustrate the interpretation of the saturation parameter ϕ, which is defined according to equation 3.21. ϕ represents the saturation of the chain in state 1: $\phi = 1$ means that all Kuhn segments are in state 1, $\phi = -1$ signifies that all Kuhn segments are in state 0 and $\phi = 0$ represents a state with equal amounts of state 0 and state 1. A choice for ϕ defines the transition width; a large value for ϕ corresponds to a wide overstretching transition and a small value of ϕ corresponds to a narrow overstretching transition. The choice for ϕ is arbitrary.

Equation 3.22 can be solved analytically. The result, by standard calculus, is given by

$$\begin{aligned} \chi &= \frac{\varepsilon_1 + \ln \gamma_1}{\gamma_1 - 1} + \frac{\ln\left[1 + \frac{2\phi}{\exp(2\lambda)\left(1-\phi^2\right)}\left(\phi + \sqrt{\phi^2 + \exp(2\lambda)\left(1-\phi^2\right)}\right)\right]}{\gamma_1 - 1} \\ &= \chi_{01}(\varepsilon_1, \gamma_1) \quad + \frac{1}{2} W_{01}(\lambda, \gamma_1, \phi). \end{aligned} \tag{3.23}$$

Equation 3.23 shows two terms. The first term is the overstretching force χ_{01}. This means that the second term gives the difference between the force corresponding to a saturation of ϕ and the overstretching force. The second term thus represents exactly half of the transition width, which we give the symbol W_{01}. The subscript 01 again indicates that the width concerns the transition from state 0 to state 1. Equation 3.23 is used for plotting the vertical lines in figure 3.7. The width is thus given by

$$W_{01} = \frac{2\ln\left[1 + \frac{2\phi}{\exp(2\lambda)\left(1-\phi^2\right)}\left(\phi + \sqrt{\phi^2 + \exp(2\lambda)\left(1-\phi^2\right)}\right)\right]}{\gamma_1 - 1}. \tag{3.24}$$

For arriving at equation 3.24 we used that the overstretching transition is antisymmetric in χ around the overstretching force χ_{01}, which allows us to multiply the second term in equation 3.23 by 2 to obtain the transition width. This antisymmetry can be proved by showing that this term, $\frac{1}{2} W_{01}$, is antisymmetric in ϕ: $\frac{1}{2} W_{01}(-\phi) = -\frac{1}{2} W_{01}(\phi)$. This means that a certain

level of saturation in state 1 (corresponding to a certain ϕ) and an equal level of saturation in state 0 (corresponding to $-\phi$) are equally far away from the overstretching force. In other words, that means that the transition is antisymmetric in χ around χ_{01}. We omit the proof here.

Now we go back to equation 3.23 for a moment, and consider the second line in the equation. Note that χ_{01} depends on ε_1 but not on λ, while for W_{01} it is the other way around. This can be easily understood by considering the origin of ε_1 and λ in our model (section 3.2); the penalty upon overstretching for a single Kuhn segment (ε_1) determines at which force the overstretching occurs, while the penalty for a 0/1-interface dictates the cooperativity and thus the width of this transition. Also note that W_{01} depends on only two system parameters: λ and γ_1; ϕ is just a number that can be chosen arbitrarily. The dependence on γ_1 is easy to understand; we recognize the term $\frac{1}{\gamma_1 - 1}$ from the expression for the position of the transition (section 3.3.1). Since the width is in essence a difference between two positions on the curve, this factor also occurs in the equation for the width. In the next paragraph we look further into the dependence of W_{01} on λ.

The cooperativity parameter λ

Note for the reader who skipped the previous: the width of the overstretching transition depends on an arbitrary definition. We introduced a parameter ϕ that we call the saturation parameter, which is a measure for the degree of saturation of the molecular chain in state 1. The transition width is a function of ϕ. The result of the calculation is given in figure 3.24.

The 2-state force-extension curves shown so far (figures 3.5, 3.6 and 3.7) correspond to the non-cooperative case ($\lambda = 0$). However, experimentally measured force-extension curves (figure 1.2) show that the overstretching transition is much sharper than in figure 3.5. This is why we introduced the cooperativity parameter λ in our model. Here we look into non-zero λ and its influence on the width of the transition. Figure 3.8 shows this width as a function of λ, according to equation 3.24.

The figure uses $\gamma_1 = 1.7$ and $\phi = \frac{1}{2}\sqrt{2} \approx 0.707$. The choice for ϕ will become clear soon. Figure 3.8 shows two distinct regimes. The right side of the figure shows the cooperative ($\lambda > 0$) regime where the width decays exponentially with increasing cooperativity. The other regime is anti-cooperative ($\lambda < 0$) and shows that the width increases linearly with increasing anticooperativity (decreasing λ). The red curve in figure 3.8 shows the exponential relation for positive λ, while the blue curve shows the linear relation for negative λ. From experiments [12, 13] we know that the overstretching transition of dsDNA is cooperative. This suggests that only the right side of figure 3.8 is relevant for our work. However, in chapter 4 we encouter a 2-state Kuhn model that is anti-cooperative in nature. This is related to the *neighbor-exclusion principle* for intercalation of dsDNA (section 2.1). We elaborate more on this in chapter 4. For now this means that we analyze both the cooperative and the anti-cooperative case of the 2-state model.

We start with the cooperative ($\lambda > 0$) 2-state Kuhn model. Figure 3.8 suggests that the transition width decreases exponentially with λ in the cooperative regime. Indeed, by taking the limit of large λ in the equation for the transition width (equation 3.24), an exponential relation is shown. Since λ only appears in exponents, this limit is already satisfied for relatively small λ, which is also suggested by figure 3.8. The obtained relation is displayed by the red curve in figure 3.8, and is given by

$$W_{\lambda>>0} \;=\; \frac{1}{\gamma_1 - 1}\,\frac{4\phi}{\sqrt{1-\phi^2}}\,\exp(-\lambda). \tag{3.25}$$

Equation 3.25 shows two prefactors. The first depends on γ_1 in the same manner that the

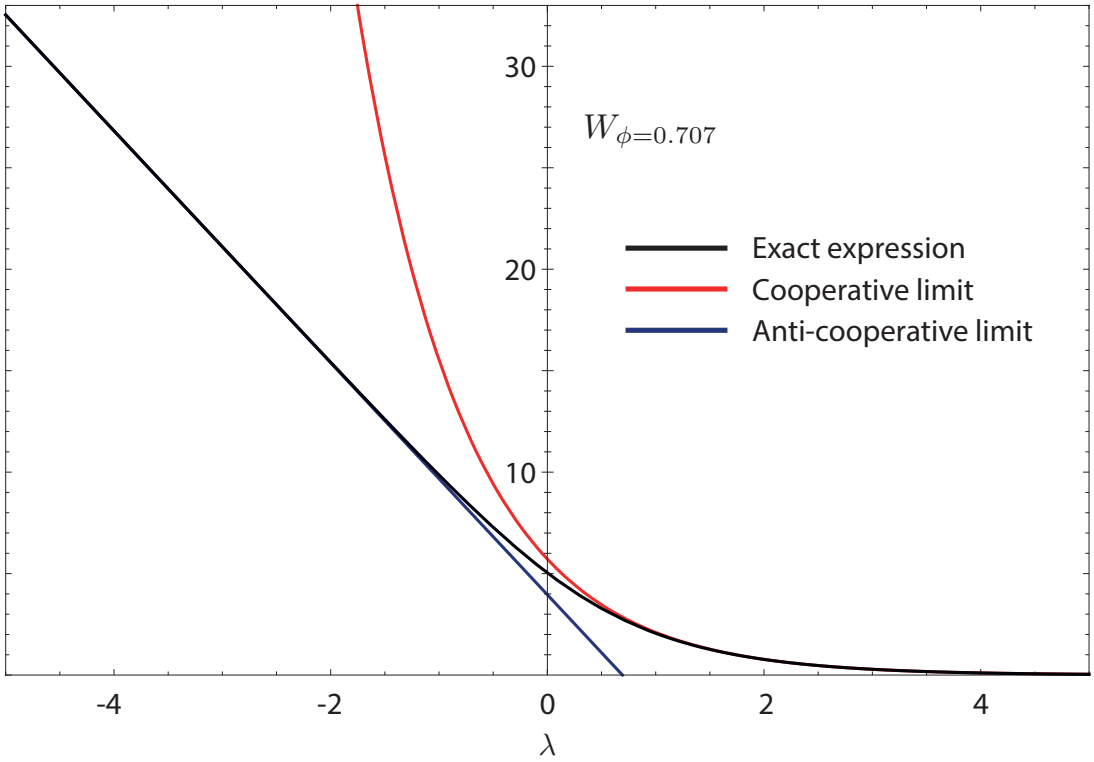

Figure 3.8: The width of the overstretching transition, defined by $\phi = \frac{1}{2}\sqrt{2} \approx 0.707$, as a function of the cooperativity parameter λ, according to equation 3.24. The transition width shows two distinct regimes. The left side of the figure shows the anti-cooperative regime ($\lambda < 0$), where the width increases linearly with decreasing λ, or increasing anti-cooperativity. The right side shows the cooperative regime ($\lambda > 0$), where the width decreases exponentially with λ. The elongation factor is $\gamma_1 = 1.7$.

general expression for the width (equation 3.24) does. The second prefactor is a function of ϕ. As explained in the text above and in figure 3.7 this is just a number that depends on the definition for the width. For $\phi = \frac{1}{2}\sqrt{2}$ (figure 3.8) this number is 4. We speculate that the exponential decay is related to a Boltzmann distribution. The width of the transition tells us something about the influence of entropy on the transition. Entropy maximization corresponds to as much mixing between states 0 and 1 as possible, which corresponds to maximization of the transition width. But as λ (the free energy penalty for a 0/1-interface) increases, the free energy penalty for a such a mix of states increases. The probability that such a state occurs scales with the Boltzmann factor of this free energy penalty. This causes the probability of a mix state to decrease exponentially with λ. We speculate that this causes the transition width to decrease exponentially with λ as well.

An example of a cooperative force-extension curve is given in figure 3.9. The figure shows the non-cooperative curve of figures 3.5, 3.6 and 3.7 together with a cooperative curve ($\lambda = 2$) with the same values for ε_1 and γ_1. The vertical lines indicate the transition widths according to equation 3.24 with $\phi = \frac{1}{2}\sqrt{2}$.

We conclude the cooperative case with a final remark about the validity of equation 3.25. We mentioned that we assume $\lambda >> 0$ to obtain equation 3.25. This is, however, an approximation. We actually have to assume that $\lambda >> \frac{1}{2}\ln\left(\frac{\phi^2}{1-\phi^2}\right)$ to derive equation 3.25. For $\phi \to 0$ and $\phi \to 1$ this deviates significantly from $\lambda >> 0$. However, it does not make sense to take a ϕ very close to either 0 or 1, since in that case we define a width that is either very small or very large. Hence those numbers do not reflect a sensible choice for the transition width. Since we are free to choose ϕ, we choose $\phi = \frac{1}{2}\sqrt{2}$. In that case $\lambda >> \frac{1}{2}\ln\left(\frac{\phi^2}{1-\phi^2}\right)$ reduces to $\lambda >> 0$. This choice for ϕ is used in figures 3.8 and 3.9.

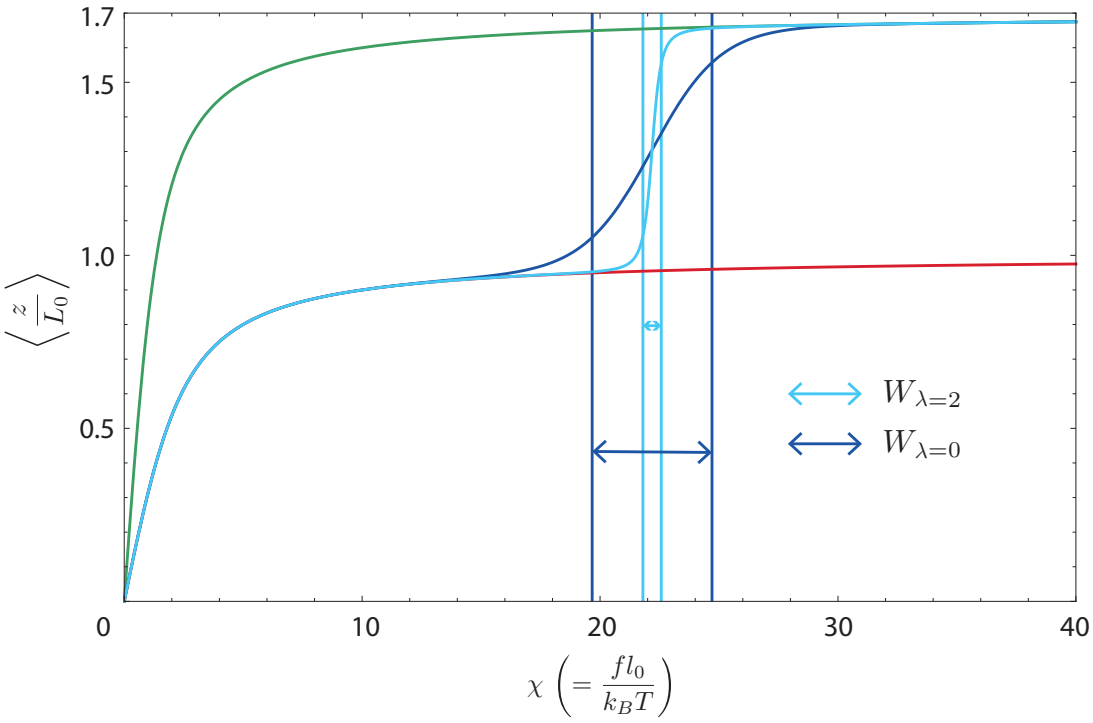

Figure 3.9: 2-state force-extension curves with $\lambda = 0$ (dark blue) and $\lambda = 2$ (light blue), with state 0 FJC (red) and state 1 FJC (green) as references. The vertical lines indicate the transition widths ($\phi = \frac{1}{2}\sqrt{2}$), and show that the cooperative curve ($\lambda = 2$) has a much smaller transition width than the non-cooperative curve ($\lambda = 0$).

The anti-cooperative 2-state model

The other regime in figure 3.8 is the anti-cooperative regime, which corresponds to $\lambda < 0$ and is given by the left side of the figure. A negative value for the cooperativity parameter λ induces an energy bonus for a 0/1-interface and therefore favors a mixing of states 0 and 1. Naturally, this leads to a wider overstretching transition. As briefly mentioned before, we study the anti-cooperative case because we encouter it when studying the intercalated state of dsDNA in chapter 4. The biological background is studied there, for now we just focus on the model.

We derive an expression for the width in the anti-cooperative case by taking the opposite limit that we took in the cooperative case: $\lambda << \frac{1}{2}\log\left(\frac{\phi^2}{1-\phi^2}\right)$. We approximate this again by $\lambda << 0$. The result is displayed by the blue curve in figure 3.8, and is given by

$$W_{\lambda<<0} = \frac{-4\lambda}{\gamma_1 - 1} + \frac{2\ln\left(\frac{4\phi^2}{1-\phi^2}\right)}{\gamma_1 - 1} \tag{3.26}$$

The second term in the expression is just a constant that depends on the definition of the width. The first term is more interesting. It shows that the width increases linearly with decreasing λ, as suggested by the left side of figure 3.8. We show an example of a force-extension curve to illustrate the influence of negative λ on the transition width and to explain the linearity and the prefactor 4. This force-extension curve is shown in figure 3.10, which shows the same data as figure 3.9 but replaces the cooperative $\lambda = 2$ curve with the anti-cooperative $\lambda = -3$ curve.

Figure 3.10 reveals an interesting aspect of the anti-cooperative overstretching transition; it shows a more complicated shape than the cooperative and non-cooperative transitions. Both

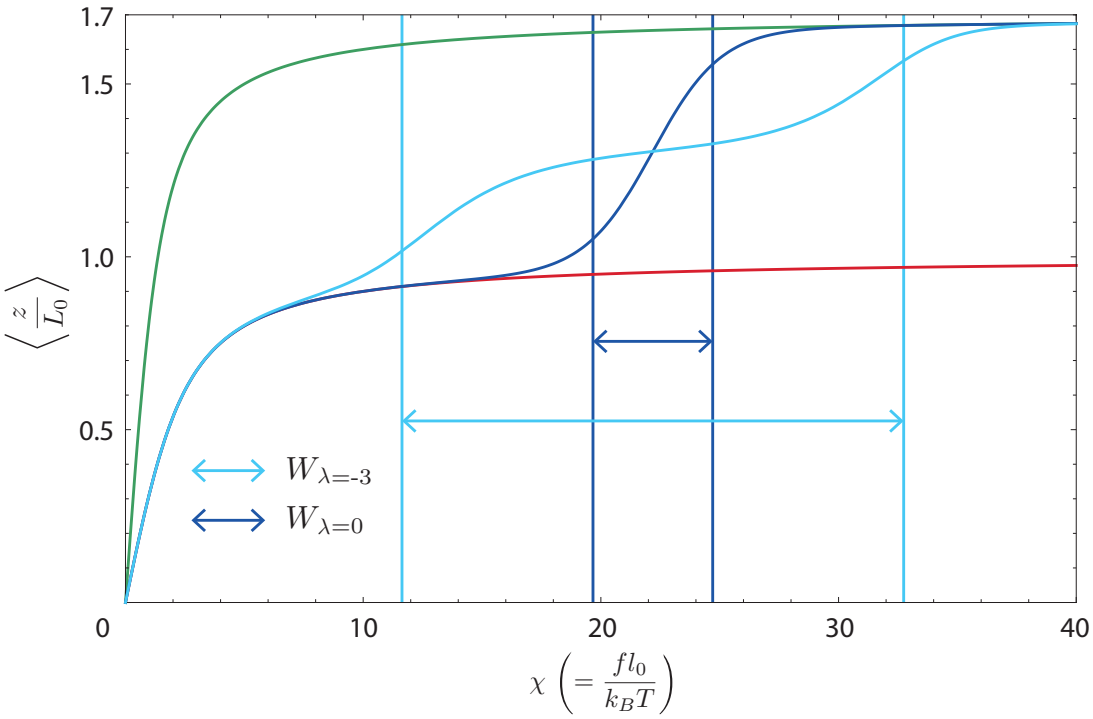

Figure 3.10: 2-state force-extension curves with $\lambda = 0$ (dark blue) and $\lambda = -3$ (light blue), with state 0 FJC (red) and state 1 FJC (green) as references. The transition width of the anti-cooperative case ($\lambda = -3$) is much larger than the width of the non-cooperative case ($\lambda = 0$). The anti-cooperative curve shows a transition that consists of two regions with relatively high slope at the edges of the transition, and a region with relatively small slope in between. We call the latter the 0/1-plateau, and it represents a state of the chain that shows an alternating pattern of Kuhn segments in states 0 and 1. The figure is plotted with $\phi = \frac{1}{2}\sqrt{2}$ and $\gamma_1 = 1.7$.

the cooperative and the non-cooperative overstretching transition show a convex force-extension curve for forces smaller than the overstretching force ($\chi < \chi_{01}$) and a concave curve for forces larger than the overstretching force ($\chi > \chi_{01}$). This is, however, not true for the anti-cooperative transition. The transition shows two regions with relatively high slope at the transition edges with a large region in between that has a relatively small slope. This plateau in the middle of the transition describes a state of the chain that shows an alternating pattern of segments in state 0 and state 1, resembling the Neél state that is found in anti-ferromagnetic systems. This 0/1-plateau exists because at forces around the overstretching force the free energy bonus for a 0/1-interface is larger than the difference between free energies corresponding to the individual states 0 and state 1. In other words, the interfacial bonus λ dominates the other free energies in the system. In this regime the chain is relatively insensitive for changes in force, so it can be considered as a separate macroscopic state of the chain. This gives the macroscopic chain states 0/0 (all segments in state 0), 0/1 (alternating pattern of states 0 and 1) and 1/1 (all segments in state 1) with two transitions, between 0/0 and 0/1 and between 0/1 and 1/1. The distance in force between those two transitions gives a good indication of the width of the complete overstretching transition.

We now use a heuristic argument to understand why the transition width increases linearly with λ. Consider a chain that is in the 0/0 state. What force $f_{00\to01}$ do we need to stretch it towards the 0/1 state? The work done by the force to stretch half of the segments to state 1 has to overcome the free energy penalty corresponding to that state. So, for each segment that is excited in state 1, it has to overcome the free energy penalty ε_1 and it has to pay the free energy penalty for a 0/1-interface λ twice, once for each neighbor that remains in state 0. Equating

the work and the energy penalty gives,

$$(\gamma_1 - 1) l_0 f_{00\to01} \approx k_B T(\varepsilon_1 + 2\lambda). \tag{3.27}$$

Note that the free energy penalty for a 0/1-interface is actually a free energy bonus because λ is negative. Equation 3.27 can be rearranged to obtain an indication for the normalized force required for the $0/0 \to 0/1$ transition,

$$\chi_{00\to01} \approx \frac{\varepsilon_1 + 2\lambda}{\gamma_1 - 1}. \tag{3.28}$$

We use the same argument for the transition from a chain in state 0/1 that is stretched to state 1/1. The only difference with the $0/0 \to 0/1$ transition is that this time the 0/1-interface disappears instead of arises. This gives

$$(\gamma_1 - 1) l_0 f_{01\to11} \approx k_B T(\varepsilon_1 - 2\lambda), \tag{3.29}$$

which can be rearranged to

$$\chi_{01\to11} \approx \frac{\varepsilon_1 - 2\lambda}{\gamma_1 - 1}. \tag{3.30}$$

We obtain an indication of the width of the total overstretching transition by calculating the difference between the forces in equations 3.28 and 3.30. This result is given by

$$W_{\lambda<<0} \approx \chi_{01\to11} - \chi_{00\to01} = \frac{-4\lambda}{\gamma_1 - 1}, \tag{3.31}$$

which is equal to the first term in equation 3.26. So the width increases linearly with decreasing λ with a prefactor of 4 because the width is determined by the difference in required work between creating and destroying a 0/1-interface.

3.4. Analyzing the experimental data

In section 3.3 we completely analyzed the force-extension relation of the 2-state Kuhn model. We showed the shape of the 2-state force-extension curve, defined the overstretching transition in terms of position and width and analyzed their depence on the system parameters ε_1, λ and γ_1. We gave special attention to the influence of the sign of λ, resulting in a cooperative ($\lambda > 0$) or anti-cooperative ($\lambda < 0$) overstretching transition. This section relates these concepts to experimental data of dsDNA. First we compare data of the overstretching transition of dsDNA to our model in section 3.4.1, and in section 3.5 we try to explain the influence of intercalating particles on the force-extension curve of dsDNA by comparing our 2-state model to corresponding experimental data (figure 1.4).

3.4.1. The overstretching transition

Figure 1.2 in section 1.1 showed an experimental force-extension curve of dsDNA, together with a theoretical fit of Storm and Nelsons Ising-DPC model [15]. Now we compare these data to our model. Qualitatively we already know that our model captures the essential features of figure 1.2; we saw that our 2-state model is capable of producing a force-extension curve with a cooperative overstretching transition in figure 3.9. The next step is a quantative comparison: what values of the parameters of our model, ε_1, λ and γ_1, correspond to the experimental data? The latter is evident: $\gamma_1 = 1.7$; the elongation factor γ_1 dictates the maximum extension and the length increase of the chain at the overstretching transition, which was found to be 1.7 by Cluzel *et al.* [12] and Smith *et al.* [13].

The other parameters require more analysis. We start with ε_1. We found in section 3.3.1 that this is the parameter that determines the position of the overstretching transition. Therefore, we use the experimentally observed position of the overstretching transition, 65 pN [12, 13], to estimate ε_1. We rewrite equation 3.17 to express ε_1 in terms of the unit-bearing force f_{01},

$$\varepsilon_1 \;=\; \frac{f_{01} l_0 (\gamma_1 - 1)}{k_B T} - \ln \gamma_1. \tag{3.32}$$

We substitute numbers for the quantities in equation 3.32 to obtain a value for the free energy penalty ε_1. We use $\gamma_1 = 1.7$, $k_B = 1.38 \cdot 10^{-2}$ pN nm K^{-1}, $f_{01} = 65$ pN and $T = 300$ K. For l_0 we use the contour length of a single base pair, $l_0 = 0.34$ nm [62]. Substituting these numbers in equation 3.32 gives $\varepsilon_1 = 3.2$, and for the total overstretching free energy penalty $\varepsilon_1 + \ln \gamma_1 = 3.7$. Recall that ε_1 is defined as a dimensionless quantity (section 3.2.3), so the unit-bearing free energy penalty upon overstretching is $3.7\, k_B T$. This number is in the order of relatively weak intramolecular interactions like Van der Waals interactions ($\sim 1\, k_B T$ [31]) or the net free energy of a hydrogen bond in a aqueous solution ($1 - 2\, k_B T$ [31]). Hydrophobic energies between hydrophobic objects and water have interactions energies of about 7 $k_B T$ nm^{-2} [93], so these might play a role as well. We also note that $3.7\, k_B T$ is substantially smaller than the strength of a covalent bond ($90 - 350\, k_B T$) [31]. This indicates that the free energy penalty for overstretching of $3.7\, k_B T$ is in the right order of magnitude. It is large enough to overcome the intramolecular forces that govern the spatial structure of the dsDNA, but small enough that the primary structure of the molecule is left intact. Indeed, the overstretching changes the spatial structure of the dsDNA, but it leaves the primary structure (the backbones) intact.

Note that the relatively small free energy penalty of $3.7\, k_B T$ suggests that thermal fluctuations that cause DNA to overstretch locally should occur regularly, even in the absence of a stretching force. After all, the corresponding Boltzmann factor (equation 3.19) becomes $\exp(-3.7) \approx 0.025$. According to equation 3.20, this yields a ratio of Kuhn segments in state 1 and Kuhn segments in state 0 of $\sim \frac{1}{40}$, suggesting that approximately 1 in 40 Kuhn segments should be in state 1 at any moment due to spontaneous overstretching. This number seems to be too large, but of course the free energy penalty for the 0/1-interface has to be taken into account as well. After estimating a number for the cooperativity parameter, we briefly come back to this point.

The last parameter is the cooperativity parameter λ, which is related to the transition width (section 3.3.2). We determine λ by using equation 3.24, the general expression for the transition width. To do so we need a number for the width: Smith *et al.* [13] note that the force range over which the overstretching transition occurs is ~ 2 pN. In order to calculate λ from this force range, using equation 3.24, we need to know what value of ϕ to use. Smith *et al.* [13] do not specify their definition of width, they just mention that the width is ~ 2 pN. We estimate that a reasonable choice for the width corresponds to a ϕ in the region $0.7 - 0.95$. We illustrate this estimate in figure 3.11.

Figure 3.11 shows four 2-state force-extension curves with $\varepsilon_1 = 3.2$, $\gamma_1 = 1.7$ and varying λ. The values of λ are based on the transition width of ~ 2 pN, which corresponds to 0.16 in terms of the dimensionless force χ (equation 3.7), and which is shown in the figure by vertical lines. The cooperativity parameters (λ) of the 2-state force-extension curves are chosen such that the transition width is equal to 0.16 with $\phi = 0.7$, $\phi = 0.8$, $\phi = 0.9$ and $\phi = 0.95$ respectively. The figure illustrates why we estimate ϕ to be a number between 0.7 and 0.95; the four graphs could all lead to an estimate of the transition width of ~ 2 pN. The corresponding values of λ (equation 3.24) are 3.6, 3.9, 4.3 and 4.7 respectively. Based on the observation by Smith *et al.* we are not able to determine λ in two significant digits; we take $\lambda = 4$. λ was defined (section 3.2) as a dimensionless free energy, so the unit-bearing free energy penalty for a 0/1-interface is about $4\, k_B T$.

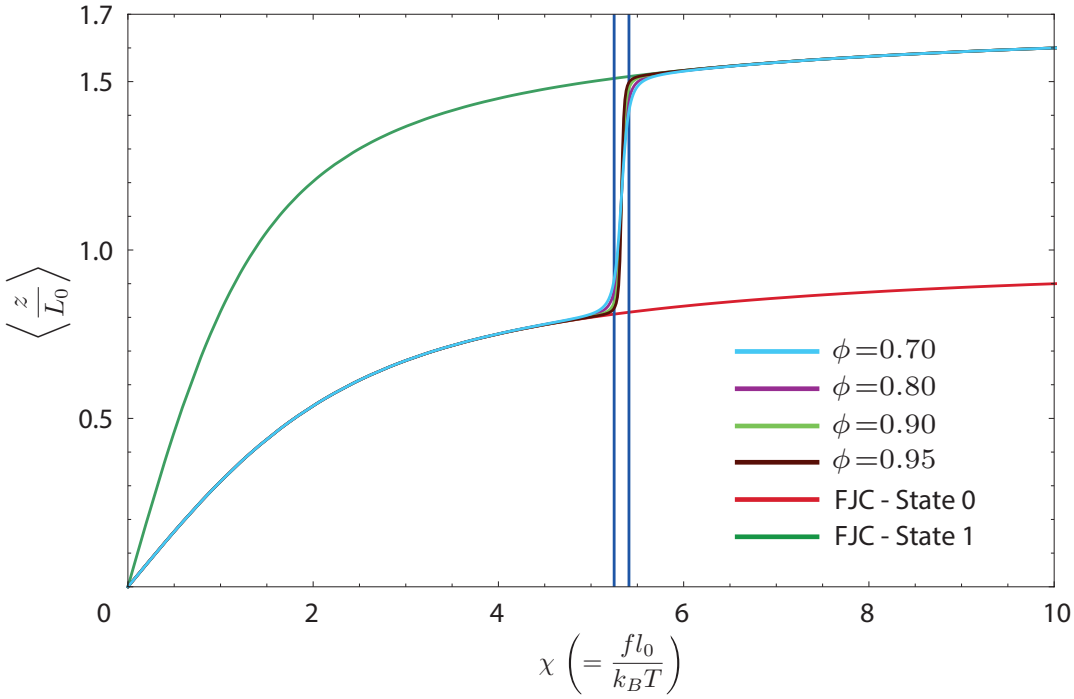

Figure 3.11: This figure is used to estimate the cooperativity parameter λ from experimental data. Smith *et al.* [13] report that the width of the overstretching transition is ~ 2 pN. To calculate λ from this observation, we need to know how they defined the transition width. In other words, we need to know how to define a value for the saturation parameter ϕ. We plotted the 2-state force-extension curve ($\varepsilon_1 = 3.2$, $\gamma_1 = 1.7$) for $\phi = 0.7$, $\phi = 0.8$, $\phi = 0.9$ and $\phi = 0.95$, with corresponding λ such that the transition width is found to be 2 pN, or 0.16 in dimensionless units (equation 3.7). The corresponing values of λ are 3.6, 3.9, 4.3 and 4.7 respectively. Since all of these choices for ϕ seem to be reasonable, we take $\lambda = 4$.

We now briefly come back to the topic of spontaneous overstretching, that we discussed in the context of ε_1. We see now that, for a single Kuhn segment to overstretch, a free energy barrier of $\varepsilon_1 + 2\lambda \approx 12\, k_B T$ has to be overcome. The probability that a thermal fluctuation would cause this in the absence of a stretching force can now be calculated from equations 3.19 and 3.20 to be $\sim 10^{-5}$. This analysis strongly suggests that the existence of a free energy penalty for an interface between B-DNA and overstretched DNA prevents dsDNA from overstretching spontaneously.

With $\gamma_1 = 1.7$, $\varepsilon_1 = 3.2$ and $\lambda = 4$ we estimated numbers for all model parameters. This allows us to compare our model to experimental data. Figure 3.12 shows the theoretical curve of the 2-state model (a) and the experimental data with corresponding Ising-DPC fit [15] (b). Note that the force-axes of figures 3.12a (dimensionless) and 3.12b (in pN) differ. This is, however, not a problem. As explained above, the parameters in the 2-state model are chosen such that the position (ε_1), width (λ) and extent (γ_1) of the overstretching transition match with the experimental data. We plot figure 3.12 to compare the shapes of the curves and to see whether our 2-state model captures the essential features of the dsDNA force-extension curve.

Based on figure 3.12, we conclude that our 2-state model does capture the essential features of the dsDNA force-extension curve. Both figures 3.12a and 3.12b show an initial entropic stretching regime (section 3.1) followed by overstretching transitions with comparable widths. The most important difference between the two figures is the degree of saturation towards a normalized length of 1 in the entropic regime. The experimental data (figure 3.12b) shows a very rapid increase in extension in the first 10 pN, followed by a plateau with a normalized

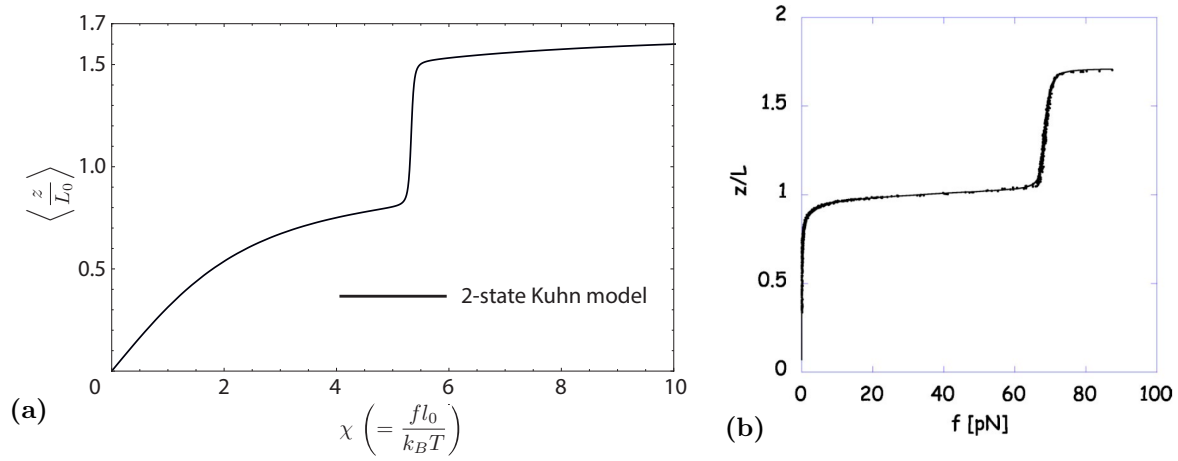

Figure 3.12: The force-extension curve of dsDNA. Figure (a) shows the theoretical result of the 2-state Kuhn model and shows the dimensionless force $\chi \equiv \frac{fl_0}{k_BT}$ on the x-axis, figure (b) shows experimental data with corresponding Ising-DPC fit [15] and shows the force in pN on the x-axis. The parameters of the 2-state model in (a) ($\varepsilon_1 = 3.2$, $\lambda = 4$, $\gamma_1 = 1.7$) are chosen such that the position, width and extent of the overstretching transition match those of the experimental data in (b). The most obvious difference between figures (a) and (b) is the degree of saturation towards a normalized length of 1 in the entropic regime (force smaller than the overstretching force). This deviation was anticipated (section 3.2.1) and is caused by the absence of bend stifness in the 2-state Kuhn model. We find, however, that our analysis of the overstretching transition is not affected by this deviation. Since we focus on the force-extension curve in the high-force regime, we argue that this simplification is justified.

extension of approximately 1 over a force range of $\sim$55 pN before the dsDNA overstretches. The 2-state model, however, shows a much slower increase of the normalized extension in the entropic regime. Even at the overstretching force, the normalized extension $\frac{z}{L_0}$ is still smaller than 0.9. The reason for this difference is the absence of bend stiffness in our model; a chain that resists bending has a persistence length that is significantly longer than the segment length, making the chain easier to stretch. Recall that the persistence length of dsDNA is about 53 nm, more than 150 times the segment length (0.34 nm) [15]. To illustrate this point, we plot the force-extension curves of a freely jointed chain with a segment length of 0.34 nm and a discrete persistent chain with a segment length of 0.34 nm and a persistence length of 53 nm in figure 3.13, where the x-axis shows the force in pN. The figure gives the force-extension curves on a force range of $0 - 65$ pN, which corresponds to the entropic regime in figure 3.12. The curves show that the DPC is significantly easier to stretch than the FJC. We conclude that the slow saturation to a normalized extension of 1 of our model (figure 3.12a) with respect to the experimental data (figure 3.12b) can indeed be contributed to the absence of bend stiffness in the theory.

We already anticipated this limitation of our model in section 3.2.1, where we discussed the influence of bend stiffness and concluded that is it not essential for achieving our goal; we want to *understand* the mechanisms behind the disturbing effect of intercalative particle binding on the force-extension curve of dsDNA in the high-force regime (section 1.3). In trying to achieve our goal we leave any complexity out of our model if we think that this additional complexity does not help us understanding the effect of intercalative binding in the high-force regime. We accept that these simplifications prevent us from *fitting* our model to the data, as long as we understand what physical principles dictate the experimental observations. We explained in section 3.2.1 why, in our view, bend stiffness is such a complication that is not necessary to understand the essential physical principles. In this section we found an additional argument for this view; we calculated ε_1 by using equation 3.17, which assumes that $\chi >> 1$. In other words, it assumes that the chain has reached a sufficient degree of saturation towards an extension of 1 at the overstretching force. Based on figure 3.12a one could question whether this is a good approximation. However, the exact free energy penalty, found with equation 3.15, agrees with

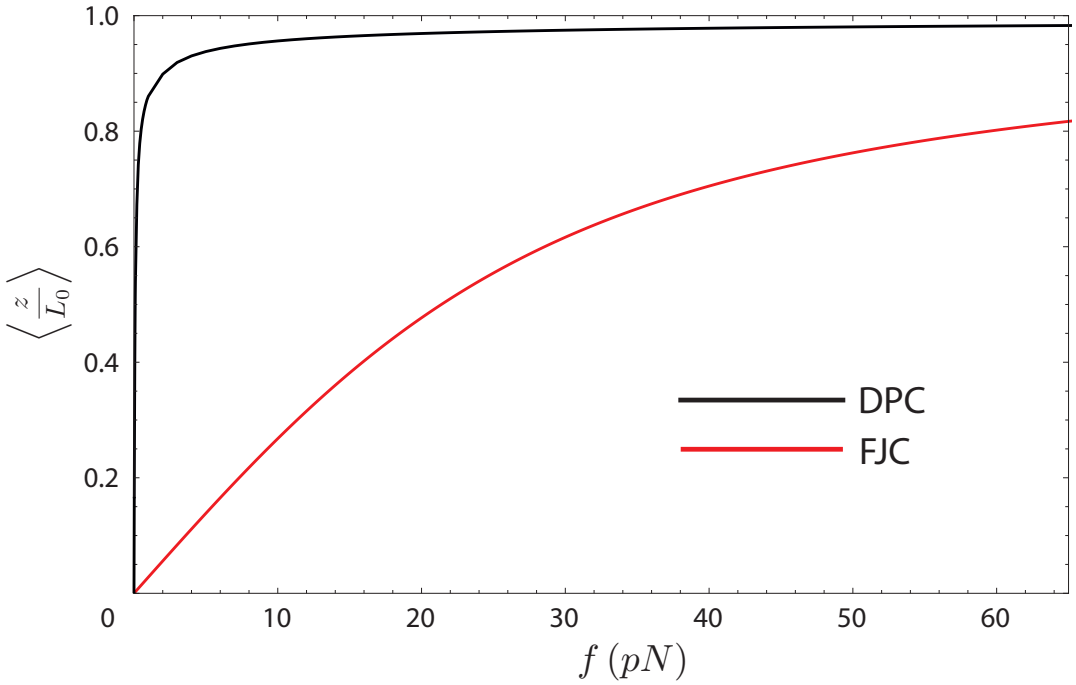

Figure 3.13: The force-extension curves of a freely jointed chain with a segment length of 0.34 nm (red) and a discrete persistent chain with a segment length of 0.34 nm and a persistence length of 53 nm (black). These numbers are representative for dsDNA. The figure shows the great impact of neglecting bend stiffness on the entropic regime of the force-extension curve; the DPC is much easier to stretch. This explains the difference in the entropic regime between the theoretical 2-state force-extension curve in figure 3.12a and the experimental data in figure 3.12b. However, we show that this difference does not affect the features of the overstretching transition, which justifies the simplification of neglecting bend stiffness.

the value of ε_1 found with equation 3.16 on five signficant digits (we use only two: $\varepsilon_1 = 3.2$). This indicates that the properties of the overstretching transition are not affected by the change in the entropic regime, and justifies our choice of neglecting bend stiffness.

Finally, we note that the entropic regime is the reason why we did not fit our model to experimental data to obtain numbers for the parameters ε_1 and λ; the large difference in the degree of saturation towards an extension of 1 prevents the model to produce a good fit. However, the relative simplicity of our model allowed us to obtain analytical expression for the transition position and width in section 3.3. From these expression we were able to obtain reliable numbers for ε_1 and λ.

3.5. The influence of intercalating particles

We saw in the previous section that our 2-state Kuhn model captures all essential features of the overstretching transition of dsDNA. The next question is whether it can also explain the influence of intercalative particles on this overstretching transition. In other words, can the 2-state Kuhn model produce a force-extension curve that captures the essential features of figures 1.4a [54] and 1.4b [21]?

We have not yet discussed how we could take intercalative particle binding into account. For now, however, we do not focus on the specific modeling. Instead, we study whether the influence of intercalative binding can be attributed to a rescaling of the parameters that are already in the 2-state model. In the end, our 2-state model only contains three independent parameters: γ_1, ε_1 and λ. If we want the 2-state Kuhn model to explain the experimental data, we should be able to do this by changing of one or more of these parameters as some function of the particle

concentration. In this section we show that *any* change of the model parameters is insufficient for explaining figures 1.4a and 1.4b.

We consider γ_1 first. The low concentration curves of both figures 1.4a and 1.4b show that this parameter has to remain 1.7 even in the presence of intercalators: they show a change in the overstretching transition, which indicates the influence of the intercalators, but they show a length of 1.7 times B-DNA for forces larger than the overstretching transition. The 20 nM curve in figure 1.4a and the 10 nM curve in figure 1.4b give the best examples of this behavior. A consequence of this observation is that γ_1 has to be a constant in the model. However, the large-concentration curves (125 nM, 1000 nM and 2500 nM) in figure 1.4b show that the dsDNA molecule is able to reach a normalized extension that is larger than 1.7. In other words, lengths that are larger than γ_1 are achieved under certain circumstances. This is not possible in the 2-state Kuhn model. We need to add an additional parameter to be able to explain this.

In addition to the problems with the large extensions, there are more arguments to support the claim that the 2-state model is insufficient for explaining experimental data. In section 2.2.2 we analyzed figure 1.4 and concluded that a good theoretical model has to be able to explain a couple of features. One of those features is the fact that the extension *increases* for small forces and *decreases* for large forces. The only way to achieve this in the 2-state Kuhn model is by introducing anti-cooperativity ($\lambda < 0$) in the transition. In the same experimental curves (figure 1.4b: 5, 10, 20 and 25 nM) we observe a shift of the overstretching transition towards higher forces. However, this overstretching transition clearly remains cooperative ($\lambda > 0$). While in principle the 2-state model could explain both the anti-cooperativity (negative λ) and the shifting of the overstretching transition (increasing ε_1), it can never do both; it is not possible to create a force-extension curve that shows an extension larger than 1 for forces that occur before a cooperative overstretching transition. We conclude that our 2-state model is not able to explain the influence of intercalative particle binding on the force-extension curve of dsDNA, purely because the mechanics are very different in the presence of particles.

Chapter 4

Modeling particle binding and the 3-state Kuhn model

In this chapter we present an elastic model of dsDNA that takes into account the intercalative binding of particles to DNA: the 3-state Kuhn model. This model is based on the 2-state Kuhn model (chapter 3), and adds a third molecular state to the model. We motivate this model in section 4.1, after which we present the model in section 4.2. In sections 4.3 and 4.4 we analyze the 3-state Kuhn model mathematically. This allows us to come back to our research aim in section 4.5, where we explain the physical principles behind the influence of intercalators on the overstretching transition of dsDNA. In section 4.6 we quantify this influence, and in section 4.7 we predict the force-extension curve of a dsDNA-intercalator complex in a force-regime beyond the overstretching transition.

4.1. Expanding the 2-state Kuhn model

We concluded chapter 3 with the observation that the 2-state Kuhn model captures the essential features of the high-force regime of the dsDNA force-extension curve. However, we also concluded that the 2-state Kuhn model is not able to produce force-extension curves that resemble experimental data. Therefore the 2-state Kuhn model does not contribute to our understanding of the interaction between intercalators and dsDNA and how these interactions affect the force-extension curve. Our next step is to expand our 2-state model so that it is able to explain the experimental observations. In this section we address the question of how we should do this. We use two kinds of arguments: biophysical knowledge about intercalative binding to dsDNA (section 2.1) and the observations that we did by studying the experimental force-extension curves (section 2.2.2).

We discussed in section 2.1 that, in an intercalation process, a planar molecule or a planar part of a molecule is inserted between normally neighboring base pairs in a plane perpendicular to the helical axis [46]. This results in an increase of the distance between adjacent base pairs from 0.34 nm to 0.68 nm [66–68]. In other words, dsDNA stretches locally to twice its normal contour length if an intercalator is bound. If we want to model this intercalation correctly, the corresponding Kuhn segment should also be twice as long as the standard segment length. This gives rise to the introduction of a third molecular state in our model, which we call state 2. State 2 represents intercalated DNA and is twice as long as B-DNA: $\gamma_2 = 2$. Here γ_2 is the elongation factor of state 2, defined in the same way as γ_1 in section 3.2. In the absence of intercalators, this state is energetically unfavorable because of the large stress in the DNA backbone caused by the elongation. This is why we do not see evidence for the existence of this state in force-extension curves that do not take into account intercalation. However, if an intercalator binds the dsDNA, the corresponding free energy penalty might be overcome by the free energy bonus for binding. This might explain the high-concentration curves in figure 1.4b,

that show a normalized extension larger than 1.7.

We also discussed in section 2.1 that, at moderate stretching forces, a bound intercalator prohibits other intercalators to bind at adjacent binding sites on the dsDNA [72, 73], which is called the neighbor-exclusion principle [66]. Nordmeier *et al.* [76] and Coury *et al.* [77] found that the neighbor-exclusion principle leads to an 1.5-fold elongation of the contour length at saturation, but later Yan and Marko [57] predicted that at high stretching forces the maximum binding could be increased to one intercalator per base pair. Their prediction was confirmed by Vladescu *et al.* [21]. We can relate this knowledge about intercalation to the observations we did by studying the experimental force-extension curves in section 2.2.2. At moderate forces the neighbor-exclusion principle prevents the dsDNA to be completely saturated with intercalators, leading to an alternating pattern of Kuhn segments in state 0 and state 2. This leads to an effective segment length of $\frac{1+\gamma_2}{2} = 1.5$, which is in between the segment lengths of B-DNA (state 0) and overstretched DNA (state 1). This effective segment length becomes more important when more intercalators are available for binding. This might explain the length increase at forces smaller than the overstretching force and the length decrease at force larger than the overstretching force, both as a function of intercalator concentration. However, the large-concentration curves in figure 1.4 show a normalized extension longer than 1.7, even at low forces. This suggests that the neighbor-exclusion principle is not only violated at high forces [57], but also at high concentrations. If so, then state 2 might explain the effects related to both the intermediate length (1.5) and the longer length (2).

The goal of this chapter is to achieve our research aim: we want to understand the physical principles behind the effect of intercalative particle binding on the location and magnitude of the overstretching transition of double-stranded DNA. In section 2.2.2 we analyzed experimental data and presented a list of five effects of intercalators on the overstretching transition of dsDNA that we needed to understand in order to answer our primary research question. These effects are

- A force shift of the overstretching transition as a function of intercalator concentration.
- An end-to-end length that is significantly larger than 1 for forces smaller than the overstretching force.
- An end-to-end length increase at forces smaller than the original overstretching force.
- An end-to-end length decrease at forces larger than the original overstretching force.
- The disappearance of the overstretching transition for large concentrations.

In section 4.5 we explain all these effects. We show that they are a direct consequence of the addition of a third molecular state that is twice as long as B-DNA, and that is energetically favored in the presence of intercalating particles. In sections 4.2, 4.3 and 4.4 we develop the 3-state Kuhn model, and analyze it mathematically. These sections serve as a justification for the conclusions in section 4.5.

4.2. 3 states of DNA

In the previous section we discussed how we expand the 2-state model of dsDNA to create a model that is capable of explaining experimental data. We concluded that a third state is required in our model. We call it state 2, with corresponding state parameter $S_i = 2$. We use this third state to describe a part of the dsDNA that is intercalated. In this section we introduce the 3-state Kuhn model. We start by discussing how we take the binding of an intercalator into account in our model.

4.2.1. Modeling intercalative binding to dsDNA

We briefly discussed the process of intercalation in section 2.1. Upon binding to dsDNA, an intercalator is inserted between normally neighboring base pairs in a plane perpendicular to the helical axis, which locally alters the structure of the dsDNA. This is a complicated process in which many chemical groups are involved. However, completely in line with the modeling of the overstretching transition in chapter 3, we use the approach of coarse-graining here. We average over all microscopic details of the dsDNA and we use effective parameters that capture the essential features of the intercalation process. We model the locally altered structure of dsDNA by changing the segment length of the Kuhn segment that is intercalated. The intercalated segment is twice as long as B-DNA, thus $\gamma_2 = 2$.

In addition to the length modification, a free energy is associated with changing the Kuhn segment from B-DNA to intercalated DNA. This is completely analogous to the introduction of state 1 in chapter 3. However, the free energy penalty for state 2 is more complicated than the penalty for state 1, because particle binding is involved. We study mono-intercalators (section 2.1), so one intercalator binds one base pair. In our model, one base pair corresponds to one Kuhn segment. Therefore, we describe the binding of intercalators by a Langmuir-like adsorption model [94], in a similar way that is used, for example, in the context of templated polymerization [95, 96]. Every Kuhn segment can either bind exactly one intercalator or no intercalator at all. The free energy penalty that is related to changing a Kuhn segment from state 0 to state 2 and binding an intercalator, ΔE_2, is given by

$$\Delta E_2 \;=\; \varepsilon_2 - \mu. \tag{4.1}$$

The first term, ε_2 is the free energy penalty that is associated with changing the dsDNA from state 0 to state 2. This free energy contains contributions from deforming the dsDNA into a new configuration, binding the intercalator and the interplay between binding and deformation. It also contains a contribution related to the interaction of unbound intercalators with the surrounding solution; when an intercalator binds the dsDNA, it leaves the solution, so the disappearance of interactions between an intercalator and the solution contributes to the free energy ε_2. We do not distinguish between the free energies of deformation and binding because we assume that a Kuhn segment is only in state 2 if a particle intercalates this Kuhn segment. While the dsDNA could, in principle, assume the state 2 configuration in the absence of a particle, we conclude from experimental data that it does not [12, 13], even at large forces.

The second term is the chemical potential, μ, of free intercalators in solution, which are available for binding to the DNA molecule. We define the chemical potential as the Gibbs free energy per particle. The chemical potential term is a consequence of entropy, and expresses that more particles bind to the dsDNA if more particles are available in solution. We assume that the solution is ideal [97], in which case the chemical potential μ is given by

$$\mu \;=\; k_B T \ln\left(\frac{C}{55.6}\right), \tag{4.2}$$

Here C is the concentration of intercalators in solution in moles per liter (M). The number 55.6 gives the molar concentration in moles per liter of the solvent, which is water. The reciprocal of this density is a typical volume scale of the solvent, which is the appropriate volume scale for this problem. In the remainder of this thesis, we will express the chemical potential in units of the thermal energy $k_B T$, as we did with all energies. Thus,

$$\mu \;=\; \ln\left(\frac{C}{55.6}\right). \tag{4.3}$$

In using equation 4.3 we assume a simplification. The chemical potential μ is a measure of the concentration of free intercalators in solution. If an intercalator binds to the dsDNA molecule, the number of bound intercalators increases and therefore the amount of free intercalators decreases. In other words, μ is a function of the number of Kuhn segments in state 2. To avoid this complication, we assume that the number of free intercalators is much larger than the number of bound intercalators, which allows us to treat the number of free intercalators as a constant. We justify this assumption by noting that, in the experimental setup used for obtaining force-extension data [84], only one dsDNA molecule is available for intercalative binding. Thus, the number of binding locations is much smaller than the number of free intercalators. This allows us to treat μ as a constant that only depends on the experimentally controlled intercalator concentration.

The introduction of state 2 with segment length $\gamma_2 l_0$ and free energy penalty $\varepsilon_2 - \mu$, together with state 0 and state 1, gives the three states of the 3-state Kuhn model. They are schematically summarized in figure 4.1.

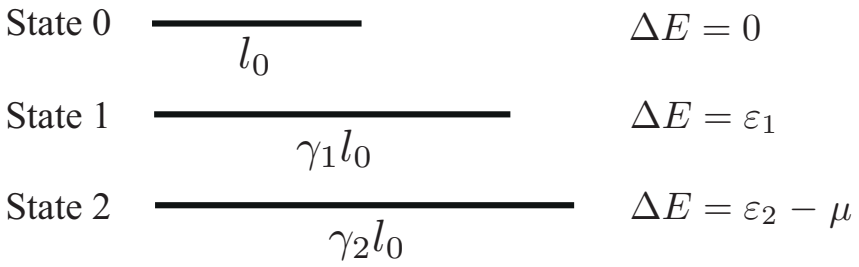

Figure 4.1: Three states of DNA in the 3-state Kuhn model. State 0 represents B-DNA and is the ground state of dsDNA with a segment length of l_0. State 1 represents overstretched DNA with a length of $\gamma_1 l_0$. A free energy penalty ε_1 is associated with the transition from state 0 to state 1. State 2 represents intercalated DNA with a length of $\gamma_2 l_0$. A free energy penalty $\varepsilon_2 - \mu$ is associated with the transition from state 0 to state 2, which signifies the binding of an intercalator to the dsDNA.

4.2.2. Cooperativity and anti-cooperativity

In section 3.2 we introduced a cooperativity parameter λ, that penalizes an interface between a Kuhn segment in state 0 and a Kuhn segment in state 1 (a 0/1-interface), in our 2-state model. We based this parameter on experimental observations [12, 13] of the overstretching transition, that taught us that the transition was cooperative in nature, leading to $\lambda > 0$. Here we repeat this procedure. Figure 4.1 displays the three states of DNA in our 3-state model. Any of these states can be neighbors to each other, so we need more than one cooperativity parameter to obtain a correct description for our 3-state model. As we did in chapter 3, we base our choices on experimental findings.

To start with, we model the interactions between states 0 and 1 in the same manner as we did in chapter 3. So λ is a free energy penalty for a 0/1-interface, while we do not penalize a 0/0-interface or a 1/1-interface. In addition, we use experimental observations regarding intercalated dsDNA to assign cooperativity parameters to interfaces where state 2 is involved. First, we consider a 2/2-interface. We already discussed this interface, in a somewhat different context, in section 2.2.2. We discussed the neighbor-exclusion principle that inhibits two neighboring Kuhn segments to both be in state 2. We also discussed that, in the high force regime, this exclusion principle is violated. Based on these experimental observations, we introduce a free energy penalty for a 2/2-interface, which we call δ. Indeed, if δ is chosen positive, this might explain both experimental observations; at low forces the penalty prevents a 2/2-interface to occur, but at high forces the amount of work done becomes important. State 2 is the longest state ($\gamma_2 = 2$), so if the stretching force is sufficiently large it might overcome the free energy

penalty δ and allow neighboring segments to both be in state 2.

Finally we add a free energy penalty η for a 1/2-interface. We base this on the work of Biebricher *et al.*, whose preliminary results [98] show that intercalated dsDNA molecules do not overstretch cooperatively if they are stretched fast. That is, if the timescale of stretching is much smaller than the timescale of the dsDNA-intercalator interactions. This suggests that intercalated DNA is stabilized against overstretching. Relating this to our model, their observations suggest that Kuhn segments in the ground state (state 0, B-DNA) have more difficulty overstretching (to state 1) if other Kuhn segments are in the intercalated state (state 2). We model this by assigning a positive free energy penalty to a 1/2-interface ($\eta > 0$). We note that these force-extension curves of Biebricher *et al.* are not representative for this work; they stretch fast, so their system is not in equilibrium. Our calculations assume equilibrium, which reflects that the dsDNA-intercalator interactions occur on much faster timescales than the stretching. However, the free energy penalties in the model should not depend on the timescales involved. The remaining interfaces (0/0, 1/1 and 0/2) are not penalized. We present a tabular overview of the cooperativity parameters λ, δ and η and the interfaces where they work in table 4.1.

	$S_{i+1} = 0$	$S_{i+1} = 1$	$S_{i+1} = 2$
$S_i = 0$	0	λ	0
$S_i = 1$	λ	0	η
$S_i = 2$	0	η	δ

Table 4.1: The cooperativity parameters of the 3-state Kuhn model. The row number gives the state of the i^{th} Kuhn segment, while the column number gives the state of Kuhn segment $i + 1$. The symbols in the table give the free energy penalties that are associated with the interfaces between segment i and $i + 1$. In our study λ, δ and η are all positive.

The reason that we do not assign free energy penalties or bonuses to 0/0-, 1/1- and 0/2-interfaces, is that these penalties could be gauged away without changing the model. As an example, say that we would assign a free energy penalty κ to a 1/1-interface. This would give us penalties for a 0/1-interface (λ), a 1/1-interface (κ) and a 1/2-interface (η). In other words, we penalize state 1 for having *any* interface. Every Kuhn segment in our model always has two neighboring Kuhn segments and thus two interfaces. Since we cannot change the number of interfaces a Kuhn segment has, penalizing a Kuhn segment in state 1 for having *any* interface is effectively the same thing as penalizing the Kuhn segment *itself* for being in state 1. However, we already have a free energy penalty for a Kuhn segment in state 1: ε_1. This allows us to reduce the hypothetical 1/1-penalty κ to zero and simultaneously rescale the 0/1-penalty λ, the 1/2 penalty η and the state 1 penalty ε_1, without changing the physics of the system[1]. In other words, introducing a free energy for a 1/1-interface, κ, does not add any new physics to our model, but rather leads to a rescaling of the other parameters. For this reason we do not penalize a 1/1-interface.

The same argument applies to the other interfaces that we do not penalize. Thus, the zeros in table 4.1 are not simplifications, and λ, δ and η describe the most general case of cooperativity in the 3-state model. Finally, note that the reasoning above assumes that there are no edge effects in play, since it uses that every Kuhn segment has two neighbors. In chapter 3 we assumed a very large number of particles to calculate our partition function ($N \to \infty$), and we use the same assumption in this chapter. Therefore, edge effects can indeed be neglected.

We conclude this section by showing a possible configuration of the 3-state Kuhn model in figure 4.2. The figure shows Kuhn segments in states 0, 1 and 2, together with the according

[1]The interested reader can verify that the this rescaling has to be done according to $\lambda \to \lambda - \frac{1}{2}\kappa$, $\eta \to \eta - \frac{1}{2}\kappa$, and $\varepsilon_1 \to \varepsilon_1 + \kappa$.

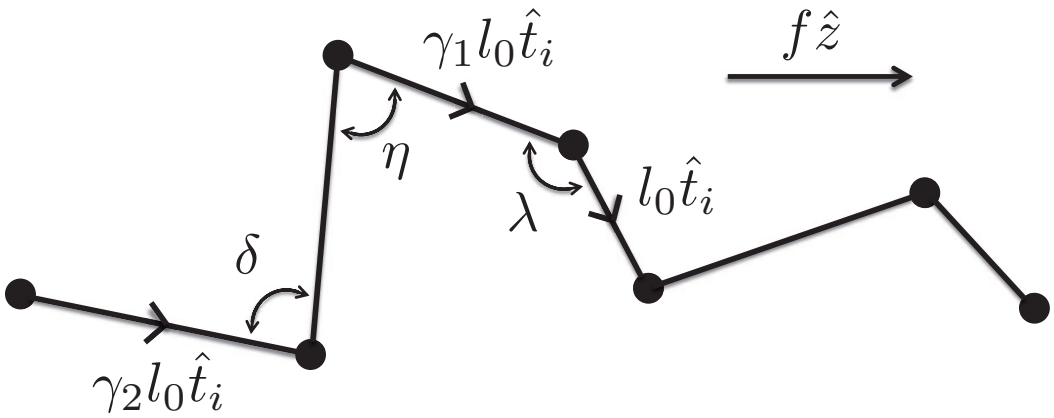

Figure 4.2: A possible configuration of the 3-state Kuhn model. The configuration shows Kuhn segments in states 0 (B-DNA), 1 (overstretched DNA) and 2 (intercalated DNA), with corresponding segment lengths l_0, $\gamma_1 l_0$ and $\gamma_2 l_0$ respectively. The cooperativity parameters λ, δ and η penalize 0/1-interfaces, 2/2-interfaces and 1/2-interfaces respectively.

Kuhn vectors $l_0\hat{t}_i$, $\gamma_1 l_0\hat{t}_i$ and $\gamma_2 l_0\hat{t}_i$. The figure also shows the free energy penalties for a 0/1-interface (λ), a 2/2-interface (δ) and a 1/2-interface (η). Recall that the free energy penalties for states 1 and 2 are given in figure 4.1.

4.2.3. Methods and calculations*

Now that we have defined our 3-state Kuhn model, we calculate the corresponding force-extension curve. As we did for the 2-state Kuhn model (section 3.2.3), we start by formulating the free energy functional of the 3-state Kuhn model, $\varepsilon^{3-\text{state}}[\{\hat{t}_i\}, \{S_i\}]$. It is given by

$$\frac{\varepsilon^{3-\text{state}}[\{\hat{t}_i\}, \{S_i\}]}{k_B T} = \sum_{i=1}^{N} \left[- \frac{f l_0 \left(\delta_{S_i,0} + \gamma_1 \delta_{S_i,1} + \gamma_2 \delta_{S_i,2}\right)}{k_B T} \hat{t}_i \cdot \hat{z} + \varepsilon_1 \delta_{S_i,1} + (\varepsilon_2 - \mu)\, \delta_{S_i,2} \right]$$
$$+ \sum_{i=1}^{N-1} \left[\lambda \left(\delta_{S_i,0}\delta_{S_{i+1},1} + \delta_{S_i,1}\delta_{S_{i+1},0}\right) + \eta \left(\delta_{S_i,1}\delta_{S_{i+1},2} + \delta_{S_i,2}\delta_{S_{i+1},1}\right) + \delta \left(\delta_{S_i,2}\delta_{S_{i+1},2}\right) \right]. \quad (4.4)$$

The expression looks more complicated than the 2-state free energy functional, but it essentially contains the same terms. The first term in the first summation represents the work done by the chain. In this work term, $l_0 \left(\delta_{S_i,0} + \gamma_1 \delta_{S_i,1} + \gamma_2 \delta_{S_i,2}\right)$ gives the length of the i^{th} Kuhn segment. Here $\delta_{S_i,n}$ is the Kronecker delta, which is equal to 1 if $S_i = n$ and equal to 0 otherwise. This gives l_0 for the segment length if $S_i = 0$, $\gamma_1 l_0$ if $S_i = 1$ and $\gamma_2 l_0$ if $S_i = 2$. The second and third term give the free energy penalties ε_1 and $\varepsilon_2 - \mu$ for Kuhn states in state 1 and state 2 respectively. The second summation, that runs from $i = 1$ to $i = N - 1$, gives the free energies associated with interfaces between Kuhn segments. It penalizes 0/1-interfaces (λ), 1/2-interfaces (η) and 2/2-interfaces (δ). Note the difference between δ and $\delta_{i,j}$: the former gives the free energy penalty for a 2/2-interface, while the latter is the Kronecker delta with elements i and j.

From here on, the calculation of the force-extension is analogous to the 2-state force-extension calculation. We do not repeat it here, but rather refer to section 3.2.3 for an outline of the required calculations. We do not present the final result for the force-extension relation in an equation, because the resulting expression is quite unwieldy. Instead, we present the results of the 3-state Kuhn model in graphical form in the upcoming sections. We refer to Appendix A.3 for an explanation of why the calculation generates such an unwieldy expression. The interested reader can also find an outline of the required steps for the derivation of the 3-state

force-extension relation in Appendix A.3.

4.3. The force-extension curve of the 3-state Kuhn model

In this section we analyze the force-extension relation of the 3-state Kuhn model, which is the result of the calculations in section 4.2.3. Here we focus on the mathematical analysis of the force-extension relation and the corresponding properties, and in section 4.6 we relate these properties to the experimental data of figure 1.4.

We begin this analysis by showing an example of a 3-state force-extension in figure 4.3. The free energies ($\varepsilon_1 = 7$, $\varepsilon_2 = 1$, $\lambda = 4$, $\delta = 8$, $\eta = 8$, $\mu = -10$) do not represent experimental data, which is discussed in section 4.6. The elongation factors are $\gamma_1 = 1.7$ and $\gamma_2 = 2$. The

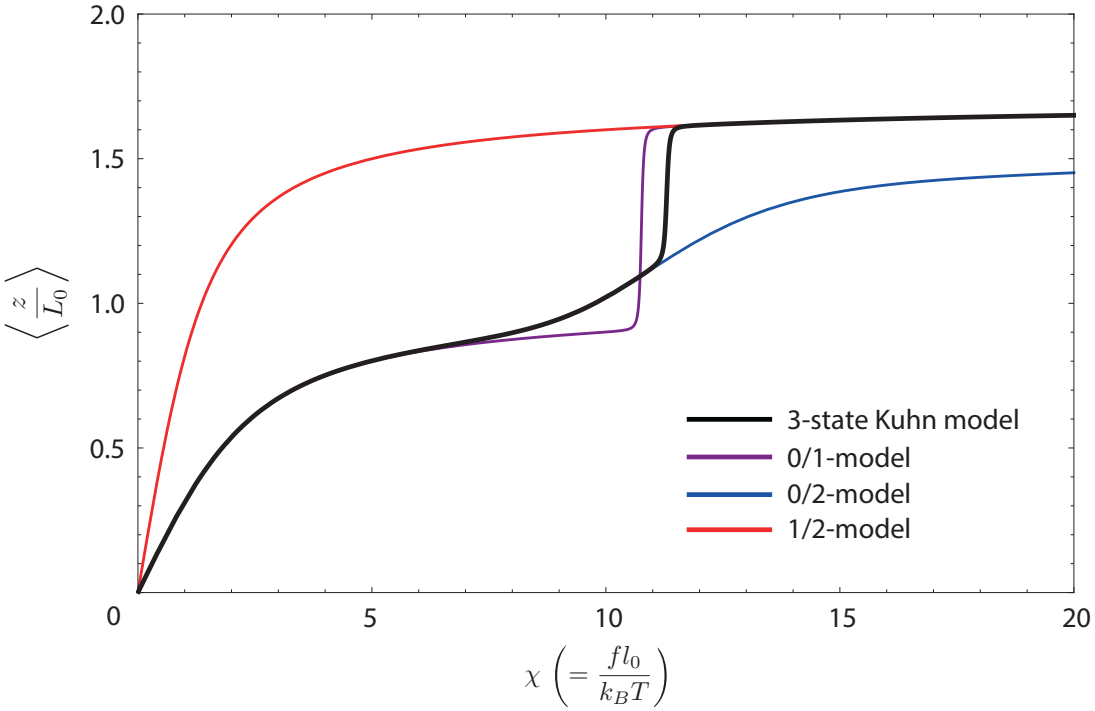

Figure 4.3: An example of a force-extension curve of the 3-state Kuhn model in the presence of intercalators is shown in black. The purple curve shows the 3-state force-extension curve in the absence of intercalating particles, and is equal to the cooperative 2-state force-extension curve from chapter 3. The black curve agrees qualitatively with experimental data (figure 1.4b, concentrations 5, 10, 20 and 25 nM). Especially note that the black curve shows four of the five effects of intercalators that we listed in chapter 2: the shift in the overstretching transition, the end-to-end increase (decrease) at force smaller (larger) than the original overstretching force and the larger than 1 end-to-end length for forces smaller than the overstretching force. The other two curves are reference curves that represent 2-state models in which one of three states is excluded. The blue curve represents a 0/2-model, which excludes state 1, and the red curve represents the 1/2-model, which excludes state 0. Similarly, the purple curve corresponds to the 0/1-model. The 3-state force-extension curve follows the 0/2-model closely for low forces and the 1/2-model for large forces. The two regimes are separated by the overstretching transition. The free energies used for the plot ($\varepsilon_1 = 7$, $\varepsilon_2 = 1$, $\lambda = 4$, $\delta = 8$, $\eta = 8$, $\mu = -10$) do not represent experimental data. The elongation factors are $\gamma_1 = 1.7$ and $\gamma_2 = 2$, and the axes are the same as the axes used in chapter 3, showing the dimensionless extension as a function of the dimensionless force.

purple curve in figure 4.3 shows the force-extension curve in the absence of intercalating particles ($\mu \to -\infty$), which is equal to the cooperative 2-state force-extension relation from chapter 3. The black curve gives the 3-state force-extension relation at a chemical potential μ that is large enough to perturb the force-extension curve. Indeed, the black curve clearly deviates from the purple curve. In fact, the black curve resembles the experimental data from figure 1.4b

(concentrations 5, 10, 20 and 25 nM) pretty well. That is, the curves show the same qualitative behavior. If we look back to the intercalator-induced effects that we want to understand (section 2.2.2), we even see that this theoretical force-extension curve already shows four of these effects: it shows an end-to-end length increase at forces smaller than the original overstretching force, an end-to-end length decrease at forces larger than the overstretching force, an end-to-end length significantly larger than 1 at forces smaller than the overstretching force, and a force-shift of the overstretching transition. This qualitative agreement with experimental data is promising, but to really understand the influence of intercalators on the force-extension curve of dsDNA, we need to quantify these effects.

We mentioned in section 4.2.3 that the force-extension relation of the 3-state Kuhn model is an unwieldy expression. This complicates the mathematical analysis and prevents us from quantifying the 3-state model in the same manner that we quantified the 2-state Kuhn model in chapter 3. However, we learn a lot about the force-extension relation of the 3-state model by studying figure 4.3. It shows three reference curves in addition to the 3-state force-extension curve. The purple curve was already mentioned briefly, and represents the chain in the absence of intercalating particles. In other words, this curve represents the chain in the absence of state 2. Therefore, we call the corresponding model the the 0/1-model, representing that it is a 2-state model which includes state 0 and state 1, but excludes state 2. Similarly, we also introduce the 0/2-model, a 2-state model in which we exclude overstretched DNA (state 1), and the 1/2-model, that excludes B-DNA (state 0). Figure 4.3 shows the 0/2-model (blue) and 1/2-model (red) as references for the 3-state force-extension curve. This leads to an interesting observation: the plotted 3-state curve (black) closely follows the force-extension curve of the 0/2-model at low forces and that of the 1/2-model at high forces. These two regimes are separated by a sharp transition: the overstretching transition. We show in section 4.5 that this is an immediate consequence of the positive free energy penalty between state 1 and state 2, η. For now we just assume $\eta > 0$, and come back to this point in section 4.5.

Note the strong analogy with the behavior of the cooperative 2-state force-extension curve, that we studied in section 3.3.2. This 2-state force-extension curve (figure 3.9) first closely follows the state 0 freely jointed chain (which we could call, analogous to the nomenclature just introduced, the 0-model) at low forces. Then, it undergoes the sharp, cooperative overstretching transition, after which it closely follows the state 1 freely jointed chain (1-model). In both cases, the more extended model can be described by two regimes in which it follows simpler models, which are separated by the overstretching transition. So, to gain more understanding of how the overstretching transition is affected by intercalative binding, we first need to understand the 0/2- and 1/2-models. However, the reader that is mainly interested in our results can skip sections 4.3.1 and 4.3.2, and continue reading in section 4.4.

4.3.1. The 0/2-model*

We start by analyzing the 0/2-model. This is a 2-state Kuhn model that arises when state 1 is excluded from the 3-state Kuhn model. In other words, it originates from the 3-state Kuhn model by taking the limit of $\varepsilon_1 \to \infty$. Hence, the energy functional $\varepsilon^{0/2-\text{model}}[\{\hat{t}_i\}, \{S_i\}]$ of the chain is given by

$$\begin{aligned}\frac{\varepsilon^{0/2-\text{model}}[\{\hat{t}_i\}, \{S_i\}]}{k_B T} &= \sum_{i=1}^{N}\left[- \frac{f l_0 \left(\delta_{S_i,0} + \gamma_2 \delta_{S_i,2}\right)}{k_B T}\, \hat{t}_i \cdot \hat{z} + \left(\varepsilon_2 - \mu\right) \delta_{S_i,2}\right] \\ &\quad + \sum_{i=1}^{N-1}\left[\delta\left(\delta_{S_i,2}\delta_{S_{i+1},2}\right)\right]. \end{aligned} \tag{4.5}$$

In chapter 3 we calculated the force-extension relation of the 2-state model, which was in fact

the 0/1-model. Equation 4.5 gives the energy functional of the 0/2-model, which is also a 2-state Kuhn model. Hence, the derivation of the force-extension relation goes completely analogous to the derivation in section 3.2.3 and Appendix A.2. We directly present the result, again in the infinite-chain limit,

$$\lim_{N\to\infty}\left\langle \frac{z_{0/2}}{L_0}\right\rangle = \frac{1}{2}\left(-\frac{2}{\chi}+\coth(\chi)+\gamma_2\coth(\gamma_2\chi)\right) + \frac{\gamma_2\left[\cosh(\gamma_2\chi)+\exp(\varepsilon_2-\mu+\delta)\left(\cosh(\chi)-\gamma_2\coth(\gamma_2\chi)\sinh(\chi)\right)\right]-\coth(\chi)\sinh(\gamma_2\chi)}{2\sqrt{4\exp(\varepsilon_2-\mu+2\delta)\gamma_2\sinh(\chi)\sinh(\gamma_2\chi)+\left(-\exp(\varepsilon_2-\mu+\delta)\gamma_2\sinh(\chi)+\sinh(\gamma_2\chi)\right)^2}}. \tag{4.6}$$

Equation 4.6 closely resembles the force-extension relation of the 0/1-model (equation 3.13). In fact, equation 4.6 can be obtained from equation 3.13 by substituting $\gamma_1 \to \gamma_2$, $\lambda \to -\frac{1}{2}\delta$ and $\varepsilon_1 \to \varepsilon_2 - \mu + \delta$. In other words, the force-extension relation of the 0/2-model is nothing new, it is just the force-extension relation of the 0/1-model with a rescaling of the three parameters of the model (γ_1, ε_1 and λ). We can understand this by considering table 4.2, which shows the cooperativity parameters of the 0/2-model.

	$S_{i+1}=0$	$S_{i+1}=2$
$S_i=0$	0	0
$S_i=2$	0	δ

Table 4.2: The cooperativity parameters of the 0/2-state Kuhn model. The row number gives the state of the i^{th} Kuhn segment, while the column number gives the state of Kuhn segment $i+1$. The numbers in the table give the free energy penalties that are associated with the interfaces between segment i and $i+1$. Together with the elongation factor γ_2 and the free energy penalty $\varepsilon_2 - \mu$ for state 2, this table characterizes the 0/2-model.

Together with the free energy penalty for state 2, $\varepsilon_2 - \mu$, and the elongation factor of state 2, γ_2, table 4.2 defines the 0/2-model. Now we can rescale these parameters, without changing the physics of the system, in a similar manner as we did in section 4.2.2 to show that our 3-state cooperativity parameters λ, δ and η give the most general case of the 3-state Kuhn model. Using the fact that only energy differences between states matter, we can rescale the free energy penalty for a 2/2-interface to 0, and simultaneously assign a penalty of $-\frac{1}{2}\delta$ for a 0/2-interface and rescale $\varepsilon_2 - \mu \to \varepsilon_2 - \mu + \delta$.[2] This leads to a new table of cooperativity parameters, given in table 4.3.
Note that this table represents the 2-state Kuhn model that we discussed in chapter 3, with a free energy penalty for an interface between different segments, and no penalties for interfaces between equal segments. Hence, this system can be mapped on the 0/1-model with the mapping $-\frac{1}{2}\delta \to \lambda$, $\gamma_2 \to \gamma_1$ and $\varepsilon_2 - \mu + \delta \to \varepsilon_1$.

The anti-cooperative 2-state Kuhn model

The analysis above shows that the 0/2-model is just an example of the anti-cooperative 2-state Kuhn model, which we analyzed in section 3.3.2. It is anti-cooperative because δ is positive,

[2] To prove that this rescaling does not change the physics of the system, consider a subsystem of n ($n \geq 1$) adjacent Kuhn segments in state 2 and both its neighbors, which are in state 0. The free energy of this subsystem is unaffected by the rescaling. A subsystem that does not contain such a string is completely in state 0 and therefore not affected by the rescaling either.

	$S_{i+1}=0$	$S_{i+1}=2$
$S_i=0$	0	$-\frac{1}{2}\delta$
$S_i=2$	$-\frac{1}{2}\delta$	0

Table 4.3: The cooperativity parameters of the 0/2-model, after rescaling. The rescaling also affects the free energy penalty for state 2, which becomes $\varepsilon_2 - \mu + \delta$. This model is now equal to the 2-state Kuhn model (with states 0 and 1) that was studied in chapter 3, with mapping $-\frac{1}{2}\delta \to \lambda$, $\gamma_2 \to \gamma_1$ and $\varepsilon_2 - \mu + \delta \to \varepsilon_1$.

thus $-\frac{1}{2}\delta$, which has the role that λ has in section 3.3, is negative. Moreover, this can be easily understood by considering the physical meaning of δ: it penalizes interfaces between two Kuhn segments in state 2. Hence, the transition from state 0 to state 2 is anti-cooperative. So we can use all results for the anti-cooperative transition, that we obtained in section 3.3, using the mapping $\gamma_1 \to \gamma_2$, $\lambda \to -\frac{1}{2}\delta$ and $\varepsilon_1 \to \varepsilon_2 - \mu + \delta$. This gives for the position of the 0/2-transition

$$\chi_{02} \;=\; \frac{\varepsilon_2 - \mu + \delta + \ln \gamma_2}{\gamma_2 - 1}, \tag{4.7}$$

and for the 0/2-transition width, in the limit of $\delta >> 0$,

$$W_{02,\delta>>0} \;=\; \frac{2\delta}{\gamma_2 - 1} + \frac{2\ln\left(\frac{4\phi^2}{1-\phi^2}\right)}{\gamma_2 - 1}. \tag{4.8}$$

Recall from section 3.3.2 that $\lambda << 0$ is already satisfied for λ relatively close to 0, as was shown by figure 3.8. That figure shows that the linear dependence of the width on λ is valid for $\lambda \lesssim -1$. Thus, equation 4.8 is valid for $\delta \gtrsim 2$. As we did in section 3.3.2, we defined the saturation parameter $\phi = \frac{1}{2}\sqrt{2}$.

We note an important difference between equations 4.7 and 4.8 and the corresponding equations for the 2-state Kuhn model of chapter 3 (the 0/1-model): the width and the position are not independent. While the width only depends on the cooperativity parameter δ, and not on the penalty $\varepsilon_2 - \mu$, the position of the transition depends on both $\varepsilon_2 - \mu$ and δ. So the cooperativity parameter influences both the width and the position of the transition. This can be understood by considering the meaning of the position of the transition. It signifies the force at which a system that is completely in state 0 (state 0 FJC) is equally likely as a system that is completely in state 2 (state 2 FJC). In chapter 3, the cooperativity parameter (λ) did not influence this since it does not play a role in either of these systems: it is only relevant on interfaces between them. However, in the 0/2-model, δ penalizes every interface in a state 2 FJC, so it shifts the position of the transition towards higher forces. Indeed, equation 4.7 shows that the position increases with increasing δ. We plot an example of a force-extension curve of the 0/2-model in figure 4.4. The free energies ($\delta = 8$, $\varepsilon_2 = 1$ and $\mu = -10$) are equal to those used in figure 4.3, and are not representative for experimental data of dsDNA; this plot is only used to analyze the 0/2-model. The elongation factor $\gamma_2 = 2$ reflects intercalative binding to dsDNA.

Figure 4.4 shows a force-extension curve of the 0/2-model in black. The shape of this curve was analyzed in section 3.3.2; it shows a wide overstretching transition, with two regimes with relative high slopes at the edges of the transition, and a relatively flat plateau in the middle. In section 3.3.2 we called this plateau the 0/1-plateau. Here we call it the 0/2-plateau, for obvious reasons. The 0/2-plateau represents a state of the chain that shows an alternating pattern of Kuhn segments in state 0 and Kuhn segments in state 2, or a 0/2-Neél state. This leads to the appearance of three macroscopic states of the chain: 0/0 (all segments in state 0), 0/2 (0/2-Neél state) and 2/2 (all segments in state 2). In between those regimes are two transitions, which

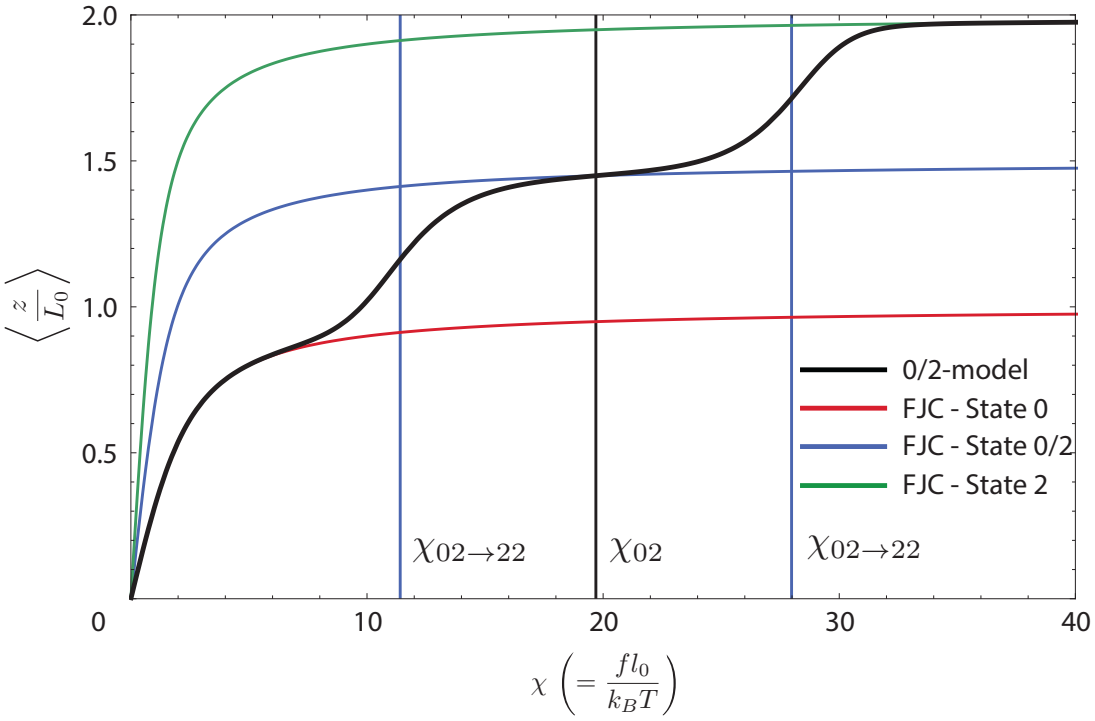

Figure 4.4: The force-extension curve of the 0/2-model (black) shows three regimes. At low forces ($\chi \lesssim 12$), all Kuhn segments are in state 0, so the 0/2-model follows the force-extension curve of the freely jointed chain with Kuhn segment l_0 (red). Moderate forces ($12 \lesssim \chi \lesssim 28$) excite Kuhn segments to state 2, but they are not large enough to excite two neighboring Kuhn segments due to the free energy penalty δ. This leads to the 0/2-plateau, which represents a 0/2-Neél state. In this regime, the 0/2-model resembles a freely jointed chain with segment length $\frac{1+\gamma_2}{2}\, l_0$ (blue). High forces ($\chi \gtrsim 28$) are large enough to overcome the energy penalty δ, so all Kuhn segments are excited towards state 2: the curve resembles a freely jointed chain with Kuhn segment $\gamma_2 l_0$ (green). The vertical blue lines indicate the positions of these transitions (equation 4.9 and 4.10), while the black vertical line gives the center of the transition from state 0 to state 2, and is given by equation 4.7. The free energies ($\delta = 8$, $\varepsilon_2 = 1$ and $\mu = -10$) are not representative for dsDNA.

are indicated by the blue vertical lines in figure 4.4. We denote the transition forces as $\chi_{00\to02}$ and $\chi_{02\to22}$ respectively, and we calculate them below. The black vertical line indicates the center of the transition from state 0 to state 2, χ_{02}. It is the force at which the free energies of macroscopic states 0/0 and 2/2 are equal, and it is given by equation 4.7. Finally, figure 4.4 shows freely jointed chains with segment lengths l_0 (red), $\frac{1+\gamma_2}{2}\, l_0$ (blue) and $\gamma_2 l_0$ (green), with $\gamma_2 = 2$, which emphasize the existence of the 0/0-, 0/2- and 2/2-regimes of the force-extension curve. Note that figure 4.4 shows the same 0/2-model force-extension curve as figure 4.3 (blue curve) does, but figure 4.4 shows a larger force range. This high-force regime of the 3-state Kuhn model, for forces significantly larger than the overstretching transition, is discussed in section 4.7.

We finish the analysis of the 0/2-model by calculating the transition forces $\chi_{00\to02}$ and $\chi_{02\to22}$. First, however, we need to define them more precisely. We define $\chi_{02\to22}$ as the force where the extension is exactly in between that of the FJC with segment length $\frac{1+\gamma_2}{2}\, l_0$ (blue curve in figure 4.4) and the FJC with segment length $\gamma_2 l_0$ (green curve in figure 4.4). Or, to put it differently, we define $\chi_{02\to22}$ as the force where the chain is halfway towards complete saturation in state 2. This means that the saturation parameter $\phi = \frac{1}{2}$. Similarly, $\chi_{00\to02}$ is defined by $\phi = -\frac{1}{2}$. Using this definition, we calculate $\chi_{00\to02}$ and $\chi_{02\to22}$ using the equations for the transition position χ_{02} (equation 4.7) and the transition width $W_{\delta>>0}$ (equation 4.8).

This gives

$$\chi_{00\to02} \;=\; \frac{\varepsilon_2-\mu+\ln\left(\frac{3}{4}\gamma_2\right)}{\gamma_2-1} \tag{4.9}$$

for the transition from macroscopic state 0/0 to macroscopic state 0/2, and

$$\chi_{02\to22} \;=\; \frac{\varepsilon_2-\mu+2\delta+\ln\left(\frac{4}{3}\gamma_2\right)}{\gamma_2-1} \tag{4.10}$$

for the transition from macroscopic state 0/2 to macroscopic state 2/2. The vertical blue lines in figure 4.4 are plotted by using equations 4.9 and 4.10.

Note that $\chi_{00\to02}$ does not depend on δ. This can be understood by realizing that it describes a transition from macroscopic state 0/0 to macroscopic state 0/2. Neither of this states shows neighboring segments in state 2, so the transition between them should not depend on δ. Instead, this transition is governed by the competition between the work done, $fl_0(\gamma_2-1)$, and the free energy cost, $\varepsilon_2-\mu+\ln\gamma_2$, of exciting a single Kuhn segment to state 2. For the explananation of the $\ln\gamma_2$ term, see section 3.3.1. Recall that this is the same competition that determines the position of the overstretching transition in the 2-state Kuhn model. Indeed, equation 4.9 closely resembles the expression for the transition position in the 2-state model (equation 3.17) with substitutions $\varepsilon_2-\mu\to\varepsilon_1$ and $\gamma_2\to\gamma_1$.

The transition between macroscopic states 0/2 and 2/2, $\chi_{02\to22}$, does depend on δ. We understand equation 4.10 by considering the free energy cost of exciting a Kuhn segment to state 2, if both its neighbors are already in state 2. This cost is the free energy penalty for state 2, $\varepsilon_2-\mu+\ln\gamma_2$, and twice the cost for a 2/2-interface, δ. This gives $\varepsilon_2-\mu+\ln\gamma_2+2\delta$ as the free energy penalty. Equation 4.10 gives the force required to overcome this free energy penalty.

4.3.2. The 1/2-model*

The analysis of the 1/2-model is analogous to the analysis of the 0/2-model, so we will show the most important results and refer to section 4.3.1 for the background. The 1/2-model originates from the 3-state Kuhn model by excluding state 0 from the system. This results in the energy functional of the chain,

$$\begin{aligned}\frac{\varepsilon^{1/2-\text{model}}[\{\hat{t}_i\},\{S_i\}]}{k_BT} \;=\; &\sum_{i=1}^{N}\left[-\frac{fl_0\left(\gamma_1\delta_{S_i,1}+\gamma_2\delta_{S_i,2}\right)}{k_BT}\,\hat{t}_i\cdot\hat{z}+\varepsilon_1\delta_{S_i,1}+\left(\varepsilon_2-\mu\right)\delta_{S_i,2}\right]\\ &+\;\sum_{i=1}^{N-1}\left[\eta\left(\delta_{S_i,1}\delta_{S_{i+1},2}+\delta_{S_i,2}\delta_{S_{i+1},1}\right)+\delta\left(\delta_{S_i,2}\delta_{S_{i+1},2}\right)\right],\end{aligned} \tag{4.11}$$

which leads, after a calculation analogous to that in section 3.2.3 and Appendix A.2 to the force-extension relation of the 1/2-model, in the infinite chain limit,

$$\begin{aligned}\lim_{N\to\infty}\left\langle\frac{z_{1/2}}{L_0}\right\rangle \;=\; &\frac{1}{2}\left(-\frac{2}{\chi}+\gamma_1\coth\left(\gamma_1\chi\right)+\gamma_2\coth(\gamma_2\chi)\right)\;+\;\gamma_1e^{\varepsilon_1+\eta+\mu}\cdot\\ &\frac{\left[\gamma_2\cosh\left(\gamma_2\chi\right)-\gamma_1\coth(\gamma_1\chi)\sinh(\gamma_2\chi)\right]+\gamma_2e^{\delta+\varepsilon_2+\eta}\left[\gamma_1\cosh\left(\gamma_1\chi\right)-\gamma_2\coth(\gamma_2\chi)\sinh(\gamma_1\chi)\right]}{2\sqrt{4\gamma_1\gamma_2e^{2\delta+\varepsilon_1+\varepsilon_2+\mu}\sinh\left(\gamma_1\chi\right)\sinh\left(\gamma_2\chi\right)+\left(e^{\varepsilon_1+\eta+\mu}\gamma_1\sinh\left(\gamma_2\chi\right)-e^{\delta+\varepsilon_2+\eta}\gamma_2\sinh\left(\gamma_1\chi\right)\right)^2}}.\end{aligned} \tag{4.12}$$

Equation 4.12 can also be obtained from the 0/1-model force-extension curve (equation 3.13) by a mapping of parameters. This can be done by substituting $\varepsilon_1\to\varepsilon_2-\mu-\varepsilon_1+\delta$, $\lambda\to\eta-\frac{1}{2}\delta$ and $\gamma_1\to\frac{\gamma_2}{\gamma_1}$, as well as multiplying the force-extension relation by γ_1 and replacing $\chi\to\gamma_1\chi$. The

rescaling of ε_1 and λ can be explained using tables similar to tables 4.2 and 4.3. The rescaling of $\gamma_1 \to \frac{\gamma_2}{\gamma_1}$ signifies that the effective elongation factor in the 1/2-model is the elongation of a Kuhn segment upon changing from state 1 to state 2. Finally, multiplication by γ_1 and replacing $\chi \to \gamma_1\chi$ correspond to rescaling the y-axis and x-axis respectively, which is required because the shortest segment length in the 1/2-model is $\gamma_1 l_0$ instead of l_0.

The position and width of the transition can be calculated from equation 4.12, similar to how we calculated the position and the width in chapter 3. The result is

$$\chi_{12} = \frac{\varepsilon_2 - \mu - \varepsilon_1 + \delta + \ln\left(\frac{\gamma_2}{\gamma_1}\right)}{\gamma_2 - \gamma_1}, \tag{4.13}$$

for the position of the transition from state 1 to state 2, χ_{12}, and

$$W_{12} = \frac{2\ln\left[1 + \frac{2\phi\exp(\delta - 2\eta)}{(1-\phi^2)}\left(\phi + \sqrt{\phi^2 + \exp(2\eta - \delta)\left(1 - \phi^2\right)}\right)\right]}{\gamma_2 - \gamma_1} \tag{4.14}$$

for the width of the 1/2-transition. In contrast to our analysis of the 0/1-model and the 0/2-model, we cannot conclude whether the transition is cooperative or anti-cooperative based on the background information from section 2.1. The cooperativity parameter of the 1/2-model is $\eta - \frac{1}{2}\delta$. We know that both η and δ are positive, but their ratio is unknown. Thus, we do not make assumptions on the sign of $\eta - \frac{1}{2}\delta$ for now, and work with the general expression for the width (equation 4.14). An example of a force-extension curve of the 1/2-model is given in figure 4.5. The figure shows an example of a cooperative case, in which $\eta > \frac{1}{2}\delta$, and thus shows a cooperative transition from a regime where the curve follows a freely jointed chain with segment length $\gamma_1 l_0$ (red) to a regime where the curve follows a freely jointed chain with segment length $\gamma_2 l_0$ (green). The vertical lines indicates the position of the transition χ_{12}, as given by equation 4.13. Note that we did not see any evidence of state 2 in the 1/2-model that was shown in figure 4.3 (red curve). This is because both 1/2-interfaces (η) and 2/2-interfaces (δ) are penalized. This transition would have been visible if a larger window on the force-axis had been used. The free energies ($\delta = 4$, $\eta = 8$, $\varepsilon_1 = 7$, $\varepsilon_2 = 1$ and $\mu = -10$) do not represent experimental data on dsDNA. The elongation factors $\gamma_1 = 1.7$ and $\gamma_2 = 2$ do represent dsDNA. We do not give an example of an anti-cooperative case ($\eta < \frac{1}{2}\delta$), but this figure would look similar to the anti-cooperative transition of the 0/2-model, as shown in figure 4.4.

The influence of intercalators

We conclude this section by answering how intercalators influence the force-extension curves of the 0/2- and 1/2-models. We observe that the widths of both the 0/2-model and the 1/2-model are independent of the chemical potential μ, and thus they are not influenced by intercalative binding. Only the positions of the transitions are affected, and both decrease with μ (equations 4.7 and 4.13). These observations can easily be understood by considering the way in which intercalators are taken into account in the model. A free energy bonus of μ is assigned to a Kuhn segment that binds an intercalator, which effectively leads to a rescaling of the free energy penalty of state 2. If more intercalators are added to the solution, μ becomes larger, and state 2 is more favored over the other states. We have seen before, in chapter 3, that rescaling the free energy penalty for a certain state shifts the position of the transition, but leaves the width unaffected.

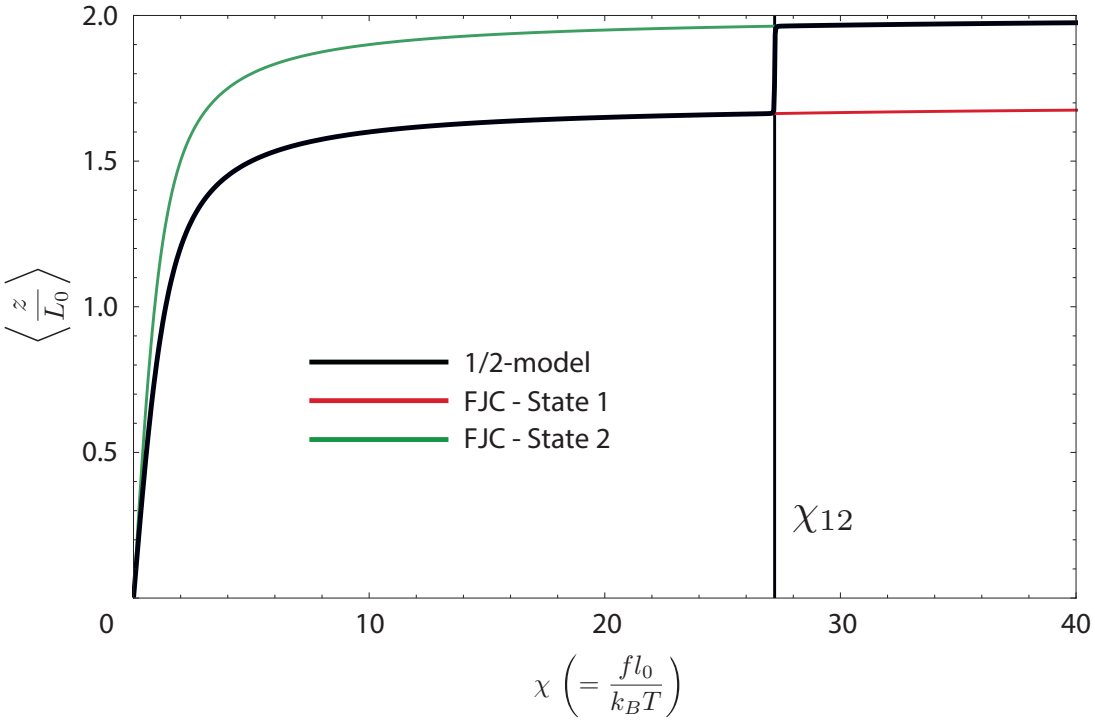

Figure 4.5: An example of a force-extension curve of the 1/2-model (black), that shows a cooperative transition ($\eta > \frac{1}{2}\delta$) from a state 1 FJC (red) to a state 1 FJC (green). The position of the transition, χ_{12}, is given by equation 4.13 and displayed by the vertical line. The 1/2-model can also produce an anti-cooperative transition if $\eta < \frac{1}{2}\delta$. The free energies ($\delta = 4$, $\eta = 8$, $\varepsilon_1 = 7$, $\varepsilon_2 = 1$ and $\mu = -10$) do not represent experimental data on dsDNA. The elongation factors $\gamma_1 = 1.7$ and $\gamma_2 = 2$ do represent dsDNA.

4.4. The overstretching transition in the 3-state model

We start this section by shortly summarizing the most import insights of sections 4.3.1 and 4.3.2 for the reader that skipped those sections. We have seen that the 0/2-model and the 1/2-model can be mapped on the 2-state Kuhn model of chapter 3, but that the width and the position of the corresponding transitions are not independent. We have seen that the 0/2-model is an anti-cooperative 2-state Kuhn model, and we calculated the positions of the transitions between the macroscopic states 0/0 (all Kuhn segments in state 0), 0/2 (alternating pattern of state 0 and 2, or 0/2-Neél state) and 2/2 (all Kuhn segments in state 2). We refer to those transition positions as $\chi_{00\to02}$ and $\chi_{02\to22}$, and both decrease when μ increases. Finally, we have seen that the cooperativity of the 1/2-model depends on the sign of $\eta - \frac{1}{2}\delta$.

Now that we understand the physics and the force-extension curves of the 0/2- and 1/2-model, we go back to the example of the 3-state force-extension curve in figure 4.3. We observed earlier that the force-extension curve of the 3-state model (black) follows the 0/2-model closely for low forces, and then undergoes the cooperative overstretching transition towards the 1/2-model. We pointed out that this is analogous to the 2-state model that follows the state 0 FJC for low forces, and then undergoes the cooperative overstretching transition to the state 1 FJC. In chapter 3 we found that the transition force χ_{01}, which gives the overstretching force in the 2-state model, is determined by the competition between the extra work upon overstretching and the free energy penalty for state 1 (equation 3.18). In other words, at the transition force the free energies, including the contribution of the work, of state 0 and state 1 are equal. We now use the same approach to determine the overstretching transition of the 3-state Kuhn model: we equate the free energy of the 0/2-model to that of the 1/2-model. As can be seen in figure 4.3, the

influence of state 2 on the 1/2-model is negligible at the force of the overstretching transition; the 1/2-model is identical to a state 1 FJC. This effect is also seen in the experimental data of figure 1.4b (0 and 10 nM), which shows a constant extension of about 1.7 times the B-DNA contour length directly after the overstretching transition. Hence, we equate the free energy of the 0/2-model to the free energy of a 1/1-model. The 1/1-model is a freely jointed chain with segment length $\gamma_1 l_0$, and every Kuhn segment receives a free energy penalty ε_1.

We already calculated the free energies of the 0/2-model (F_{02}) and the 1/1-model (F_{11}), which were intermediate results in the derivations of the force-extension curves (equations 3.11 and 3.12). The free energy of the 1/1-model, F_{11}, is given by

$$F_{11} \;=\; -k_B T N \left[\ln\left(\frac{4\pi}{\chi}\right) + \ln\left(\frac{\exp(-\varepsilon_1)\sinh(\gamma_1\chi)}{\gamma_1}\right)\right]. \tag{4.15}$$

The free energy of the 0/2-model is more complicated. We do not present F_{02} in an equation, but the theoretically interested reader can easily obtain it by substituting equation A.35 in equation A.33 (Appendix A.2) and performing the parameter mapping from the 0/1-model to the 0/2-model that was explained in section 4.3.1. Equating F_{02} and F_{11} yields a complicated equation that we do not solve analytically in the general case. We can, however, approximate it in certain force regimes. We illustrate this graphically by plotting the free energies as a function of the dimensionless force χ in figures 4.6, 4.7 and 4.8. To do so, we divide the free energy by N, obtaining the free energy per Kuhn segment, and by $k_B T$, to obtain a dimensionless free energy. Finally, we subtract the first term in equation 4.15, because it does not depend on the length of a Kuhn segment and both F_{11} and F_{02} contain it. The resulting dimensionless free energies per Kuhn segment are plotted in figure 4.6a, for a set of parameters that is suited for illustrating our methods ($\delta = 4$, $\varepsilon_1 = 7$, $\varepsilon_2 = 1$, $\mu = -16$, $\gamma_1 = 1.7$ and $\gamma_2 = 2$). The red curve shows the free energy of the 1/1-model (second term in equation 4.15) as a function of χ, while the blue curve shows the free energy of the 0/2-model. The free energy of the 1/1-model appears to be a linear function of χ for $\chi \gtrsim 1$. Indeed, in the limit of large χ, the hyperbolic sine in equation 4.15 reduces to an exponent, and the free energy is reduced to

$$\lim_{\chi>>1} \frac{F_{11}}{k_B T N} - \ln\left(\frac{4\pi}{\chi}\right) \;=\; -\ln\left(\frac{\exp(-\varepsilon_1+\gamma_1\chi)}{2\gamma_1}\right) \;=\; -\gamma_1\chi + \varepsilon_1 + \ln(2\gamma_1). \tag{4.16}$$

A linear fit of the 1/1-model free energy in figure 4.6a gives a slope of -1.7 and an offset of $8.22 \approx \varepsilon_1 + \ln(2\gamma_1)$, consistent with equation 4.16.

The 0/2-model free energy shows more complicated behavior. However, while the expression for the free energy is rather unwieldy, figure 4.6a shows an interesting feature of this free energy: it consists of three regions where the free energy is approximately a linear function of χ. Two forces mark the transitions between these regions. The transition forces are indicated by the vertical blue lines and given by $\chi_{00\to02}$ (equation 4.9) and $\chi_{02\to22}$ (equation 4.10). So, the transitions between the linear regimes of the 0/2-model free energy coincide with the transitions between the macroscopic states 0/0, 0/2 and 2/2. This suggests that the leftmost region in figure 4.6a represents the 0/0-state, the rightmost region represents the 2/2-state, and the region in between describes the 0/2-state. Indeed, linear fits of the three regions show that the regions have slopes of -1 (left), -1.5 (middle) and -2 (right), corresponding to the average elongation factors of those macroscopic states.

Using this observation, we can solve $F_{11} = F_{02}$ by assuming that the intersection between the two curves occurs at a force χ that corresponds to one of the three regimes discussed above. We can greatly simplify the expression for F_{02} in any of those three regimes, allowing us to give an analytical approximation of the solution. We now consider the three cases one by one. We have seen an example of the first case in figure 4.6a. We note that this method fails if the intersection occurs close to one of the transition forces. In that case, we solve $F_{11} = F_{02}$ numerically.

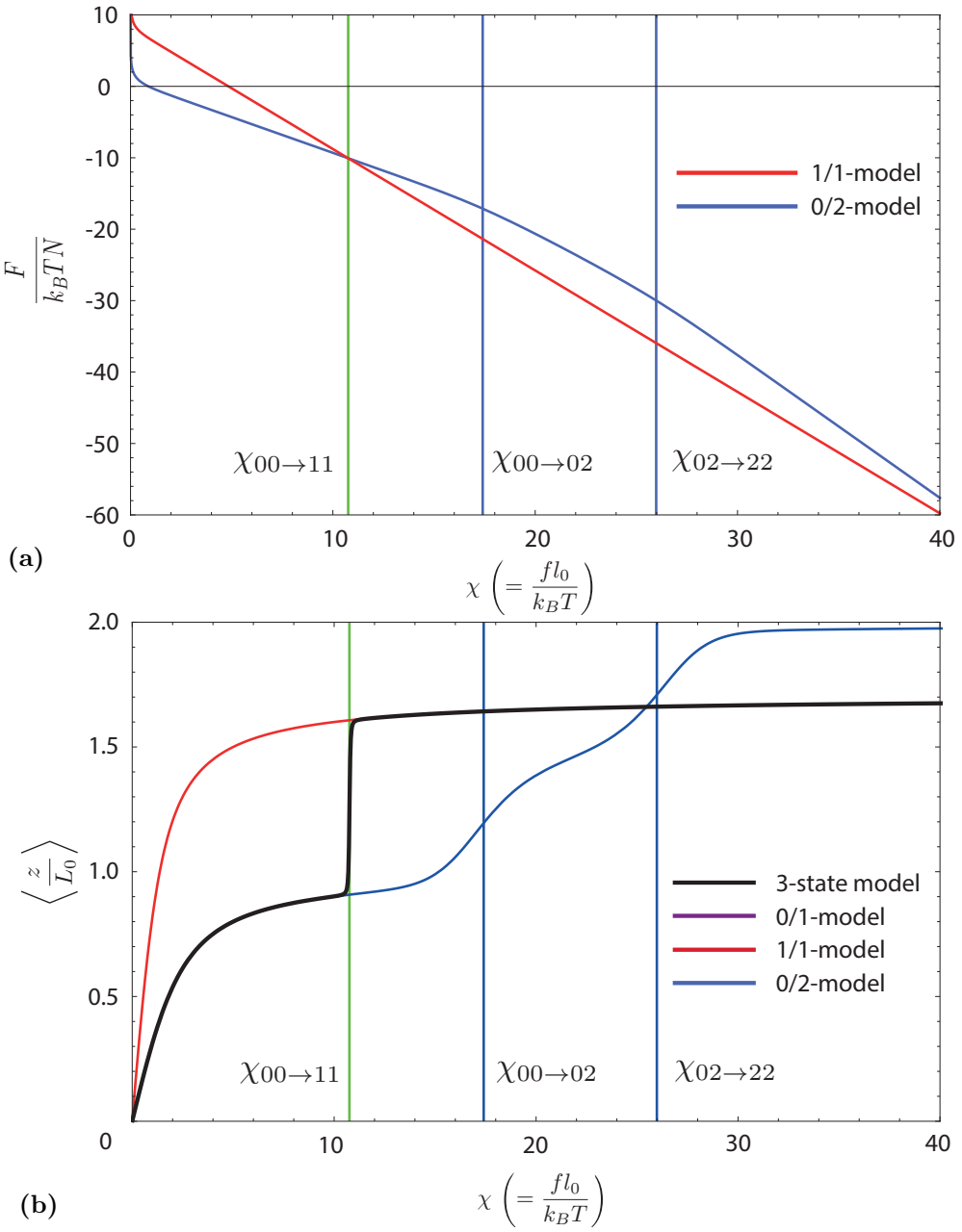

Figure 4.6: The free energies of the 0/2-model (blue) and the 1/1-model (red) are plotted in figure (a). The free energy of the 1/1-model is a linear function of the dimensionless force χ (for $\chi \gtrsim 1$), while the free energy of the 0/2-model shows three linear regimes. The forces $\chi_{00\to02}$ and $\chi_{02\to22}$ indicate the transitions between those linear regimes. The leftmost regime describes the macroscopic 0/0 state, the regime in the middle describes a macroscopic 0/2 state, and the rightmost regime represents a macroscopic 2/2 state. The intersection of both free energy curves gives the overstretching force of the 3-state model, and is indicated by the green vertical line. In this case the intersection occurs in the leftmost region of the 0/2-model, thus in the region where all segments are in state 0. Hence, intercalation (state 2) does not influence the overstretching transition, and the overstretching force is equal to that of the 2-state model of chapter 3. Figure (b) shows the corresponding force-extension curves. Indeed, the 3-state curve (black) completely overlaps the 0/1-model curve (purple). The 0/2-model is given in blue and the 1/1-model is given in red. The parameters in these plots are $\delta = 4$, $\varepsilon_1 = 7$, $\varepsilon_2 = 1$, $\mu = -16$, $\gamma_1 = 1.7$, $\gamma_2 = 2$, $\lambda = 4$ and $\eta = 8$.

The green vertical line in figure 4.6a shows the force at which $F_{11} = F_{02}$. We pointed out, earlier in this section, that this is the force where the overstretching transition occurs. In figure 4.6b we plotted the force-extension curves of the 3-state model (black), the 1/1-model (red),

the 0/2-model (blue) and the 0/1-model (purple) with the same parameters that where used in figure 4.6a, complemented with $\lambda = 4$ and $\eta = 8$. Note that the 0/1-model (purple) is not visible because it is completely covered by the 3-state model (black). Figure 4.6b shows the same x-axis as 4.6a. The green vertical line is located at the same position, and gives the position of the overstretching transition, as anticipated. Note that the blue lines indeed give the positions of $\chi_{00\to02}$ and $\chi_{02\to22}$ in figure 4.6b. We can now calculate the position of the overstretching transition analytically by considering in which regime of the 0/2-model it occurs. The green line is located to the left of both blue lines, so the 0/2-model is in the 0/0 regime at the point of the overstretching transition. This allows us to simplify the expression for F_{02} by assuming $\chi << \chi_{00\to02}$. This gives, for the overstretching force,

$$\chi_{00\to11} \;=\; \frac{\varepsilon_1 + \ln\gamma_1}{\gamma_1 - 1}, \tag{4.17}$$

where the subscript $00 \to 11$ indicates that the overstretching transition occurs from state 0/0 in the 0/2-model to the 1/1-model. Equation 4.17 is equal to the 2-state overstretching force that we known from chapter 3 (equation 3.17). This can be understood by realizing that if the overstretching occurs in the 0/0-regime, there is no influence of state 2 in the model. Hence, the 3-state model behaves as the 0/1-model in that limit. Indeed, figure 4.6b shows that the 3-state force-extension curve and the 0/1-model force-extension curve overlap completely.

Shifting the overstretching transition

In the example of figure 4.6 we saw no influence of intercalating particles, because the chemical potential ($\mu = -16$) was too small. Now we add more intercalators to the solution, which we model by increasing μ, and study how this affects the free energies and the force-extension curves. All other parameters are kept constant. Figure 4.7 shows the free energies and the force-extension curves for $\mu = -8.5$. Figure 4.7a shows two green vertical lines, indicating that there are two forces at which the free energies of the 0/2-model and the 1/1-model are equal. In between the green lines, the 1/1-model has a lower free energy, but outside the green lines the free energy of the 0/2-model is lower. In other words, there are two transitions between the 0/2-model and the 1/1-model in the force-extension curve of the 3-state Kuhn model. The first indicates the overstretching transition, while the second gives a transition from an overstretched chain (1/1-state) to the even longer state of complete intercalative saturation (2/2-state), in which every base pair is intercalated. We discuss this high-force regime in section 4.7.

Figure 4.7b shows both transitions at the positions of the green vertical lines. The same colors that were used in figure 4.6b are used here: the 3-state Kuhn model is given in black, the 0/2-model in blue, the 1/1-model in red and the 0/1-model in purple. The blue vertical lines give the positions of the transitions in the 0/2-model. The 3-state model is now clearly deviating from the 0/1-model. The overstretching transition has shifted to a higher force, and the 3-state model obtains an elongation of more than 1 for forces smaller than the overstretching force. We analyze the physical reasons for these changes in section 4.5. Here we focus on the mathematical side of the model. We now obtain approximate expressions for the transitions that are given by the green lines, by taking the appropriate limits when solving $F_{11} = F_{02}$. The overstretching transition is found in between the blue lines in figure 4.7, hence $\chi_{00\to02} << \chi << \chi_{02\to22}$, which gives

$$\chi_{02\to11} \;=\; \frac{\varepsilon_1 - \frac{1}{2}(\varepsilon_2 - \mu) + \ln\left(\frac{\gamma_1}{\sqrt{\gamma_2}}\right)}{\gamma_1 - \frac{1}{2}(\gamma_2 + 1)}. \tag{4.18}$$

Equation 4.18 has the same structure as equation 4.17, but now the parameters of state 1 (ε_1, γ_1) are replaced by the difference between state 1 and the average of states 0 and 2. Indeed, it describes the overstretching transition from a system with half of its segments in state 0 and the

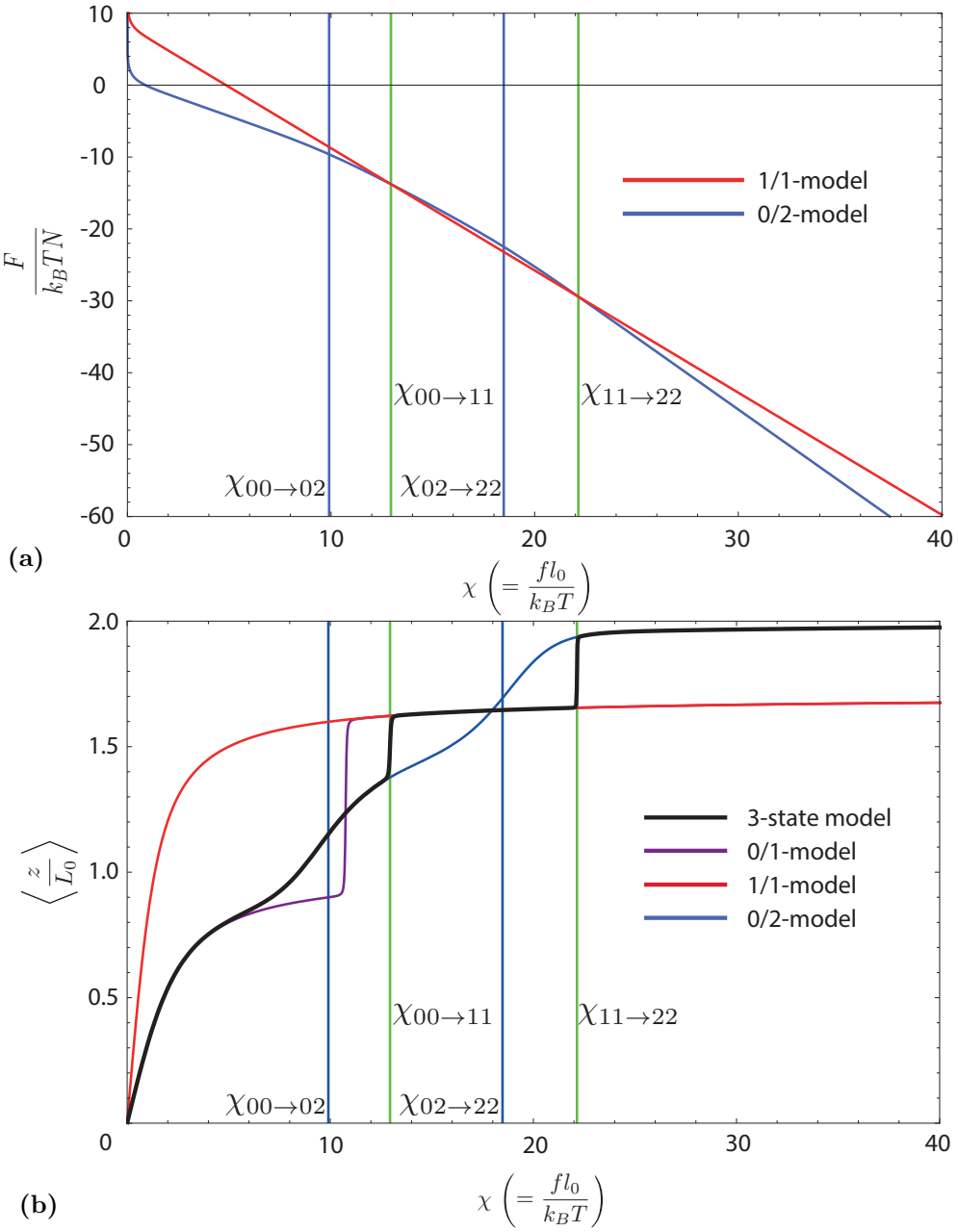

Figure 4.7: The free energies (a) and force-extension curves (b) for the same parameters that were used in figure 4.6, but the chemical potential μ is increased from -16 to -8.5. The free energies in figure (a) now show two intersections. The first is located in between the two blue vertical lines and represents the overstretching transition. Thus, the overstretching transition occurs from a state with an alternating 0/2 pattern to a completely overstretched chain (state 1). This leads to a shift of the overstretching transition towards higher forces, which can be seen by comparing the position of the 3-state overstretching transition with the overstretching transition of the 0/1-model (purple). It also leads to an elongation of more than 1 for forces smaller than the overstretching force. The second intersection is not an overstretching transition, but gives the transition from a completely overstretched state (1/1) to a completely intercalated state (2/2).

other half in state 2, to a system with all segments in state 1. We note that this expression is, strictly speaking, only valid if the anti-cooperativity of the 0/2-system is large enough that the force-extension curve is completely flat in between $\chi_{00\to02}$ and $\chi_{02\to22}$. We see in figure 4.7b that this is not the case. Hence, the position of the green lines is calculated by numerically solving the exact equation for the free energies. However, equation 4.18 gives a proper and insightful

approximation for the force, that is very close to the actual force.

The other transition in figure 4.7b is found to the right of both blue lines, thus we take $\chi >> \chi_{02\to22}$, which gives

$$\chi_{11\to22} = \frac{\varepsilon_2 - \mu - \varepsilon_1 + \delta + \ln\left(\frac{\gamma_2}{\gamma_1}\right)}{\gamma_2 - \gamma_1}. \tag{4.19}$$

Equation 4.19 is equal to equation 4.13, the transition force of the 1/2-model. Indeed, this force describes the transition from a 1/1-state to a 2/2-state, which is exactly the 1/2-transition. We stress that this transition is *not* an overstretching transition. Instead, at this force the chain changes from the overstretched state into the completely intercalated state, where every base pair is intercalated. If such a transition would occur in an experiment, this would be detectable in a force-extension measurement, but it should also be detectable with fluorescence microscopy. After all, the fluorescence intensity is a measure of the number of bound intercalators. Intercalation at every base pair should therefore significantly increase the fluorescence intensity.

The disappearance of the overstretching transition

Equations 4.18 and 4.19 show the influence of μ (and thus, of the intercalation concentration) on the overstretched state (state 1) in the force-extension curve. The overstretching force $\chi_{02\to11}$ is an increasing function of μ, while the 1/2-transition $\chi_{11\to22}$ is a decreasing function of μ. This is caused by the fact that increasing μ favors state 2 over state 1, so the free energy of the 0/2-model is lowered with respect to the free energy of the 1/1-model. Therefore, $\chi_{02\to11}$ increases, while $\chi_{11\to22}$ decreases with μ. Thus, when μ is increased, the green lines (figure 4.7b) approach each other until, eventually, they overlap. If μ is increased beyond that point, the free energies of the 1/1-model and the 0/2-model do not intersect anymore: F_{02} is lower than F_{11} for *any* force. At this chemical potential, the overstretched state (state 1) does not occur in the molecular chain anymore, and this is reflected in the force-extension curve: the disappearance of state 1 naturally leads to the disappearance of the overstretching transition. An example of such a situation is given in figure 4.8, where μ is increased from -8.5 to -5.

Figure 4.8a shows that the free energies F_{02} (blue) and F_{11} (red) do not intersect at any force. The free energy of the 0/2-model (F_{02}) is lower than the free energy of the 1/1-model (F_{11}) for *all* forces. Thus, state 1 will not occur in the DNA. Figure 4.8b shows that the corresponding 3-state force-extension curve does not show any sign of state 1; the 3-state force-extension curve (black) completely overlaps the force-extension curve of the 0/2-model (blue), and does not show the cooperative overstretching transition.

4.4.1. The influence of the chemical potential

We now aim to calculate the chemical potentials that corresponds to the changes in behavior from figure 4.6 to figure 4.7, and from figure 4.7 to figure 4.8. In other words, we aim to calculate the chemical potential at which the overstretching transition first deviates from the zero-particle overstretching transition, and the chemical potential at which the overstretching transition disappears.

We start with the first. This is the lowest chemical potential at which the 3-state force-extension curve shows a sign of state 2. This occurs approximately when the overstretching transition is located around $\chi_{00\to02}$. Or, in terms of the figures, when the green vertical line coincides with the leftmost blue vertical line. The free energy equation, $F_{02} = F_{11}$, does not give a straightforward analytical solution in between the regimes described above, so we approximate this chemical potential by equation the solution for the overstretching transition in the $\chi << \chi_{00\to02}$ regime (equation 4.17) and that in the $\chi_{00\to02} << \chi << \chi_{02\to22}$ regime (equation 4.18). This leads to

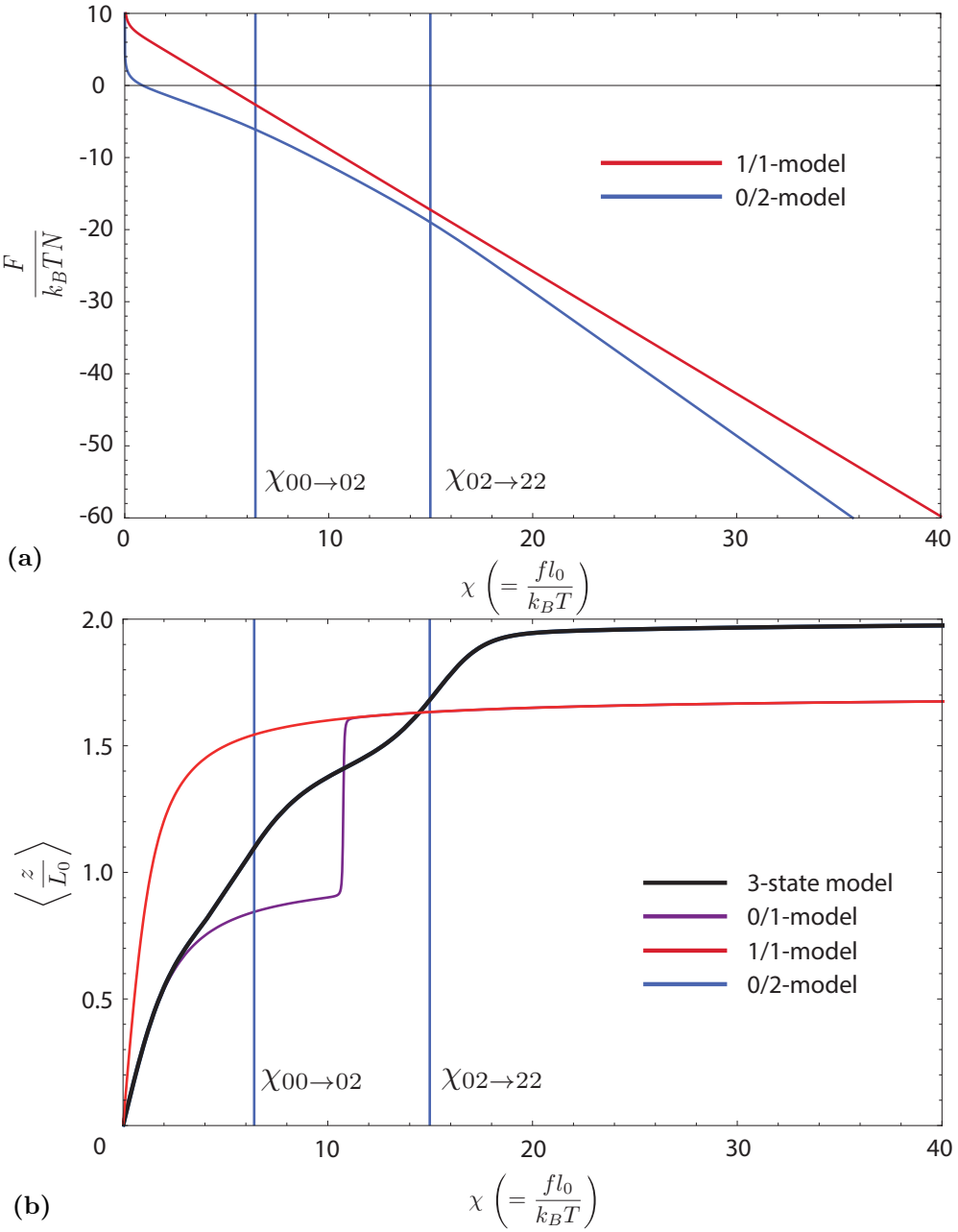

Figure 4.8: The free energies (a) and force-extension curves (b) for the same parameters that were used in figures 4.6 and 4.7, but the chemical potential μ is increased to -5. The free energies in figure (a) do not intersect: the free energy of the 0/2-model is lower than the free energy of the 1/1-model for all forces. Thus, the overstretched state (state 1) does not occur in the DNA anymore. The 3-state force-extension curve (black) in figure (b) completely overlaps the force-extension curve of the 0/2-model. There is no influence of the 1/1-model (red) in the 3-state force-extension curve, so state 1 does not play a role in the 3-state force-extension curve. Naturally, this leads to a disappearance of the overstretching transition.

$$\mu_{min} = \varepsilon_2 - \frac{\gamma_2 - 1}{\gamma_1 - 1}\varepsilon_1 + \mu_{corr}. \tag{4.20}$$

Here the subscript 'min' indicates that this is an indication for the smallest chemical potential that changes the force-extension curve of the 3-state model. The last term, μ_{corr} is a correction that is a function of γ_1 and γ_2 only, and originates from the logarithmic terms in equations 4.17 and 4.18. It is of the order of 0.1 (in dimensionless units), which is smaller than the error caused by the approximation that lead to equation 4.20. Therefore, we neglect it. The expression that

remains can be understood by rewriting it, which yields

$$\frac{\varepsilon_2 - \mu_{min}}{\gamma_2 - 1} \approx \frac{\varepsilon_1}{\gamma_1 - 1}. \tag{4.21}$$

Equation 4.21 shows that, at μ_{min}, the positions of the 00/02-transition (equation 4.9) and 0/1-transition (equation 3.17) are approximately equal. Thus, μ_{min} is the minimal chemical potential where state 2 is present in the molecular chain in the force-regime of the overstretching transition ($\chi \sim \chi_{01}$). This causes the intercalators (state 2) to change the overstretching transition.

We continue by calculating μ_{max}, the maximal chemical potential that still shows an overstretching transition. If $\mu > \mu_{max}$, the overstretching transition disappears and the force-extension curve looks like the black curve in figure 4.8b. We explained above that the disappearance of the overstretching transition is associated with the absence of an intersection between the F_{11} and F_{02} curves (figure 4.8a), while before the disappearance they intersect twice (figure 4.7a). At μ_{max}, the point of disappearance, the free energy equation has exactly one solution, so the vertical lines in figure 4.7 coincide.

We calculate μ_{max} in the same way in which we calculated μ_{min}. In the relevant regime, there is no straightforward analytical solution of $F_{11} = F_{02}$, so we approximate μ_{max} by equating the expressions for both green vertical lines, $\chi_{02\to11}$ (equation 4.18) and $\chi_{11\to22}$ (equation 4.19) This results in

$$\mu_{max} = \varepsilon_2 - \varepsilon_1 \frac{\gamma_2 - 1}{\gamma_1 - 1} + \delta \frac{2\gamma_1 - \gamma_2 - 1}{\gamma_1 - 1} + \mu_{corr}, \tag{4.22}$$

where μ_{corr} is again a small correction factor, which depends only on γ_1 and γ_2, and that we neglect. This expression gives the chemical potential where $\chi_{02\to11}$ and $\chi_{11\to22}$ are equal to each other, but also equal to $\chi_{02\to22}$ (equation 4.10), the force where the 0/2-model undergoes the transition from the macroscopic state 0/2 to the macroscopic state 2/2. Thus, at μ_{max} the macroscopic states 0/2, 1/1 and 2/2 all have the same free energy. At higher chemical potential, $\chi_{11\to22} < \chi_{02\to11}$, so as soon as the system would overstretch ($\chi_{02\to11}$), it would immediately stretch further to state 2/2. Therefore, there is no overstretching transition for $\mu > \mu_{max}$.

Together, μ_{min} and μ_{max} give an indication for the range of chemical potentials that shifts the overstretching transition. At $\mu < \mu_{min}$ the overstretching transition is not shifted, while at $\mu > \mu_{max}$ there is no overstretching transition at all. Thus, the chemical potentials μ_{shift}, that shift the overstretching transition, obey

$$\varepsilon_2 - \frac{\gamma_2 - 1}{\gamma_1 - 1}\varepsilon_2 < \mu_{shift} < \varepsilon_2 - \varepsilon_1 \frac{\gamma_2 - 1}{\gamma_1 - 1} + \delta \frac{2\gamma_1 - \gamma_2 - 1}{\gamma_1 - 1}, \tag{4.23}$$

and the window of chemical potentials that do so, W_μ, is thus given by

$$W_\mu = \delta \frac{2\gamma_1 - \gamma_2 - 1}{\gamma_1 - 1}. \tag{4.24}$$

Since γ_1 and γ_2 are known, equation 4.24 allows us to determine the value of the cooperativity parameter δ from experimental data, by studying the range of chemical potentials that show a force-extension curve with shifted overstretching transition. We do this in section 4.6.

We conclude this section with a summary in graphical form of the influence of μ on the 3-state Kuhn model. We show the 3-state force-extension curves of figures 4.6b ($\mu = -16$), 4.7b ($\mu = -8.5$) and 4.8b ($\mu = -5$) in one plot, together with the curve corresponding to $\mu = -10$. The result is given in figure 4.9. The figure shows all three regimes discussed in this section: the unaffected overstretching transition ($\mu = -16$), the shifted overstretching transition ($\mu = -10$ and $\mu = -8.5$) and the force-extension curve that shows no overstretching transition at all

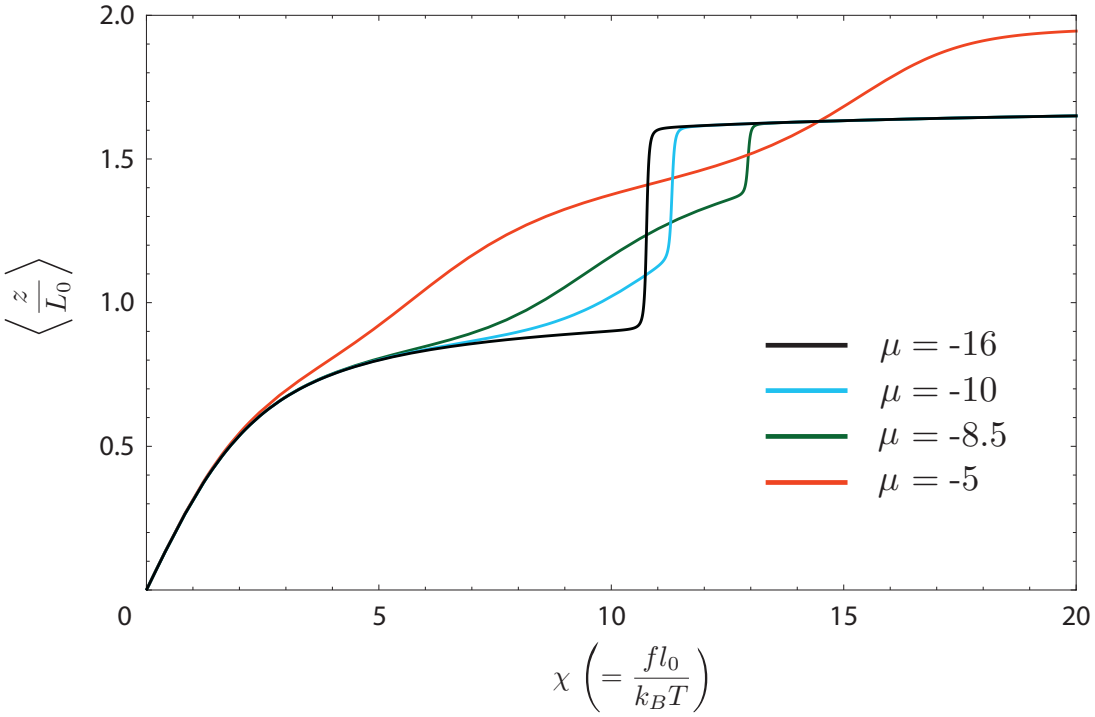

Figure 4.9: A graphical summary of section 4.4: 3-state force-extension curves are plotted for a range of chemical potentials that covers all regimes discussed in this section. The $\mu = -16$ curve shows an overstretching transition that is not affected by intercalative binding. The curves with $\mu = -10$ and $\mu = -8.5$ show an overstretching transition that is shifted towards higher forces, and the $\mu = -5$ curve shows no overstretching transition at all. The other parameters are given by $\delta = 4$, $\varepsilon_1 = 7$, $\varepsilon_2 = 1$, $\gamma_1 = 1.7$, $\gamma_2 = 2$, $\lambda = 4$ and $\eta = 8$.

($\mu = -5$). Figure 4.9 captures all five features of the experimental force-extension curves that we listed in chapter 2. In the next section we analyze the physical background of these features.

4.5. Explaining experimental observations

In section 4.4 we analyzed the overstretching transition of the 3-state Kuhn model as a function of μ. The results, as summarized in figure 4.9, show that the 3-state Kuhn model reproduces all features of the influence of intercalation that we observed in the experimental data of Vladescu *et al.* [21] (figure 2.4b). We now return to the five observations that we listed in section 2.2.2. The mathematical and graphical analysis of the 3-state Kuhn model allows us to give physical interpretations to these observations. We discuss each of the observations and analyze why they occur in the 3-state model. If we understand why the coarse-grained 3-state Kuhn model shows this behavior, we also understand the leading physical principles behind the changes in the real system. The five features of force-extension curves in the presence of intercalators, as listed in section 2.2.2, are

- A force shift of the overstretching transition as a function of intercalator concentration.
- An end-to-end length that is significantly larger than 1 for forces smaller than the overstretching force.
- An end-to-end length increase at forces smaller than the original overstretching force.
- An end-to-end length decrease at forces larger than the original overstretching force.
- The disappearance of the overstretching transition for large concentrations.

A force shift of the overstretching transition as a function of intercalator concentration.

The first intercalator-induced effect that we analyze is the most striking change in the force-extension curves: the shift of the overstretching force towards higher forces as a function of the intercalator concentration. We clearly observe this effect in figure 4.3 and quantified it in section 4.4. Obviously, the effect is caused by the increased influence of the intercalated state (state 2) in the model. Intercalated base pairs have a different length and a different free energy penalty than non-intercalated base pairs, thus they influence the force-extension curve. However, for a shift in the overstretching force to occur, as seen in figure 1.4b, another ingredient of the 3-state Kuhn model is essential: the cooperativity parameter η. Recall that η penalizes an interface between a Kuhn segment in state 1 and a Kuhn segment in state 2. Thus η represents a free energy penalty associated with an intercalated base pair neighboring an overstretched base pair. We introduced this cooperativity parameter based on the preliminary results of Biebricher *et al.* [98] in section 4.2.2, which suggest that such a free energy penalty might exist. We assumed that η is positive in the entire analysis of section 4.4, and here we show that the existence of a positive free energy penalty η is indeed essential for the shift of the overstretching transition. To do so, we plot the force-extension curves of figure 4.3 again, but we reduce η to 0. The result is plotted in figure 4.10.

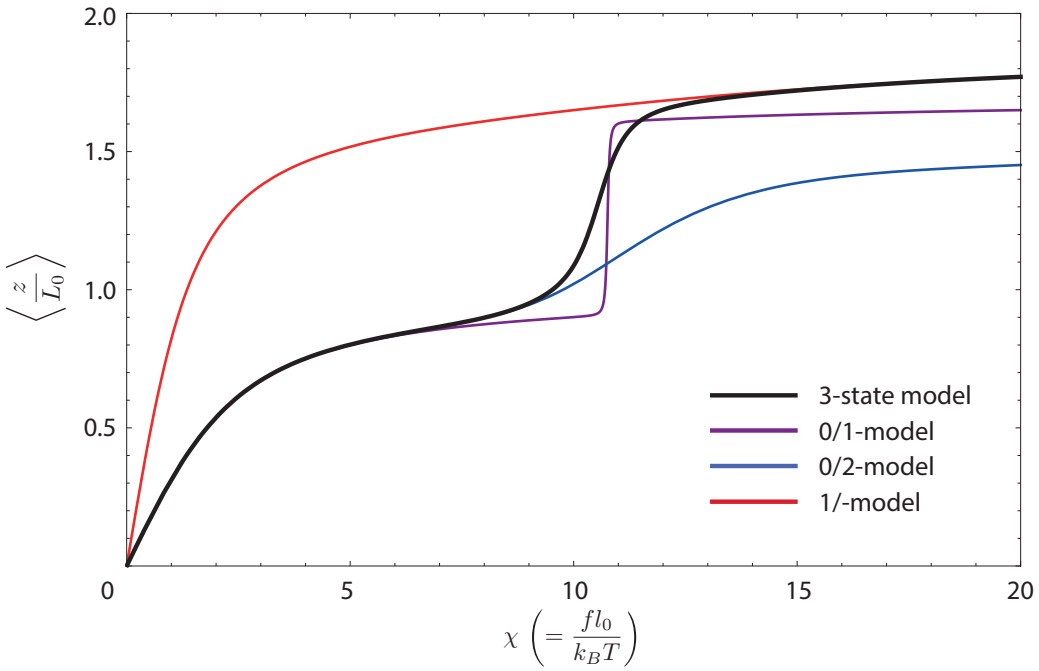

Figure 4.10: This figure shows the example of figure 4.3, but the free energy penalty for a 1/2-interface η is reduced to 0. The force-extension curve of the 3-state Kuhn model is shown (black), as well as the force-extension curves of the 0/1-model (purple), the 0/2-model (blue) and the 1/2-model (red). In the absence of a positive free energy penalty η, the overstretching transition does not shift towards higher forces as a function of μ. Instead, the overstretching transition directly disappears as soon as some Kuhn segments are intercalated. This shows that the existence of a positive η is essential for explaining the experimental data of figure 1.4b.

Figure 4.10 does not show a shift in the overstretching transition. On the contrary, it does not show a cooperative overstretching transition at all. To understand why η plays such an essential role in the shift of the overstretching transition, we consider what happens when the chemical potential μ approaches μ_{min} (equation 4.20) from below. At this chemical potential, the influence of state 2 in the 0/2-model starts around the same force as the influence of state

1 in the 0/1-model ($\chi_{00\to02} \approx \chi_{01}$). If η would be equal to 0, as in figure 4.10, states 1 and 2 could independently occur. This would lead to a macroscopic state where states 0, 1 and 2 are all present. At forces larger than the original overstretching force, $\chi > \chi_{01}$, state 1 has a lower free energy than state 0, so most Kuhn segments in state 0 are excited in state 1, while the intercalated Kuhn segments (state 2) are unaffected. This leads to a normalized extension that is larger than 1.7 because some segments are in state 1 ($\gamma_1 = 1.7$), while others are in state 2 ($\gamma_2 = 2$). Furthermore, the presence of intercalated Kuhn segments would break the cooperativity of the overstretching transition, because it allows the chain to have Kuhn segments in state 0 and Kuhn segments in state 1 in the chain simultaneously, without paying the free energy penalty λ. This is possible because the sequence of states 0-0-1-1 does pay the free energy penalty λ at the 0/1-interface, but the sequence of states 0-0-2-1-1 would not pay any interfacial free energy penalty. The 3-state Kuhn model in figure 4.10 indeed shows both these effects.

However, this picture completely changes when η is larger than 0. This penalizes a 1/2-interface, and states 1 and 2 cannot occur independently anymore. State 1 now pays a free energy penalty for interfaces with both state 0 and state 2, so both sequences 0-0-1-1 and 0-0-2-1-1 pay an energy penalty: λ for the 0/1-interface and η for the 1/2-interface respectively. Hence, the overstretching transition remains cooperative even in the presence of state 2. Furthermore, an extension of more than 1.7 is not observed at forces slightly higher than the overstretching force because states 1 and 2 do not occur simultaneously, and all Kuhn segments are in state 1 after the overstretching transition.

We have seen that a nonzero η is essential for a cooperative overstretching transition towards an elongation of 1.7 in the presence of intercalators. The last question we need to answer is why the overstretching force increases with μ. This is also an immediate consequence of η. It is caused by the fact that the overstretching transition does, in the presence of intercalators, not start from a chain with all segments in state 0. Instead, some Kuhn segments are in state 2 at the original overstretching force χ_{01}. Not only the Kuhn segments in state 0, but also the Kuhn segments in state 2, need to change into state 1 at the overstretching transition. However, changing a Kuhn segment from state 2 to state 1 costs more free energy than changing a Kuhn segment from state 0 to state 1 at that force. Thus, changing the partly intercalated chain into a completely overstretched chain is more difficult than changing a completely state 0 chain to a completely overstretched chain. So the force needs to do more work before the overstretching transition is realized, and the overstretching transition shifts towards higher forces.

An end-to-end length that is significantly larger than 1 for forces smaller than the overstretching force.

Now we understand why the overstretching transition shifts towards higher forces, this effect is straightforward to understand. We saw that the shifted overstretching transition is a transition from a chain that is partly intercalated to an overstretched chain. Intercalated DNA is longer than B-DNA, so the chain has a normalized end-to-end length of more than 1 just before it overstretches.

An end-to-end length increase at forces smaller than the original overstretching force.

This effect is closely related to the previous effect. The difference is that the previous effect answers why the end-to-end length is larger than 1 for forces lower than the *shifted* overstretching force, while here we discuss why the end-to-end length increases with μ for forces lower than the *original* overstretching force χ_{01} (equation 3.17). However, we just saw that the overstretching transition only shifts if there are already intercalated Kuhn segments at the original

overstretching force. Thus, for $\chi < \chi_{01}$, intercalators change the chain from a completely B-DNA state to a largely largely B-DNA state, with some intercalated Kuhn segments. State 2 (intercalated) is longer than state 0 (B-DNA), which causes the end-to-end length to increase.

An end-to-end length decrease at forces larger than the original overstretching force.

In between the original and the shifted transitions, the average segment length is in between l_0 and $\gamma_1 l_0 = 1.7\, l_0$, because in this force regime up to 50% of the Kuhn segments is intercalated, which corresponds to an average segment length of $\frac{\gamma_2+1}{2} l_0 = 1.5\, l_0$. The introduction of this effective state with a segment length in between those of states 0 and 1 causes both the end-to-end length decrease at $\chi > \chi_{01}$ and the increase at $\chi < \chi_{01}$.

The disappearance of the overstretching transition for large concentrations.

We studied this effect in section 4.4. We attribute this effect to the intercalator binding at every base pair at large μ. When $\mu \to \mu_{max}$ (equation 4.22), the overstretching transition shifts towards higher forces. At the same time, the free energy of the macroscopic 2/2-state decreases as a function of μ as well. Hence, the transition from state 1/1 to state 2/2 ($\chi_{11\to22}$) shifts towards lower forces. We saw in section 4.4 that when these transition forces are equal, the overstretching transition disappears. At such high chemical potentials, the free energy of the intercalated state is so low that the 0/2-model is favored over the 1/1-model even at forces that are normally not large enough to allow intercalation at every base pair. Hence, the overstretched state (state 1) itself disappears from the chain, and so does the overstretching transition.

We now understand the physical principles behind the five effects of intercalative binding on the location and extent of the overstretching transition of dsDNA. Thus, we have answered our research question and we have achieved the primary goal of this thesis. However, our 3-state Kuhn model allows for a further analysis of the influence of intercalators on the force-extension curve of dsDNA. The next two sections are dedicated to this further analysis.

4.6. A quantative comparison to experimental data

In section 4.4 we performed calculations on the effects of intercalator binding in the 3-state Kuhn model, and showed that the experimentally observed effects can be reproduced with the 3-state model. Now we seek to quantify the comparison between the 3-state model and the experimental data. First we study the shift of the overstretching force quantitatively, after which we determine values for the parameters in our model.

4.6.1. Quantifying the force shift of the overstretching transition

The experimental data of Vladescu *et al.* (figure 1.4b [21]) show the force-extension curves of dsDNA as a function of the ethidium concentration. Five of these curves show an overstretching transition. We plot the corresponding overstretching force as a function of concentration in figure 4.11.

Figure 4.11 shows that the overstretching force f_{over} in pN is a linear function of the intercalator concentration in the regime of 0 - 25 nM. We compare this to the quantative predictions of our 3-state Kuhn model. We calculated the overstretching force as a function of the chemical potential μ in section 4.4, resulting in equation 4.18. This expression shows that the dimensionless overstretching force $\chi_{02\to11}$ is a linearly increasing function of μ, which suggests that the overstretching force would increase logarithmically with the particle concentration, according to equation 4.3. This is in contradiction with the experimental data in figure 4.11.

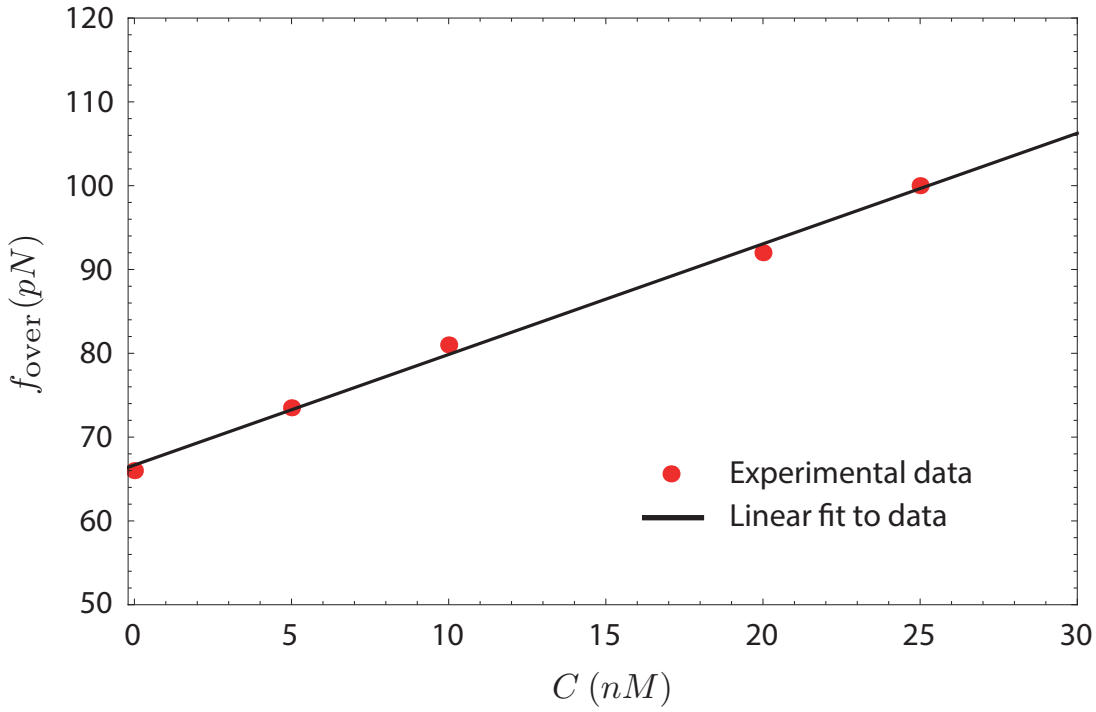

Figure 4.11: The overstretching force f_{over} in pN as a function of the intercalator concentration C in nM, according to the experimental data of Vladescu *et al.* [21]. The red dots correspond to the force-extension curves in figure 1.4b that show an overstretching transition. The black line gives a linear fit to the data.

However, equation 4.18 was derived in section 4.4 under the assumption that $\chi_{00\to02} << \chi << \chi_{02\to22}$. This assumption reflects that, at the overstretching force, the 0/2-model is in a 0/2-Neél state. In other words, this assumes that the force-extension curve of the 0/2-model is approximately flat at the overstretching transition. The 3-state curve overlaps with the 0/2-model at forces lower than the overstretching force, thus the 3-state curve is also assumed to be approximately flat before it overstretches. Figure 1.4b shows that this is not true for the experimental data. The extensions all increase significantly up to the overstretching transitions. This indicates that the overstretching transition occurs in the force regime $\chi \sim \chi_{00\to02}$, where the number of intercalated Kuhn segments is increasing as a function of force. This force regime is in between the regimes corresponding to equations 4.17 and 4.18. Therefore, we calculate the overstretching force as a function of μ in this regime by numerically solving $F_{02} = F_{11}$.

Based on figure 4.11, we expect the shift in the overstretching transition to be linear with intercalation concentration. So, using the relation between C and μ (equation 4.3), we expect the force shift to increase exponentially with the chemical potential μ. To check whether our model agrees with the data of the force-shift in figure 4.11, we plot the logarithm of the force shift, $\ln(\chi_{\text{over}}(\mu) - \chi_{\text{over}}(\mu \to -\infty))$, as a function of the chemical potential μ. Here $\chi_{\text{over}}(\mu)$ gives the overstretching force as function of the chemical potential, and $\chi_{\text{over}}(\mu \to -\infty)$ gives the overstretching transition in the absence of intercalators. The result is presented in figure 4.12.

Figure 4.12 uses the same model parameters as figures 4.6, 4.7 and 4.8 ($\gamma_1 = 1.7$, $\gamma_2 = 2$, $\varepsilon_1 = 7$, $\varepsilon_2 = 1$, $\delta = 4$, $\eta = 8$ and $\lambda = 4$), but the chemical potential μ is varied from -16 to -8. This includes the examples of both figure 4.6 ($\mu = -16$) and figure 4.7 ($\mu = -8.5$). The fit shows the linear dependence of the logarithmic force-shift as a function of μ. Thus, we can write

$$\ln\Big[\chi_{\text{over}}(\mu) - \chi_{\text{over}}(\mu \to -\infty)\Big] \;=\; a \cdot \mu + b, \tag{4.25}$$

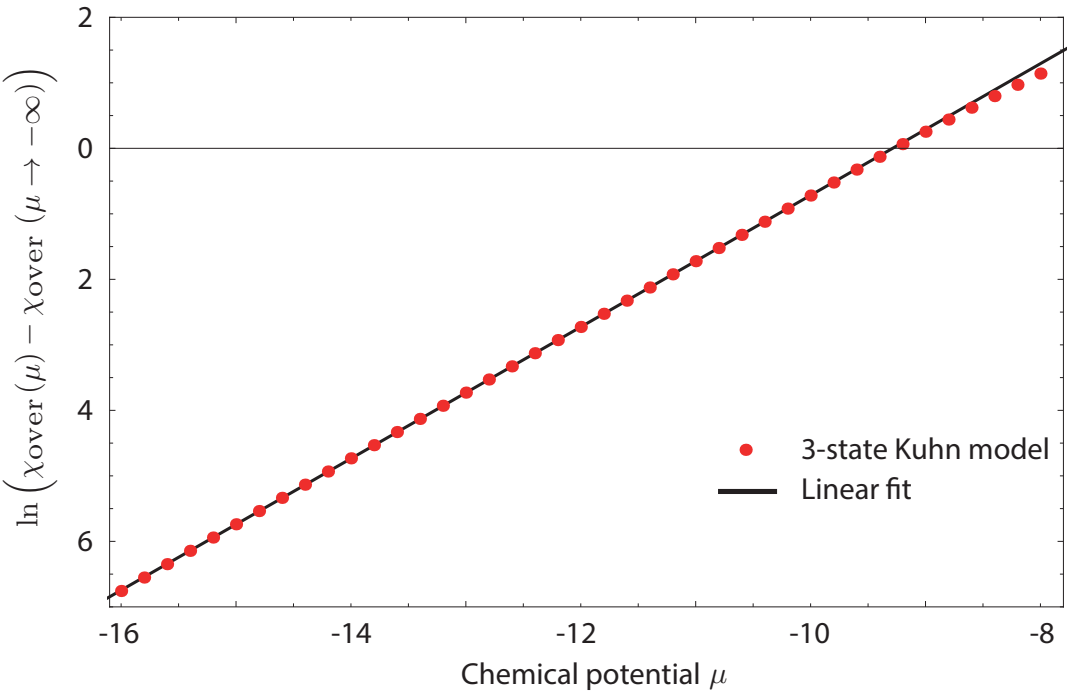

Figure 4.12: The logarithm of the force shift of the overstretching transition in the 3-state Kuhn model is plotted as a function of the chemical potential, in the regime where $\chi \sim \chi_{00\to02}$. The red dots are produced by numerically equating the free energies of the 0/2-model and the 1/1-model, $F_{02} = F_{11}$. The fit shows that this logarithm increases linearly with the chemical potential, so the force shift itself increases exponentially with the chemical potential. The validity of this exponential regime ends around $\mu = -9$, where the dots start deviating from the fit. The model parameters used for this plot are $\gamma_1 = 1.7$, $\gamma_2 = 2$, $\varepsilon_1 = 7$, $\varepsilon_2 = 1$, $\delta = 4$, $\eta = 8$ and $\lambda = 4$.

where a and b are the slope and intercept of the linear fit respectively. We now rewrite this expression,

$$\begin{aligned}\chi_{\text{over}}(\mu) &= \chi_{\text{over}}(\mu \to -\infty) + \exp(a \cdot \mu + b) \\ &= \chi_{\text{over}}(\mu \to -\infty) + \exp\left(a \ln\left(\frac{C}{55.6}\right) + b\right) \\ &= \chi_{\text{over}}(\mu \to -\infty) + \exp(b) \cdot \left(\frac{C}{55.6}\right)^a, \end{aligned} \tag{4.26}$$

where we used equation 4.3 in the second step. We now determine the dependence of the fitting parameters a and b on the parameters of the 3-state Kuhn model to compare our model to the experimental data. We omit the analysis and present the results directly. First, the slope a is independent of all model parameters and is always equal to 1. Thus, the 3-state Kuhn model gives a linear dependence of the overstretching force on the concentration,

$$\chi_{\text{over}}(\mu) = \chi_{\text{over}}(\mu \to -\infty) + \frac{\exp(b)}{55.6} \cdot C, \tag{4.27}$$

which agrees with the experimental data shown in figure 4.11. The value of the intercept b does depend on the system parameters, and is given by

$$b = \frac{\gamma_2 - 1}{\gamma_1 - 1}\varepsilon_1 - \varepsilon_2 + b_{corr}, \tag{4.28}$$

where b_{corr} is a correction on the value of b that depends on γ_1 and γ_2, which we neglect for

simplicity. To understand the value of the intercept, we substitute it in the first line of equation 4.26,

$$\chi_{\text{over}}(\mu) = \chi_{\text{over}}(\mu \to -\infty) + \exp\left(\mu + \frac{\gamma_2 - 1}{\gamma_1 - 1}\,\varepsilon_1 - \varepsilon_2\right). \tag{4.29}$$

We note that the value of b is exactly minus the smallest chemical potential that shifts the overstretching transition, μ_{min} (equation 4.20). So we can rewrite equation 4.29 to obtain

$$\chi(\mu) = \chi(\mu \to -\infty) + \exp(\mu - \mu_{min}). \tag{4.30}$$

This gives a new interpretation of μ_{min}. Since the overstretching transition shifts exponentially with μ, there is no smallest chemical potential that shifts the overstretching transition. Instead, it is the characteristic chemical potential of the exponential increase of the overstretching force. The exponential nature of this force-shift is related to the exponential increase, as a function of force, of intercalated Kuhn segments in the force-regime before the overstretching transition. This exponential increase of intercalated segments was found by Biebricher *et al.* [98] and by Roel Roijmans [54], and is also predicted by our 3-state Kuhn model.

We emphasize that equations 4.25 to 4.30 are only valid for relatively small shifts in the overstretching transition. The validity of these equations ends when either the overstretching transition enters the force regime where the 0/2-model shows the alternating 0/2-state (in which case equation 4.18 is valid) or when the overstretching transition disappears because $\mu > \mu_{max}$ (equation 4.22). In figure 4.12 this is observed at a chemical potential of about -9, where the calculations start to deviate from the linear fit.

4.6.2. The parameters of the 3-state Kuhn model

In this section we connect the theory of the 3-state Kuhn model to available experimental data to determine values for the parameters of the model, γ_1, γ_2, ε_1, ε_2, λ, δ, and η.

To start with, the introduction of intercalators in the model cannot change the parameters that are related to overstretched DNA (state 1) only. Thus, $\varepsilon_1 = 3.2$, $\lambda = 4$ and $\gamma_1 = 1.7$. Furthermore, we already know that $\gamma_2 = 2$ based on the biological background information of section 2.1. This leaves the free energies ε_2, δ and η. We start by estimating the free energy penalty δ, that penalizes interfaces between two intercalated Kuhn segments and is thus responsible for the neighbor-exclusion principle (section 2.1). We saw that δ dictates the position of the transition between the macroscopic states 0/2 and 2/2 in the 0/2-model (equation 4.10). Unfortunately, the 3-state Kuhn model does not show this transition under the circumstances used for obtaining figure 1.4b. The 3-state model shows, however, that the window of chemical potentials that shift the overstretching transition is a function of δ as well (equation 4.24). We now estimate δ by studying the force-extension curves in figure 1.4b that are influenced by intercalators. The figure shows overstretching transitions for the curves with concentrations of 0, 5, 10, 20 and 25 nM. The 5 nM curve shows a shift of the overstretching transition of about 8 pN, corresponding to 0.7 in dimensionless units according to the definition of $\chi \equiv \frac{fl_0}{k_BT}$. Thus, it corresponds roughly to μ_{min}, which would show a shift of 1 in dimensionless units (equation 4.30). Hence, figure 1.4b shows a concentration increase with a factor 5 (25 nM with respect to 5 nM), corresponding to an increase in μ of $\ln(5) \approx 1.6$. From this, the minimum value of δ in the experimental data is ~ 3, obtained by equation 4.24. However, the first force-extension curve that does not show an overstretching transition is obtained with a concentration of 125 nM, which corresponds to a factor 25 concentration increase, or an increase in μ of $\ln(25) \approx 3.2$. Thus, the maximum value of δ is determined by equation 4.24 to be ~ 6. Thus we estimate the cooperatity parameter δ to be between 3 and 6. More data in between concentrations 25 nM and 125 nM is required to give a better estimate.

Next, we evaluate ε_2. Recall that $\varepsilon_2 - \mu$ is the free energy penalty for state 2. We relate μ to the experimental intercalator concentration C according to equation 4.3, which gives the

value of μ for every force-extension curve in figure 1.4b. We use these values, together with the linear shift of the overstretching force as a function of concentration, to calculate ε_2. We found this linear dependence both in the experimental data of Vladescu *et al.* [21] (figure 4.11) and in our theory (equation 4.27). To compare theory and experiment, we first multiply the theoretical result, equation 4.27, by $\frac{k_BT}{l_0}$ to obtain the dimension of force, substitute equation 4.28 for b, and then equate the experimentally and theoretically found slopes to obtain ε_2. The slope of figure 4.11 is 1.3 pN/nM, thus

$$\frac{k_BT \exp\left(\frac{\gamma_2-1}{\gamma_1-1}\varepsilon_1 - \varepsilon_2\right)}{55.6\, l_0} \cdot C \;=\; 1.3 \cdot 10^9 \cdot C, \tag{4.31}$$

where the slope of figure 4.11 is multiplied by 10^9 because C is the intercalator concentration in M (instead of nM), and $\frac{k_BT}{l_0}$ is expressed in pN. We solve equation 4.31 for ε_2 and substitute the known values of ε_1, γ_1 and γ_2, to obtain $\varepsilon_2 \approx -18$. Thus the free energy penalty $\varepsilon_2 = -18k_BT$, where the minus sign shows that it is actually a free energy bonus. ε_2 contains contributions from deformations in the dsDNA and from the binding free energy of an intercalator. Since state 2 is not observed experimentally [12, 13], the deformation in the dsDNA is very likely to give a positive contribution to ε_2. Thus, the binding free energy of dsDNA intercalation is a free energy bonus of at least $\sim 20\, k_BT$. The other free energies in our model ($\varepsilon_1 = 3.2$, $\lambda = 4$, $3 < \delta < 6$) are significantly smaller, so the question arises why this interaction free energy is so large. However, we are not the first to find free energies for interactions between dsDNA and intercalators in this order. For example, Řeha *et al.* [99] found stacking energies between ethidium and A-T base pairs, at a mutual distance of 0.33 nm, in the order of $\sim 38\, k_BT$ using computer simulations. Note that 0.33 nm is approximately the distance between ethidium and the nearest base pair in intercalated dsDNA, since it is half the distance between neighboring base pairs. Using similar methods, the stacking energies between different base pairs were found to be in the order of $-11\, k_BT$ to $-19\, k_BT$, depending on the type of nucleotide [100]. The difference between these interactions gives an indication of the binding free energy for intercalation, and this difference is indeed in the order of $-20k_BT$. Řeha and co-workers attributed this large interaction free energy to electrostatic and dispersion forces, because the intercalator is electrically charged and highly polarizable [99]. Indications for the role of electrostatics were also found experimentally: Waring [89] found that an increasing salt concentration in the solution significantly decreases the interaction strength between dsDNA and ethidium. This suggests that the electrostatic interaction is reduced due to charge screening. Additionally, other effects might contribute to the binding free energy as well. For example, hydrophobic forces are suggested to play a role in ethidium-dsDNA interactions [101]. This might be related to the fact that ethidium molecules, which are partly hydrophobic, break their contact with water when they intercalate dsDNA. We perform a rough estimate of this hydrophobic interaction energy to check whether this force could play a significant role. We estimate the surface of an ethidium molecule to be in the order of 1 nm^2, based on the size of a C-C bond ($0.120 - 0.154$ nm [102]), while the hydrophobic interaction free energy of a hydrophobic object with water is about $7\, k_BT\, \mathrm{nm}^{-2}$ [93]. Since an ethidium molecule has two sides, the total hydrophobic energy is in the order of $14k_BT$. This estimate shows that hydrophobic forces might, next to electrostatic and dispersion forces, play a significant role in the binding free energy of ethidium to dsDNA.

The last parameter is the cooperativity parameter η, which penalizes 1/2-interfaces. We concluded (section 4.5) that a positive value of η is essential for the shift of the overstretching force. However, to obtain a number for η we need to observe coexistence of states 1 and 2. We do not clearly observe such coexistence in the experimental data, so we can only determine a lower limit for η. Figure 1.4b shows that the overstretching transition remains very sharp even when the force shift is rather large, which is the case in the 25 nM curve. Our model shows that the width of the overstretching transition is inversely proportional to the difference in length

between the state before the transition and the state after the transition. In the case of the 25 nM curve, this difference is rather small, but still the overstretching transition remains sharp. We conclude form this that η must be relatively large. By comparing the data to our model, we estimate $\eta \gtrsim 6$. More information about η could be obtained from experimental data of even higher forces, a regime that we discuss in section 4.7.

Summarizing, we have used experimental data to find estimates for all our model parameters. The elongation factors are $\gamma_1 = 1.7$ and $\gamma_2 = 2$, the cooperativity parameters are given by $\lambda = 4$, $3 < \delta < 6$ and $\eta > 6$, and the free energy penalties for states 1 and 2 are given by $\varepsilon_1 = 3.2$ and $\varepsilon_2 = -18$. All free energies (λ, δ, η, ε_1 and ε_2) are given in units of the thermal energy k_BT. We conclude this section by comparing the resulting force-extension curves to experimental data. Figure 4.13 shows the theoretical curves (a) corresponding to the experimental data [21] in (b). Note that the axes of the theoretical plot (figure 4.13a) are adjusted to the axes of the experimental plot to allow for a better comparison. Furthermore, note that the extension axis in figure (b) starts at 0.25 nm instead of 0.

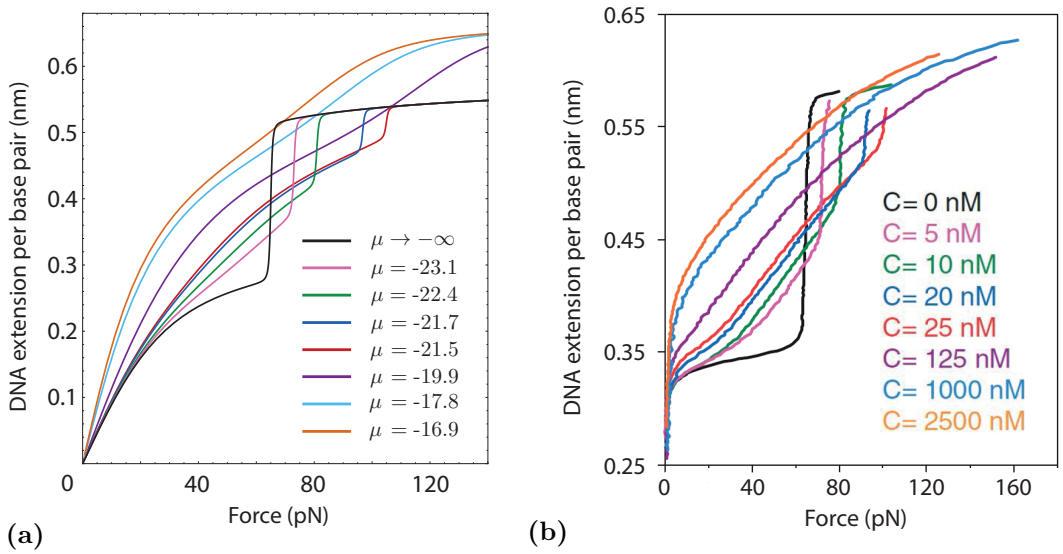

Figure 4.13: The theoretical force-extension curves of the 3-state Kuhn model (a) corresponding to the experimental data of Vladescu *et al.* [21] in (b). The chemical potentials in (a) correspond to the concentrations in (b) according to equation 4.3, and corresponding curves in (a) and (b) are plotted in the same color. The similarity between (a) and (b) is evident. The low-force regimes differ because of the lack of bend stiffness in the model. The force shift of the overstretching transition, however, is captured very well in the theoretical curves. The theoretical high concentration curves ($\mu = -19.9$, $\mu = -17.8$ and $\mu = -16.9$) also resemble the experimental curves very well.

The chemical potentials in figure (a) are chosen such that they correspond to the concentrations in figure (b), according to equation 4.3. Corresponding curves are plotted in the same color. The agreement between figures 4.13a and 4.13b is evident. The low-force regime of the theoretical curves (a) deviates from the the experimental curves (b) due to the previous discussed absence of bend stiffness. However, the observed force shift of the overstretching transition is captured very well in the theoretical curves, as well as the disappearance of the overstretching transition for higher concentrations and the corresponding elongations beyond 1.7. The theoretical high-concentration curves ($\mu = -19.9$, $\mu = -17.8$ and $\mu = -16.9$) deviate slightly from the experimental curves because they show slightly larger extensions than the corresponding experimental curves. This is best seen around the force of the original overstretching transition (65 pN), where the experimental curves intersect the zero-intercalator (black) curve at lower extension than the theoretical curves do. This is probably related to bend stiffness. Husale *et*

al. [103] and Vladescu *et al.* [20] found that the persistence length of ethidium intercalated dsDNA is smaller than the persistence length of bare dsDNA. The high-concentration curves represent dsDNA with a high degree of intercalation, so this explains why the theoretical curves slightly overestimate the length increase of the high-concentrations curves with respect to the low concentration curves.

We conclude with the observation that figure 4.13 shows that the theoretical curves resemble the experimental curves very well, and that the 3-state Kuhn model captures all essential features of the influence of intercalative particle binding on the overstretching transition of dsDNA.

4.7. Intercalation at every base pair in the high-force regime

We conclude this chapter by analyzing a regime in the force-extension curve that is not described in the data of Vladescu *et al.* [21]. This is the force regime well above the overstretching transition. The force-extension curves of figure 4.13b stop in or shortly after the overstretching transition. In this section we predict the behavior of these force-extension curves in higher force-regimes. Our 3-state Kuhn model has shown to work very well at forces around the overstretching force, and now we explore its behavior in this highest-force regime.

The high-concentration curves in figure 4.13 ($\mu = -19.9$, $\mu = -17.8$ and $\mu = -16.9$) show normalized extensions of more than 1.7, approaching 2. We interpret this as a violation of the neighbor-exclusion principle (section 2.1), leading to intercalation at every base pair. However, the 3-state Kuhn model also predicts this violation for lower chemical potentials. We predict that the curves in figure 4.13b that show a shift in the overstretching force (5, 10, 20 and 25 nM) would show this violation as well if the curves would be extended to larger forces. In other words, we predict that these curves also show a normalized extension that approaches 2 if the stretching force is increased sufficiently.

We base this prediction on our analysis of the 0/2- and 1/2-models. Both show that, if forces are sufficiently large, the macroscopic 2/2-state will be excited (figures 4.4 and 4.5). In this state the neighbor-exclusion principle is violated and every base pair is intercalated. This is caused by the fact that the stretching force does work on the chain. The macroscopic 2/2-state corresponds to the longest possible molecular chain, twice as long as B-DNA. Hence, the 2/2-state maximizes the work that the stretching force can do. If this force is sufficiently large, the work dominates the free energy penalties, including δ, and thus violates the neighbor-exclusion principle. Recall from chapter 2 that the exclusion principle is believed [21] to be mediated by structural changes in the dsDNA backbone, rather than by direct steric repulsion. The large stretching forces promote these structural changes because they allow the force to do more work.

To demonstrate this effect, we show the force-extension curves of figure 4.13a again, but now we extend the force axis to 240 pN. The result is given in figure 4.14. It shows that, indeed, all force-extension curves approach a normalized length of 2 (0.68 nm per base pair) if the force is large enough. The only exception is the black curve, which represents dsDNA in the absence of intercalative binding. The curves show cooperative transitions from the 1/1-model to the 0/2-model, as discussed in section 4.4. The corresponding transition forces can be calculated by solving $F_{02} = F_{11}$. If $\chi >> \chi_{02\rightarrow 22}$, the solution can be approximated by equation 4.19. This approximation is accurate for the $\mu = -23.1$ and $\mu = -22.4$ curves in figure 4.14. The cooperativity parameter of the transition is given by $\eta - \frac{1}{2}\delta$ (section 4.3.2). We estimated $3 < \delta < 6$ and $\eta > 6$ for ethidium binding to dsDNA, so the transition is indeed cooperative. However, it is possible that there exist DNA-intercalator complexes for which $\eta < \frac{1}{2}\delta$, in which case the transition to state 2/2 at high forces would be anti-cooperative.

In our analysis of the high-force regime we have assumed that the DNA molecule does not rupture if stretching forces of the order of 100 pN are applied. The 3-state Kuhn model does not take breaking into account, so we cannot predict whether this assumption is valid. However, it is reported in literature [3] that dsDNA molecules have been stretched to forces in the order

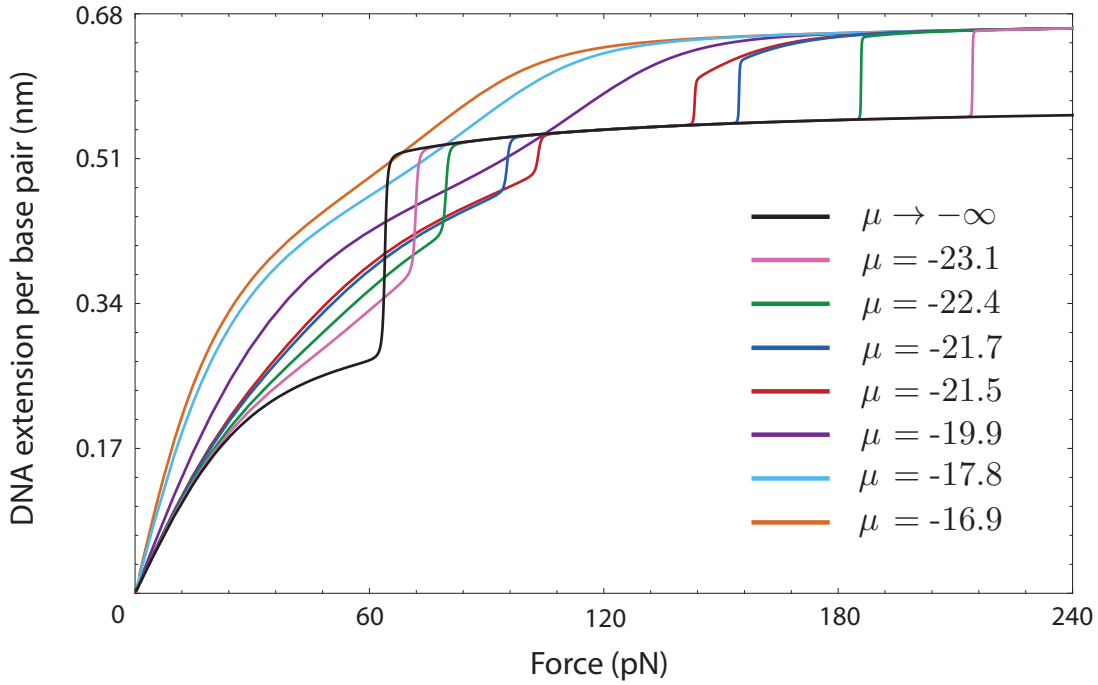

Figure 4.14: The force-extension curves of figure 4.13a are plotted again, but the force axis is extended to a force of 240 pN. The 3-state Kuhn model predicts that, in the presence of intercalating dye, all force-extension curves are stretched to a state in which every Kuhn segment (base pair) is intercalated, if the stretching force is large enough. This violation of the neighbor-exclusion principle is attributed to the work done by the stretching force, which overcomes the free energy penalty δ at high forces. The higher the chemical potential is, the smaller the force that is required for intercalation at every base pair.

of 1000 pN before they broke. Under the circumstances of these experiments, we expect to find intercalation at every base pair before the DNA molecule breaks.

Summarizing, our model explains normalized extensions that are larger than 1.7, which are observed in experimental data [21] at large concentrations, by violation of the neighbor-exclusion principle. Our model predicts that large stretching forces also induce violation of this exclusion principle. In both cases this happens because state 2 is energetically favored over the other states. In the first case state 2 is favored because its free energy penalty, $\varepsilon_2 - \mu$, becomes small if the chemical potential μ is large enough. In the latter case state 2 is favored because it is longer than the other states, and thus favored because it allows the stretching force to do more work.

Chapter 5

Conclusions & outlook

This chapter is concerned with the main conclusions of our work, followed by an outlook to possible future research. We finish with a section in which we discuss the technological relevance of our work.

5.1. Conclusions

In this thesis we developed multi-state Kuhn models to gain an understanding of the physical principles behind the effect of intercalative particle binding on the location and magnitude of the overstretching transition of double-stranded DNA. We performed an analysis on experimental data of this effect, and used this analysis as a starting point of our theoretical study. We concluded that a 2-state Kuhn model, while appropriate for bare dsDNA, is not sufficient for explaining the influence of intercalators on the high-force regime of the force-extension curve. We expanded our model with a third molecular state, representing intercalated DNA, obtaining the 3-state Kuhn model. We compared our theory to experimental data to estimate numbers for the parameters in the 3-state Kuhn model. Using these numbers to produce force-extension curves, we showed remarkable agreement between the experimental and theoretical curves in the high-force regime. This demonstrates that our 3-state Kuhn model captures all essential features of the effect of intercalative particle binding on the overstretching transition of double-stranded DNA, and therefore that the 3-state Kuhn model gives an appropriate description of dsDNA-intercalator complexes.

The agreement between our theory and experimental data allowed us to explain what physical principles dictate the intercalator-induced changes in the force-extension curve of dsDNA. The most remarkable changes that are observed in experimental data are the intercalator-induced shift of the overstretching force and the total disappearance of the overstretching transition for large intercalator concentrations. Both effects, as well as smaller side effects, can completely be explained by the introduction of a third molecular state, in addition to B-DNA and overstretched DNA. This third state is twice as long as B-DNA, and is excited by anti-cooperative binding of intercalators. This leads to a molecular chain that is partly intercalated at average intercalator concentrations, with an effective length that is in between those of B-DNA and overstretched DNA. We showed that this partly intercalated DNA is energetically favored over overstretched DNA, which causes the overstretching transition to shift towards higher forces. When the intercalator concentration is increased further, the anti-cooperative nature of binding can be overcome, which leads to intercalation at every base pair. This causes the overstretching transition to disappear. Moreover, we showed that a free energy penalty for an interface between overstretched DNA and intercalated DNA is essential in order to obtain the force shift of the overstretching transition.

Finally, our 3-state Kuhn model predicts the force-extension curve of dsDNA-intercalator complexes in the force-regime beyond the overstretching transition. This force-regime is not

reported in experimental literature. We predict that every dsDNA molecule in the presence of intercalators will eventually elongate to a length that is twice the original contour length, if the stretching force is large enough. This elongation is caused by intercalation of every base pair at such a stretching force. This effect should be visible in force-extension data, but also in fluorescence data.

5.2. Outlook

In this thesis we focused on gaining a deeper understanding of the physical principles behind the effect of intercalative binding on the force-extension curve of double-stranded DNA. We kept our model as simple as possible, because this allowed us to analyze the mathematical and physical properties of our model extensively. This analysis enabled us to understand the physical principles behind the effect of intercalators on the overstretching transition of dsDNA, and therefore it enabled us to achieve our goal. A consequence of this approach is that we neglected certain dsDNA properties that were not essential for gaining the desired understanding. The best example of this is the absence of bend stiffness in our model, which causes our low-force regime to deviate from the experimentally observed low-force regime. A straightforward extension of our model would include bend stiffness between adjacent Kuhn segments. Another possible extension of the 3-state Kuhn model would be the introduction of extensible Kuhn segments, which would behave like Hookean springs instead of perfectly rigid rods. However, the stretch modulus of B-DNA is known to be well above 1000 pN [15, 31]. Upon overstretching, the stretch modulus of dsDNA is even increased by an order of magnitude [15]. Since overstretching occurs around 65 pN, we do not expect that introducing extensibility of Kuhn segments would induce significant changes in the model. The force-extension relation of an extended 3-state Kuhn model could be calculated numerically and used to fit experimental data. We predict that the introduction of bend stiffness, and possibly the extensibility of Kuhn segments, is sufficient for obtaining a good fit to experimental data.

We suggest that an other important future direction is the introduction of reaction dynamics to our model. We have focused on equilibrium only, because this was appropriate for the experimental data that we explained. However, some intercalators show much slower binding kinetics than those of ethidium [48, 98, 104, 105]. This results in intercalative binding on timescales in the order of or larger than the timescale of stretching. Our theory is inappropriate for such intercalators because we assume the complete system to be in thermal, mechanical and chemical equilibrium. Indeed, experimentalists find different force-dependent behavior for these intercalators, including hysteresis effects [48, 98, 105]. A useful extension of our 3-state Kuhn model would be the the introduction of binding kinetics, which should lead to a dynamic model for intercalative binding that is valid for both fast and slow intercalators. In addition, a dynamic model could be used to study the distribution of overstretched and intercalated Kuhn segments on the dsDNA molecule, whereas we have only discussed the average degree of overstretching and intercalation on the dsDNA molecule.

5.3. Technological relevance

In the introduction of this thesis we described the motivation for our work. Intercalative binding to double-stranded DNA is an important mechanism in the study of dsDNA using fluorescent dyes. The interaction of intercalators with dsDNA has also been studied for the purpose of rational drug design, and it is likely that intercalation plays a role in certain cellular processes that involve particle binding to dsDNA. Our work contributes to a better understanding of dsDNA-intercalator interactions and therefore contributes to the understanding of the processes described above.

However, our work also has potential applicability in the context of designer materials. Double-stranded DNA has shown to be a very interesting material in this context. Branched dsDNA molecules have been used to create two and three dimensional structures completely composed of DNA, ranging from a μm to a cm scale [6–8, 106]. Suggested applications of these designed DNA structures include nanorobotics [6] and biomedical applications such as drug delivery, tissue engineering and cell transplant therapy [106]. Um *et al.* [106] report that the properties of these dsDNA structures can be tuned by using other molecules to interact with the dsDNA. They suggest that this allows DNA to be engineered as a designer material. Our work on the interactions between dsDNA and intercalative molecules might be applied in this context, where intercalators might be used to control the mechanical properties of the DNA structures. The insights about these interactions obtained in our work might assist the rational design of the properties of such structures.

Finally, our methods might be applied in a wider context of interactions between small molecules and macromolecules. We modeled the interaction between intercalators and dsDNA, but due to our method of coarse-graining we only used a few typical properties of these interactions. We largely worked with phenomenological free energies. The success of this approach in our work suggests that similar approaches might be successful in other interactions between macromolecules and small molecules as well.

References

[1] B. Alberts, A. Johnson, J. Lewis, M. Raff, K. Roberts, and P. Walter, *Molecular biology of the cell*. Garland Science, 2008.

[2] T. Strick, J.-F. Allemand, V. Croquette, and D. Bensimon, "Twisting and stretching single dna molecules," *Progress in Biophysics and Molecular Biology*, vol. 74, no. 1–2, pp. 115 – 140, 2000. Single Molecule Biochemistry and Molecular Biology.

[3] C. Bustamante, S. B. Smith, J. Liphardt, and D. Smith, "Single-molecule studies of dna mechanics," *Current Opinion in Structural Biology*, vol. 10, no. 3, pp. 279 – 285, 2000.

[4] C. Bustamante, Z. Bryant, and S. B. Smith, "Ten years of tension: single-molecule dna mechanics," *Nature*, vol. 421, no. 6921, pp. 423–427, 2003.

[5] S. Kumar and G. Mishra, "Stretching single stranded dna," *Soft Matter*, vol. 7, no. 10, pp. 4595–4605, 2011.

[6] N. C. Seeman, "Structural dna nanotechnology," in *NanoBiotechnology Protocols* (S. Rosenthal and D. Wright, eds.), vol. 303 of *Methods in Molecular Biology™*, pp. 143–166, Humana Press, 2005.

[7] N. C. Seeman, "From genes to machines: Dna nanomechanical devices," *Trends in biochemical sciences*, vol. 30, no. 3, pp. 119–125, 2005.

[8] N. C. Seeman, "An overview of structural dna nanotechnology," *Molecular Biotechnology*, vol. 37, no. 3, pp. 246–257, 2007.

[9] T. Strick, J.-F. Allemand, D. Bensimon, A. Bensimon, and V. Croquette, "The elasticity of a single supercoiled dna molecule," *Science*, vol. 271, no. 5257, pp. 1835–1837, 1996.

[10] S. B. Smith, L. Finzi, and C. Bustamante, "Direct mechanical measurements of the elasticity of single dna molecules by using magnetic beads," *Science*, vol. 258, no. 5085, pp. 1122–1126, 1992.

[11] C. Bustamante, J. Marko, E. Siggia, and S. B. Smith, "Entropic elasticity of lambda-phage dna," *Science*, vol. 265, p. 1599, 1994.

[12] P. Cluzel, A. Lebrun, C. Heller, R. Lavery, J.-L. Viovy, D. Chatenay, and F. Caron, "Dna: An extensible molecule," *Science*, vol. 271, no. 5250, pp. 792–794, 1996.

[13] S. Smith, Y. Cui, and C. Bustamente, "Overstretching b-dna: The elastic response of individual double-stranded and single-stranded dna molecules," *Science*, vol. 271, no. 5250, pp. 795–799, 1996.

[14] P. Flory, *Statistical Mechanics of Chain Molecules*. Interscience, 1969.

[15] C. Storm and P. C. Nelson, "Theory of high-force dna stretching and overstretching," *Phys. Rev. E*, vol. 67, p. 051906, 2003.

[16] O. Kratky and G. Porod, "Röntgenuntersuchung gelöster fadenmoleküle," *Recl. Trav. Chim. Pays-Bas*, vol. 68, pp. 1106–1122, 1949.

[17] N. Saito, K. Takahashi, and Y. Yunoki, "The statistical mechanical theory of stiff chains," *Journal of the Physical Society of Japan*, vol. 22, no. 1, pp. 219–226, 1967.

[18] J. F. Marko and E. D. Siggia, "Stretching dna," *Macromolecules*, vol. 28, no. 26, pp. 8759–8770, 1995.

[19] S. Cocco, J. Yan, J.-F. Léger, D. Chatenay, and J. F. Marko, "Overstretching and force-driven strand separation of double-helix dna," *Phys. Rev. E*, vol. 70, p. 011910, 2004.

[20] I. D. Vladescu, M. J. McCauley, M. E. Nuñez, I. Rouzina, and M. C. Williams, "Quantifying force-dependent and zero-force dna intercalation by single-molecule stretching," *Nature methods*, vol. 4, no. 6, pp. 517–522, 2007.

[21] I. D. Vladescu, M. J. McCauley, I. Rouzina, and M. C. Williams, "Mapping the phase diagram of single dna molecule force-induced melting in the presence of ethidium," *Phys. Rev. Lett.*, vol. 95, p. 158102, 2005.

[22] I. Rouzina and V. A. Bloomfield, "Force-induced melting of the {DNA} double helix 1. thermodynamic analysis," *Biophysical Journal*, vol. 80, no. 2, pp. 882 – 893, 2001.

[23] I. Rouzina and V. A. Bloomfield, "Force-induced melting of the {DNA} double helix. 2. effect of solution conditions," *Biophysical Journal*, vol. 80, no. 2, pp. 894 – 900, 2001.

[24] M. C. Williams, I. Rouzina, and M. J. McCauley, "Peeling back the mystery of dna overstretching," *Proceedings of the National Academy of Sciences*, vol. 106, no. 43, pp. 18047–18048, 2009.

[25] H. Fu, H. Chen, J. F. Marko, and J. Yan, "Two distinct overstretched dna states," *Nucleic acids research*, p. gkq309, 2010.

[26] X. Zhang, H. Chen, H. Fu, P. S. Doyle, and J. Yan, "Two distinct overstretched dna structures revealed by single-molecule thermodynamics measurements," *Proceedings of the National Academy of Sciences*, vol. 109, no. 21, pp. 8103–8108, 2012.

[27] X. Zhang, H. Chen, S. Le, I. Rouzina, P. S. Doyle, and J. Yan, "Revealing the competition between peeled ssdna, melting bubbles, and s-dna during dna overstretching by single-molecule calorimetry," *Proceedings of the National Academy of Sciences*, vol. 110, no. 10, pp. 3865–3870, 2013.

[28] J. R. Wenner, M. C. Williams, I. Rouzina, and V. A. Bloomfield, "Salt dependence of the elasticity and overstretching transition of single dna molecules," *Biophysical journal*, vol. 82, no. 6, pp. 3160–3169, 2002.

[29] J. F. Allemand, D. Bensimon, R. Lavery, and V. Croquette, "Stretched and overwound dna forms a pauling-like structure with exposed bases," *Proceedings of the National Academy of Sciences*, vol. 95, no. 24, pp. 14152–14157, 1998.

[30] J. F. Leger, G. Romano, A. Sarkar, J. Robert, L. Bourdieu, D. Chatenay, and J. F. Marko, "Structural transitions of a twisted and stretched dna molecule," *Phys. Rev. Lett.*, vol. 83, pp. 1066–1069, 1999.

[31] P. Nelson, *Biological Physics: Energy, Information, Life*. W. H. Freeman, 2003.

[32] K. Morikawa and M. Yanagida, "Visualization of individual dna molecules in solution by light microscopy: Dapi staining method," *Journal of biochemistry*, vol. 89, no. 2, pp. 693–696, 1981.

[33] S. Matsumoto, K. Morikawa, and M. Yanagida, "Light microscopic structure of dna in solution studied by the 4',6-diamidino-2-phenylindole staining method," *Journal of Molecular Biology*, vol. 152, no. 2, pp. 501 – 516, 1981.

[34] A. N. Glazer and H. S. Rye, "Stable dye-dna intercalation complexes as reagents for high-sensitivity fluorescence detection," *Nature*, vol. 359, no. 6398, pp. 859–861, 1992.

[35] P. R. Bianco, L. R. Brewer, M. Corzett, R. Balhorn, Y. Yeh, S. C. Kowalczykowski, and R. J. Baskin, "Processive translocation and dna unwinding by individual recbcd enzyme molecules," *Nature*, vol. 409, no. 6818, pp. 374–378, 2001.

[36] C. Monico, M. Capitanio, G. Belcastro, F. Vanzi, and F. S. Pavone, "Optical methods to study protein-dna interactions in vitro and in living cells at the single-molecule level," *International journal of molecular sciences*, vol. 14, no. 2, pp. 3961–3992, 2013.

[37] I. Heller, T. P. Hoekstra, G. A. King, E. J. Peterman, and G. J. Wuite, "Optical tweezers analysis of dna–protein complexes," *Chemical reviews*, vol. 114, no. 6, pp. 3087–3119, 2014.

[38] P.-M. Lam and Y. Zhen, "Discrete persistent-chain model for protein binding on dna," *Phys. Rev. E*, vol. 83, p. 041912, 2011.

[39] J. R. Broach, "Making the right choice— long-range chromosomal interactions in development," *Cell*, vol. 119, no. 5, pp. 583 – 586, 2004.

[40] R. G. Roeder, "The eukaryotic transcriptional machinery: complexities and mechanisms unforeseen," *Nat Med*, vol. 9, no. 10, pp. 1239–1244, 2003.

[41] B. Alberts, D. Bray, A. Johnson, N. Lewis, K. Roberts, and P. Walter, *Essential Cell Biology: An Introduction to the Molecular Biology of the Cell*. Garland, New York, 1997.

[42] L. H. Hurley, "Dna and its associated processes as targets for cancer therapy," *Nature Reviews Cancer*, vol. 2, no. 3, pp. 188–200, 2002.

[43] D. A. Koster, K. Palle, E. S. Bot, M.-A. Bjornsti, and N. H. Dekker, "Antitumour drugs impede dna uncoiling by topoisomerase i," *Nature*, vol. 448, no. 7150, pp. 213–217, 2007.

[44] T. Paramanathan, I. Vladescu, M. J. McCauley, I. Rouzina, and M. C. Williams, "Force spectroscopy reveals the dna structural dynamics that govern the slow binding of actinomycin d," *Nucleic acids research*, vol. 40, no. 11, pp. 4925–4932, 2012.

[45] F. Leng, W. Priebe, and J. B. Chaires, "Ultratight dna binding of a new bisintercalating anthracycline antibiotic," *Biochemistry*, vol. 37, no. 7, pp. 1743–1753, 1998.

[46] L. Lerman, "Structural considerations in the interaction of dna and acridines," *Journal of molecular biology*, vol. 3, no. 1, pp. 18–IN14, 1961.

[47] L. Lerman, "The structure of the dna-acridine complex," *Proceedings of the National Academy of Sciences of the United States of America*, vol. 49, no. 1, p. 94, 1963.

[48] C. Murade, V. Subramaniam, C. Otto, and M. L. Bennink, "Interaction of oxazole yellow dyes with dna studied with hybrid optical tweezers and fluorescence microscopy," *Biophysical Journal*, vol. 97, no. 3, pp. 835 – 843, 2009.

[49] T. T. Perkins, D. E. Smith, and S. Chu, "Single polymer dynamics in an elongational flow," *Science*, vol. 276, no. 5321, pp. 2016–2021, 1997.

[50] A. N. Glazer, K. Peck, and R. A. Mathies, "A stable double-stranded dna-ethidium homodimer complex: application to picogram fluorescence detection of dna in agarose gels.," *Proceedings of the National Academy of Sciences*, vol. 87, no. 10, pp. 3851–3855, 1990.

[51] J. van Mameren, E. J. Peterman, and G. J. Wuite, "See me, feel me: methods to concurrently visualize and manipulate single dna molecules and associated proteins," *Nucleic acids research*, vol. 36, no. 13, pp. 4381–4389, 2008.

[52] A. Candelli, G. J. Wuite, and E. J. Peterman, "Combining optical trapping, fluorescence microscopy and micro-fluidics for single molecule studies of dna–protein interactions," *Physical Chemistry Chemical Physics*, vol. 13, no. 16, pp. 7263–7272, 2011.

[53] P. Gross, G. Farge, E. J. Peterman, and G. J. Wuite, "Combining optical tweezers, single-molecule fluorescence microscopy, and microfluidics for studies of dna–protein interactions," *Methods in enzymology*, vol. 475, pp. 427–453, 2010.

[54] R. Roijmans, "Characterization of the double stranded dna stain sytox orange," Master's thesis, Eindhoven University of Technology, 2012.

[55] "http://www.chimicare.org/curiosita/la-chimica-dei-materiali/dose-ed-effetto-connubio-perfetto-i-meccanismi-tossicita-delle-sostanze/," 2014.

[56] H. Zhang and J. F. Marko, "Maxwell relations for single-dna experiments: Monitoring protein binding and double-helix torque with force-extension measurements," *Phys. Rev. E*, vol. 77, p. 031916, Mar 2008.

[57] J. Yan and J. F. Marko, "Publisher's note: Effects of dna-distorting proteins on dna elastic response [phys. rev. e 68, 011905 (2003)]," *Phys. Rev. E*, vol. 68, p. 039901, 2003.

[58] H. Zhang and J. F. Marko, "Intrinsic and force-generated cooperativity in a theory of dna-bending proteins," *Phys. Rev. E*, vol. 82, p. 051906, 2010.

[59] S. Cocco, J. Marko, R. Monasson, A. Sarkar, and J. Yan, "Force-extension behavior of folding polymers," *The European Physical Journal E*, vol. 10, no. 3, pp. 249–263, 2003.

[60] J. Marko and E. Siggia, "Driving proteins off {DNA} using applied tension," *Biophysical Journal*, vol. 73, no. 4, pp. 2173 – 2178, 1997.

[61] J. Rudnick and R. Bruinsma, "Dna-protein cooperative binding through variable-range elastic coupling," *Biophysical Journal*, vol. 76, no. 4, pp. 1725 – 1733, 1999.

[62] J. D. Watson, F. H. Crick, *et al.*, "Molecular structure of nucleic acids," *Nature*, vol. 171, no. 4356, pp. 737–738, 1953.

[63] D. T. Zallen, "Despite franklin's work, wilkins earned his nobel," *Nature*, vol. 425, no. 6953, pp. 15–15, 2003.

[64] A. Ghosh and M. Bansal, "A glossary of dna structures from a to z," *Acta Crystallographica Section D: Biological Crystallography*, vol. 59, no. 4, pp. 620–626, 2003.

[65] J. Černỳ and P. Hobza, "Non-covalent interactions in biomacromolecules," *Physical Chemistry Chemical Physics*, vol. 9, no. 39, pp. 5291–5303, 2007.

[66] H. M. Berman and P. R. Young, "The interaction of intercalating drugs with nucleic acids," *Annual review of biophysics and bioengineering*, vol. 10, no. 1, pp. 87–114, 1981.

[67] J. Cairns, "The application of autoradiography to the study of dna viruses," in *Cold Spring Harbor symposia on quantitative biology*, vol. 27, pp. 311–318, Cold Spring Harbor Laboratory Press, 1962.

[68] G. Cohen and H. Eisenberg, "Viscosity and sedimentation study of sonicated dna–proflavine complexes," *Biopolymers*, vol. 8, no. 1, pp. 45–55, 1969.

[69] H. S. Rye, S. Yue, D. E. Wemmer, M. A. Quesada, R. P. Haugland, R. A. Mathies, and A. N. Glazer, "Stable fluorescent complexes of double-stranded dna with bis-intercalating asymmetric cyanine dyes: properties and applications," *Nucleic acids research*, vol. 20, no. 11, pp. 2803–2812, 1992.

[70] F. Johansen and J. P. Jacobsen, "1h nmr studies of the bis-intercalation of a homodimeric oxazole yellow dye in dna oligonucleotides," *Journal of Biomolecular Structure and Dynamics*, vol. 16, no. 2, pp. 205–222, 1998.

[71] X. Yan, R. C. Habbersett, J. M. Cordek, J. P. Nolan, T. M. Yoshida, J. H. Jett, and B. L. Marrone, "Development of a mechanism-based, dna staining protocol using sytox orange nucleic acid stain and dna fragment sizing flow cytometry," *Analytical biochemistry*, vol. 286, no. 1, pp. 138–148, 2000.

[72] D. M. Crothers, "Calculation of binding isotherms for heterogeneous polymers," *Biopolymers*, vol. 6, no. 4, pp. 575–584, 1968.

[73] W. Bauer and J. Vinograd, "Interaction of closed circular dna with intercalative dyes: Ii. the free energy of superhelix formation in sv40 dna," *Journal of molecular biology*, vol. 47, no. 3, pp. 419–435, 1970.

[74] S. C. Jain and H. M. Sobell, "Visualization of drug-nucleic acid interactions at atomic resolution. vii. structure of an ethidium/dinucleoside monophosphate crystalline complex, ethidium: uridylyl (3'-5') adenosine," *Journal of Biomolecular Structure and Dynamics*, vol. 1, no. 5, pp. 1161–1177, 1984.

[75] S. C. Jain and H. M. Sobell, "Visualization of drug-nucleic acid interactions at atomic resolution. viii. structures of two ethidium/dinucleoside monophosphate crystalline complexes containing ethidium: cytidylyl (3'-5') guanosine," *Journal of Biomolecular Structure and Dynamics*, vol. 1, no. 5, pp. 1179–1194, 1984.

[76] E. Nordmeier, "Absorption spectroscopy and dynamic and static light-scattering studies of ethidium bromide binding to calf thymus dna: implications for outside-binding and intercalation," *The Journal of Physical Chemistry*, vol. 96, no. 14, pp. 6045–6055, 1992.

[77] J. E. Coury, L. Mcfail-Isom, L. D. Williams, and L. A. Bottomley, "A novel assay for drug-dna binding mode, affinity, and exclusion number: scanning force microscopy," *Proceedings of the National Academy of Sciences*, vol. 93, no. 22, pp. 12283–12286, 1996.

[78] L. Finzi and J. Gelles, "Measurement of lactose repressor-mediated loop formation and breakdown in single dna molecules," *Science*, vol. 267, no. 5196, pp. 378–380, 1995.

[79] P. Liebesny, S. Goyal, D. Dunlap, F. Family, and L. Finzi, "Determination of the number of proteins bound non-specifically to dna," *Journal of Physics: Condensed Matter*, vol. 22, no. 41, p. 414104, 2010.

[80] M. C. Williams, J. R. Wenner, I. Rouzina, and V. A. Bloomfield, "Effect of ph on the overstretching transition of double-stranded dna: evidence of force-induced dna melting," *Biophysical Journal*, vol. 80, no. 2, pp. 874–881, 2001.

[81] M. C. Williams, J. R. Wenner, I. Rouzina, and V. A. Bloomfield, "Entropy and heat capacity of dna melting from temperature dependence of single molecule stretching," *Biophysical Journal*, vol. 80, no. 4, pp. 1932–1939, 2001.

[82] A. Bensimon, A. Simon, A. Chiffaudel, V. Croquette, F. Heslot, and D. Bensimon, "Alignment and sensitive detection of dna by a moving interface," *Science*, vol. 265, no. 5181, pp. 2096–2098, 1994.

[83] A. Ashkin, J. Dziedzic, J. Bjorkholm, and S. Chu, "Observation of a single-beam gradient force optical trap for dielectric particles," *Optics letters*, vol. 11, no. 5, pp. 288–290, 1986.

[84] G. J. Wuite, R. J. Davenport, A. Rappaport, and C. Bustamante, "An integrated laser trap/flow control video microscope for the study of single biomolecules," *Biophysical Journal*, vol. 79, no. 2, pp. 1155–1167, 2000.

[85] A. Ashkin, "Forces of a single-beam gradient laser trap on a dielectric sphere in the ray optics regime," *Biophysical journal*, vol. 61, no. 2, pp. 569–582, 1992.

[86] L. P. Ghislain, N. A. Switz, and W. W. Webb, "Measurement of small forces using an optical trap," *Review of Scientific Instruments*, vol. 65, no. 9, pp. 2762–2768, 1994.

[87] L. P. Ghislain and W. W. Webb, "Scanning-force microscope based on an optical trap," *Optics Letters*, vol. 18, no. 19, pp. 1678–1680, 1993.

[88] D. Suh and J. B. Chaires, "Criteria for the mode of binding of dna binding agents," *Bioorganic & medicinal chemistry*, vol. 3, no. 6, pp. 723–728, 1995.

[89] M. Waring, "Complex formation between ethidium bromide and nucleic acids," *Journal of molecular biology*, vol. 13, no. 1, pp. 269–282, 1965.

[90] H. M. Sobell, C.-C. Tsai, S. C. Jain, and S. G. Gilbert, "Visualization of drug-nucleic acid interactions at atomic resolution: Iii. unifying structural concepts in understanding drug-dna interactions and their broader implications in understanding protein-dna interactions," *Journal of molecular biology*, vol. 114, no. 3, pp. 333–365, 1977.

[91] C.-C. Tsai, S. C. Jain, and H. M. Sobell, "X-ray crystallographic visualization of drug-nucleic acid intercalative binding: structure of an ethidium-dinucleoside monophosphate crystalline complex, ethidium: 5-iodouridylyl (3'-5') adenosine," *Proceedings of the National Academy of Sciences*, vol. 72, no. 2, pp. 628–632, 1975.

[92] H. A. Kramers and G. H. Wannier, "Statistics of the two-dimensional ferromagnet. part i," *Phys. Rev.*, vol. 60, pp. 252–262, Aug 1941.

[93] R. Phillips, J. Kondev, and J. Theriot, *Physical Biology of the Cell*. Garland Science, 2009.

[94] I. Langmuir, "The adsorption of gases on plane surfaces of glass, mica and platinum.," *Journal of the American Chemical society*, vol. 40, no. 9, pp. 1361–1403, 1918.

[95] P. G. Janssen, S. Jabbari-Farouji, M. Surin, X. Vila, J. C. Gielen, T. F. de Greef, M. R. Vos, P. H. Bomans, N. A. Sommerdijk, P. C. Christianen, *et al.*, "Insights into templated supramolecular polymerization: Binding of naphthalene derivatives to ssdna templates of different lengths," *Journal of the American Chemical Society*, vol. 131, no. 3, pp. 1222–1231, 2008.

[96] S. Jabbari-Farouji and P. van der Schoot, "Competing templated and self-assembly in supramolecular polymers," *Macromolecules*, vol. 43, no. 13, pp. 5833–5844, 2010.

[97] P. Atkins and J. De Paula, *Physical Chemistry*. Oxford Univ Press, 2006.

[98] A. Biebricher, I. Heller, and G. J. L. Wuite. Private communications, May 2014.

[99] D. Řeha, M. Kabelác, F. Ryjác?ek, J. Šponer, J. E. Šponer, M. Elstner, S. Suhai, and P. Hobza, "Intercalators. 1. nature of stacking interactions between intercalators (ethidium, daunomycin, ellipticine, and 4', 6-diaminide-2-phenylindole) and dna base pairs. ab initio quantum chemical, density functional theory, and empirical potential study," *Journal of the American Chemical Society*, vol. 124, no. 13, pp. 3366–3376, 2002.

[100] J. Šponer, J. Leszczynski, and P. Hobza, "Nature of nucleic acid-base stacking: nonempirical ab initio and empirical potential characterization of 10 stacked base dimers. comparison of stacked and h-bonded base pairs," *The Journal of Physical Chemistry*, vol. 100, no. 13, pp. 5590–5596, 1996.

[101] F. Gago, "Stacking interactions and intercalative dna binding," *Methods*, vol. 14, no. 3, pp. 277–292, 1998.

[102] C. R. Company, *CRC Handbook of Chemistry and Physics*. No. v. 65, CRC Press, 1984.

[103] S. Husale, W. Grange, and M. Hegner, "Dna mechanics affected by small dna interacting ligands," *Single Molecules*, vol. 3, no. 2-3, pp. 91–96, 2002.

[104] G. G. Holman, M. Zewail-Foote, A. R. Smith, K. A. Johnson, and B. L. Iverson, "A sequence-specific threading tetra-intercalator with an extremely slow dissociation rate constant," *Nature chemistry*, vol. 3, no. 11, pp. 875–881, 2011.

[105] A. Sischka, K. Toensing, R. Eckel, S. D. Wilking, N. Sewald, R. Ros, and D. Anselmetti, "Molecular mechanisms and kinetics between dna and dna binding ligands," *Biophysical journal*, vol. 88, no. 1, pp. 404–411, 2005.

[106] S. H. Um, J. B. Lee, N. Park, S. Y. Kwon, C. C. Umbach, and D. Luo, "Enzyme-catalysed assembly of dna hydrogel," *Nature materials*, vol. 5, no. 10, pp. 797–801, 2006.

[107] H. Anton and C. Rorres, *Elementary Linear Algebra*. Wiley International, 2005.

List of symbols

Table A: Alphabetically ordered list of the symbols, including interpretation and dimension, as used in this thesis.

Symbol	Interpretation	Dimension
a	Slope of linear fit	-
b	Intercept of linear fit	-
b_{corr}	Small correction to b	-
C	Concentration of intercalators	M
E_ν	Energy of a general state ν	pN nm
$\vec{e}_+$	Eigenvector of $\underline{\underline{T}}$ corresponding to λ_+	-
$\vec{e}_-$	Eigenvector of $\underline{\underline{T}}$ corresponding to λ_-	-
f	Stretching force	pN
F	Free energy	pN nm
$f_{00\to01}$	Transition force between states 0/0 and 0/1 in the 0/1-model	pN
$f_{00\to11}$	Transition force between states 0/0 and 1/1 in the 3-state model	pN
f_{01}	Transition force between states 0 and 1 in the 0/1-model	pN
F_{02}	Free energy of the 0/2-model	pN nm
F_{11}	Free energy of the 1/1-model	pN nm
i	Number of Kuhn segment	-
k_B	Boltzmann's constant	pN nm K^{-1}
k_BT	Thermal energy	pN nm
l_0	Length of a Kuhn segment in state 0	nm
L_0	Contour length	nm
$\underline{\underline{M}}$	A general matrix	-
N	Number of Kuhn segments	-
P_ν	Probability of a system to be in state ν	-
S	Entropy	pN nm K^{-1}
S_i	State parameter of the i^{th} Kuhn segment	-
$\{S_i\}$	Collection of all state parameters S_i	-
S_{mix}	Mixing entropy	pN nm K^{-1}
State 0	Microscopic state representing B-DNA	-
State 0/0	Macroscopic state: all segments in state 0	-
State 0/1	Macroscopic state: alternating states 0 and 1	-
State 0/2	Macroscopic state: alternating states 0 and 2	-
State 1	Microscopic state representing overstretched DNA	-
State 1/1	Macroscopic state: all segments in state 1	-
State 1/2	Macroscopic state: alternating states 1 and 2	-
State 2	Microscopic state representing intercalated DNA	-
State 2/2	Macroscopic state: all segments in state 2	-
$\underline{\underline{T}}$	Transfer matrix	-

Continued on next page.

Table A – Continued from previous page.

Symbol	Interpretation	Dimension
T	Temperature	K
$\hat{t}_i$	Unit vector in direction of i^{th} Kuhn segment	-
$\{\hat{t}_i\}$	Collection of all unit vectors $\hat{t}_i$	-
$\vec{V}$	Vector used in the transfer matrix method	-
$\vec{v}$	A general vector	-
v_+	Multiple of inner product of $\vec{V}$ and $\vec{e}_+$	-
v_-	Multiple of inner product of $\vec{V}$ and $\vec{e}_-$	-
$\vec{w}$	A general vector	-
W	Width of a general 2-state transition	-
W_{01}	Width of the 0/1-transition	-
W_{02}	Width of the 0/2-transition	-
W_μ	Range of chemical potentials that shift the overstretching transition	-
z	End-to-end length	nm
$\hat{z}$	Unit vector in the z-direction	-
Z	Partition function	-
α	Exponent of divergence of f	-
γ_1	Elongation factor of state 1	-
$\gamma_1 l_0$	Length of a Kuhn segment in state 1	nm
γ_2	Elongation factor of state 2	-
$\gamma_2 l_0$	Length of a Kuhn segment in state 2	nm
δ	Free energy penalty for a 2/2-interface	-
ΔE	Free energy penalty for a general state	-
ΔE_2	Free energy penalty for state 2	-
ε_1	Free energy penalty for state 1	-
$\varepsilon_2 - \mu$	Free energy penalty for state 2	-
$\varepsilon^{0/2-\text{model}}$	Free energy of the 0/2-model	pN nm
$\varepsilon^{1/2-\text{model}}$	Free energy of the 1/2-model	pN nm
$\varepsilon^{2-\text{state}}$	Free energy of the 2-state Kuhn model	pN nm
$\varepsilon^{3-\text{state}}$	Free energy of the 3-state Kuhn model	pN nm
ε^{FJC}	Free energy of the freely jointed chain	pN nm
η	Free energy penalty for a 1/2-interface	-
θ	Polar angle	-
κ	Hypothetical free energy penalty for a 1/1-interface	-
λ	Free energy penalty for a 0/1-interface	-
λ_+	Largest eigenvalue of the transfer matrix $\underline{\underline{T}}$	-
λ_-	Smallest eigenvalue of the transfer matrix $\underline{\underline{T}}$	-
μ	Chemical potential	-
μ_{corr}	Small corrections to μ_{max} and μ_{min}	-
μ_{max}	Largest chemical potential that shows an overstretching transition	-
μ_{min}	Characteristic chemical potential of exponential increase	-
μ_{shift}	All chemical potentials that shift the overstretching transition	-
ν	A particular microstate of a system	-
ϕ	[1]: Azimuthal angle	-
	[2]: Saturation parameter	-
χ	Dimensionless force $\frac{fl_0}{k_B T}$	-
$\chi_{00\to01}$	Transition force between states 0/0 and 0/1 in the 0/1-model	-
$\chi_{00\to02}$	Transition force between states 0/0 and 0/2 in the 0/2-model	-

Continued on next page.

Table A – Continued from previous page.

Symbol	Interpretation	Dimension
$\chi_{00\to11}$	Transition force between states 0/0 and 1/1 in the 3-state model	-
χ_{01}	Transition force between states 0 and 1 in the 0/1-model	-
χ_{02}	Transition force between states 0 and 2 in the 0/2-model	-
$\chi_{02\to11}$	Transition force between states 0/2 and 1/1 in the 3-state model	-
$\chi_{11\to22}$	Transition force between states 1/1 and 2/2 in the 3-state model	-
χ_{12}	Transition force between states 1 and 2 in the 1/2-model	-
χ_{over}	Force of the general overstretching transition	-
$\langle\ \rangle$	Thermal average	-

Appendix A

Derivations of force-extension relations

In chapters 3 and 4 we present the force-extension relations for the 1-state, 2-state and 3-state Kuhn models, and only outlines of the physics involved in calculating these relations, but mathematical details were omitted. This Appendix gives the detailed derivations of the force-extension relations of the 1-state (section A.1), 2-state (section A.2) and 3-state (section A.3) Kuhn models.

A.1. The 1-state Kuhn model

The starting point of the force-extension calculation of the 1-state Kuhn model is given by equations 3.1 and 3.2,

$$\frac{\varepsilon^{\mathrm{FJC}}[\{\hat{t}_i\}]}{k_B T} = -\frac{f l_0}{k_B T} \sum_{i=1}^{N} \hat{t}_i \cdot \hat{z}, \tag{A.1}$$

and

$$Z = \sum_{\{\hat{t}_i\}} \exp\left(-\frac{\varepsilon[\{\hat{t}_i\}]}{k_B T}\right). \tag{A.2}$$

Equation A.2 represents a summation over all possible microstates of the chain, where each microstate is defined by the orientation of all N unit vectors $\hat{t}_i$. A summation over all states of a single Kuhn segment is therefore represented by an integral over all orientations of the corresponding unit vector. Using this, and substituting equation A.1 for the energy, gives

$$Z = \int \mathrm{d}\hat{t}_1 \int \mathrm{d}\hat{t}_2 ... \int \mathrm{d}\hat{t}_N \, \exp\left(\frac{f l_0}{k_B T} \sum_{i=1}^{N} \hat{t}_i \cdot \hat{z}\right) = \prod_{i=1}^{N} \int \mathrm{d}\hat{t}_i \, \exp\left(\frac{f l_0}{k_B T} \, \hat{t}_i \cdot \hat{z}\right). \tag{A.3}$$

The last step in equation A.3 shows that all unit vectors are independent and non-interacting, which causes the partition function to factorize in the partition function of N individual Kuhn segments. Since all unit vectors are identical, this leads to

$$Z = \left[\int \mathrm{d}\hat{t} \, \exp\left(\frac{f l_0}{k_B T} \hat{t} \cdot \hat{z}\right)\right]^N. \tag{A.4}$$

The next step is evaluating the integral over all possible orientations of the unit vector $\hat{t}$, which gives all points on a unit sphere. The integral $\int d\hat{t}$ therefore represents an integral over the polar angle θ and the azimuthal angle ϕ. The polar angle θ was defined in figure 3.1 as the angle between $\hat{t}$ and the z-direction. This allows us to express the inner product in equation A.4 in

terms of θ, $\hat{t} \cdot \hat{z} = \cos\theta$. This gives

$$Z = \left[\int_0^{2\pi} \mathrm{d}\phi \int_0^{\pi} \sin(\theta)\mathrm{d}\theta \ \exp\left(\frac{fl_0}{k_B T}\cos\theta\right)\right]^N. \tag{A.5}$$

The integral over θ can be evaluated by substituting $\cos\theta = u$, whereas the integral over ϕ simply gives 2π. This leads to the following steps:

$$Z = \left[2\pi \int_{-1}^{1} \mathrm{d}u \ \exp\left(\frac{fl_0}{k_B T}u\right)\right]^N = \left[\frac{4\pi k_B T}{fl_0} \sinh\left(\frac{fl_0}{k_B T}\right)\right]^N, \tag{A.6}$$

where $\sinh x \equiv \frac{1}{2}(\exp x - \exp(-x))$ is the hyperbolic sine function. Now that we have calculated the partition function, we can continue with the steps already outlined in section 3.1.1. We use equations 3.3 and 3.4, from which we obtain

$$F = -k_B T \ln(Z) = -k_B T \ln\left(\left[\frac{4\pi k_B T}{fl_0} \sinh\left(\frac{fl_0}{k_B T}\right)\right]^N\right) \tag{A.7}$$

for the free energy, and

$$\langle z \rangle = -\frac{\partial F}{\partial f} = N l_0 \left[\coth\left(\frac{fl_0}{k_B T}\right) - \frac{k_B T}{fl_0}\right] \tag{A.8}$$

for the expectation value of the extension. This result is also presented in equation 3.5.

A.2. The 2-state Kuhn model

We repeat the steps of Appendix A.1 for the 2-state Kuhn model. Starting point is the energy functional of the 2-state Kuhn model and the recipe to calculate the partition function. They are given by equations 3.9 and 3.10,

$$\frac{\varepsilon^{\text{2-state}}[\{\hat{t}_i\},\{S_i\}]}{k_B T} = \sum_{i=1}^{N}\left[-\frac{fl_0\left[1+S_i\left(\gamma_1-1\right)\right]}{k_B T}\,\hat{t}_i\cdot\hat{z}+\varepsilon_1 S_i\right] + \sum_{i=1}^{N-1}\lambda(1-\delta_{S_i,S_{i+1}}), \tag{A.9}$$

and

$$Z = \sum_{\{\hat{t}_i\}}\sum_{\{S_i\}} \exp\left(-\frac{\varepsilon[\{\hat{t}_i\},\{S_i\}]}{k_B T}\right). \tag{A.10}$$

Again we substitute the energy functional in the partition function and replace the summation over the unit vectors by integrals. This gives

$$Z = \int \mathrm{d}\hat{t}_1 \sum_{S_1=0,1} \int \mathrm{d}\hat{t}_2 \sum_{S_2=0,1} \ldots \int \mathrm{d}\hat{t}_N \sum_{S_N=0,1} \exp\left(\sum_{i=1}^{N}\left[\frac{fl_0\left[1+S_i\left(\gamma_1-1\right)\right]}{k_B T}\,\hat{t}_i\cdot\hat{z}-\varepsilon_1 S_i\right] + \sum_{i=1}^{N-1}\lambda\left(\delta_{S_i,S_{i+1}}-1\right)\right). \tag{A.11}$$

In the derivation of the force-extension relation of the 1-state Kuhn model our next step was to factorize the partition function in a product of the partition functions of N independent Kuhn segments. Unfortunately, we cannot do that here. The last term in equation A.11 gives the energy penalty for a 0/1-interface, and depends on both Kuhn segment i and Kuhn segment $i+1$. Therefore, neighboring Kuhn segments interact and are not independent: the partition

function does not factorize.

However, while the state parameters S_i and S_{i+1} interact, the unit vectors $\hat{t}_i$ and $\hat{t}_{i+1}$ do not. Therefore, we first carry out the integrals in equation A.11 for which the partition function does factorize. We will leave the summations unaffected for now. We first evaluate the integral over a single unit vector and leave the rest out of the equations. Later we substitute this result back in equation A.11. We call the result of the integral I[1],

$$I \;=\; \int \mathrm{d}\hat{t}_i \;\exp\left(\frac{f l_0\left[1+S_i\left(\gamma_1-1\right)\right]}{k_B T}\,\hat{t}_i\cdot\hat{z}\right), \tag{A.12}$$

which was already evaluated in Appendix A.1 for the 1-state Kuhn model (equations A.4 to A.6). The only difference is that l_0 has been substituted with $l_0\left[1+S_i\left(\gamma_1-1\right)\right]$, allowing us to immediately write down

$$I \;=\; \frac{4\pi}{\chi\left[1+S_i\left(\gamma_1-1\right)\right]}\;\sinh\Big(\chi\left[1+S_i\left(\gamma_1-1\right)\right]\Big), \tag{A.13}$$

where we have used the same definition for χ as we did in equation 3.7 in section 3.1.1,

$$\chi \;=\; \frac{f l_0}{k_B T}. \tag{A.14}$$

Now we can substitute this result in equation A.11 for the integrals over all N unit vectors. A little rearranging yields

$$\begin{aligned} Z \;=\; \sum_{S_1=0,1}\sum_{S_2=0,1}\cdots\sum_{S_N=0,1}\prod_{i=1}^{N}\left[\frac{4\pi}{\chi\left[1+S_i\left(\gamma_1-1\right)\right]}\;\sinh\Big(\chi\left[1+S_i\left(\gamma_1-1\right)\right]\Big)\exp\left(-\varepsilon_1 S_i\right)\right] \\ \cdot\prod_{i=1}^{N-1}\left[\exp\Big[\lambda\left(\delta_{S_i,S_{i+1}}-1\right)\Big]\right]. \end{aligned} \tag{A.15}$$

The last term of equation A.15 prevents the partition function to factorize, and therefore makes the calculation more difficult than the calculation in Appendix A.1. To solve this problem, we use the so called *transfer matrix method* [92]. This methods uses linear algebra to solve certain partition functions that do not factorize because the particles do not behave independently. We do not explain the transfer matrix method in a separate section, but we explain each step of the method at the point in the calculation where we need it.

[1] In calculating the partition function we sum over all possible microstates, by integrating over the entire phase space of the chain. The configurational part of this phase space is performed by integration over the angles θ_i and ϕ_i for all i, where θ_i and ϕ_i correspond to the i^{th} Kuhn segment. We note that this integration would be different if we would integrate over all possible positions of the end point of a Kuhn segment x, y and z with the constraint that $\sqrt{x^2+y^2+z^2} = l_0\left[1+S_i(\gamma_1-1)\right]$. In that case more microstates would be assigned to a long Kuhn segment ($\gamma_1 l_0$) than to a short Kuhn segment (l_0), because the corresponding spherical surface area is larger. This leads to an effective entropy bonus for Kuhn segments in state 1 with respect to state 0. By integration over the angles, however, the number of microstates for short and long Kuhn segments is equal, and there is no entropy bonus for state 1. This difference in entropy causes a difference in the final expression for the force-extension curve (equation A.36). We argue that integration of the angles is natural, because the angles are the actual degrees of freedom; the influence of the length is already taken into account by summation over the state parameter S_i. Finally we note that the difference in the final results is only in the rescaling of the phenomenological free energy penalty ε_1 (equation 3.17). Therefore, the choice of integration does not affect the validity of the results and conclusions in this thesis.

The transfer matrix method

As a first step towards using the transfer matrix method, we rearrange the terms in equation A.15, for reasons to become clear below, to give

$$Z = \left(\frac{4\pi}{\chi}\right)^N \sum_{S_1=0,1} V_{S_1} \sum_{S_2=0,1} V_{S_1} V_{S_2} \exp\left[\lambda\left(\delta_{S_1,S_2}-1\right)\right] \sum_{S_3=0,1} V_{S_2} V_{S_3} \exp\left[\lambda\left(\delta_{S_2,S_3}-1\right)\right] \cdot \\ \ldots \cdot \sum_{S_N=0,1} V_{S_{N-1}} V_{S_N} \exp\left[\lambda\left(\delta_{S_{N-1},S_N}-1\right)\right] V_{S_N}, \tag{A.16}$$

where we defined V_{S_i} as

$$V_{S_i} = \sqrt{\frac{1}{1+S_i\left(\gamma_1-1\right)}} \sqrt{\sinh\left(\chi\left[1+S_i\left(\gamma_1-1\right)\right]\right)} \exp\left(-\frac{1}{2}\varepsilon_1 S_i\right), \tag{A.17}$$

and V_{S_i} is a vector element of the vector $\vec{V}$, given by

$$\vec{V} = \begin{bmatrix} V_0 \\ V_1 \end{bmatrix} = \begin{bmatrix} \sqrt{\sinh\left(\chi\right)} \\ \sqrt{\frac{1}{\gamma_1}} \sqrt{\sinh\left(\gamma_1\chi\right)} \exp\left(-\frac{1}{2}\varepsilon_1\right) \end{bmatrix} \tag{A.18}$$

We would like to emphasize that equation A.16 contains the same terms as A.15, only written in a more convenient way. Now we define a 2 x 2 *transfer matrix* $\underline{\underline{T}}$, with matrix elements defined as

$$T_{S_iS_j} = V_{S_i} V_{S_j} \exp\left[\lambda\left(\delta_{S_i,S_j}-1\right)\right], \tag{A.19}$$

such that the transfer matrix $\underline{\underline{T}}$ becomes

$$\underline{\underline{T}} = \begin{bmatrix} T_{00} & T_{01} \\ T_{10} & T_{11} \end{bmatrix} \\ = \begin{bmatrix} \sinh(\chi) & \sqrt{\frac{1}{\gamma_1}} \sqrt{\sinh(\chi)\sinh\left(\gamma_1\chi\right)} \exp\left(-\frac{1}{2}\varepsilon_1-\lambda\right) \\ \sqrt{\frac{1}{\gamma_1}} \sqrt{\sinh\left(\chi\right)\sinh\left(\gamma_1\chi\right)} \exp\left(-\frac{1}{2}\varepsilon_1-\lambda\right) & \frac{1}{\gamma_1}\sinh\left(\gamma_1\chi\right)\exp\left(-\varepsilon_1\right) \end{bmatrix} \tag{A.20}$$

We now formulate the partition function of equation A.16 in terms of the elements of the transfer matrix $\underline{\underline{T}}$,

$$Z = \left(\frac{4\pi}{\chi}\right)^N \sum_{S_1=0,1} V_{S_1} \sum_{S_2=0,1} T_{S_1S_2} \sum_{S_3=0,1} T_{S_2S_3} \ \ldots \ \sum_{S_N=0,1} T_{S_{N-1}S_N} V_{S_N}. \tag{A.21}$$

We further simplify this expression by using the rules for matrix-vector multiplication: a matrix times a vector yields a new vector. The elements of the new vector are calculated from the elements of the matrix and the old vector according to

$$\vec{w} = \underline{\underline{M}}\,\vec{v} \quad \Longleftrightarrow \quad w_i = \sum_j M_{ij} v_j, \tag{A.22}$$

which we can apply to equation A.21. This gives as a first step

$$Z = \left(\frac{4\pi}{\chi}\right)^N \sum_{S_1=0,1} V_{S_1} \sum_{S_2=0,1} T_{S_1S_2} \sum_{S_3=0,1} T_{S_2S_3} \ \ldots \ \sum_{S_{N-1}=0,1} T_{S_{N-2}S_{N-1}} \left(TV\right)_{S_{N-1}}, \tag{A.23}$$

where $(TV)_{S_{N-1}}$ is a vector element of the vector $\overrightarrow{TV}$, which was obtained by the summation over S_N according to the multiplication rules in A.22. To continue, we use that matrix multiplication is *associative*, in other words we use the property

$$\underline{\underline{T}}\left(\underline{\underline{T}}\vec{V}\right) \;=\; \left(\underline{\underline{T}}\,\underline{\underline{T}}\right)\vec{V} \;=\; \underline{\underline{T}}^2\vec{V}. \tag{A.24}$$

We invoke equation A.24 to eliminate the summations in equation A.23 one by one, which leads to

$$Z \;=\; \left(\frac{4\pi}{\chi}\right)^N \sum_{S_1=0,1} V_{S_1}\left(T^{N-1}V\right)_{S_1}. \tag{A.25}$$

The summation that is left is just the inner product of the vectors $\overrightarrow{V}$ and $\overrightarrow{T^{N-1}V}$, which gives the partition function in equation A.26. Note that the result is a scalar, as it should be, and

$$Z \;=\; \left(\frac{4\pi}{\chi}\right)^N \vec{V}\cdot\underline{\underline{T}}^{N-1}\vec{V}. \tag{A.26}$$

Eigenvectors and eigenvalues

The final steps of the calculation involve evaluating the inner product in equation A.26. In principle we could simply carry out the calculation since we know both $\vec{V}$ and $\underline{\underline{T}}$, but for a significantly large number of Kuhn segments, N, this calculation is very costly. We will therefore perform these calculations using *eigenvectors* and *eigenvalues*. Equation A.27 shows the definition of both the eigenvector and the eigenvalue of a matrix: if a matrix $\underline{\underline{M}}$ multiplies a non-zero vector $\vec{e}$, and the result is a constant multiple of that vector $\vec{e}$, then $\vec{e}$ is an eigenvector of matrix $\underline{\underline{M}}$. The resulting multiplier is called the eigenvalue, and usually denoted as λ,

$$\underline{\underline{M}}\vec{e} \;=\; \lambda\vec{e}. \tag{A.27}$$

For reasons that become clear soon, we expand our vector $\vec{V}$ in the basis that is spanned by the eigenvectors of $\underline{\underline{T}}$,

$$\vec{V} \;=\; v_+\vec{e}_+ + v_-\vec{e}_-, \tag{A.28}$$

where $v_+\vec{e}_+$ and $v_-\vec{e}_-$ are the projections of the vector $\vec{V}$ onto the two distinct eigenvectors of $\underline{\underline{T}}$. Strictly speaking, we should prove that the eigenvectors of $\underline{\underline{T}}$ span $\mathbb{R}^2$, before we assume that we can expand any vector in $\mathbb{R}^2$ in the eigenvectors of $\underline{\underline{T}}$. We omit the formal proof here, but we refer to the textbook of Anton and Rorres [107]. They prove in section 7.2 of their book that if a $n \times n$ matrix has n distinct eigenvalues, then it has n linearly independent eigenvectors and therefore the eigenvectors span $\mathbb{R}^N$. As we will see in a moment, our 2 x 2 matrix $\underline{\underline{T}}$ has 2 distinct eigenvalues, so we can safely use equation A.28. We do that by substituting it in equation A.26:

$$\begin{aligned} Z \;&=\; \left(\frac{4\pi}{\chi}\right)^N (v_+\vec{e}_+ + v_-\vec{e}_-)\cdot\underline{\underline{T}}^{N-1}(v_+\vec{e}_+ + v_-\vec{e}_-) \\ &=\; \left(\frac{4\pi}{\chi}\right)^N (v_+\vec{e}_+ + v_-\vec{e}_-)\cdot\left(v_+\,\underline{\underline{T}}^{N-1}\vec{e}_+ + v_-\,\underline{\underline{T}}^{N-1}\vec{e}_-\right). \end{aligned} \tag{A.29}$$

We now use the definition of eigenvectors and eigenvalues, equation A.27, to completely eliminate

the matrix $\underline{\underline{T}}$ from the calculations:

$$\begin{aligned} Z &= \left(\frac{4\pi}{\chi}\right)^N (v_+\vec{e}_+ + v_-\vec{e}_-)\cdot\left[v_+\,\underline{\underline{T}}^{N-2}\left(\underline{\underline{T}}\vec{e}_+\right) + v_-\,\underline{\underline{T}}^{N-2}\left(\underline{\underline{T}}\vec{e}_-\right)\right] \\ &= \left(\frac{4\pi}{\chi}\right)^N (v_+\vec{e}_+ + v_-\vec{e}_-)\cdot\left[v_+\,\underline{\underline{T}}^{N-2}\left(\lambda_+\vec{e}_+\right) + v_-\,\underline{\underline{T}}^{N-2}\left(\lambda_-\vec{e}_-\right)\right] \\ &= \left(\frac{4\pi}{\chi}\right)^N (v_+\vec{e}_+ + v_-\vec{e}_-)\cdot\left[v_+\lambda_+\,\underline{\underline{T}}^{N-2}\vec{e}_+ + v_-\lambda_-\,\underline{\underline{T}}^{N-2}\vec{e}_-\right] \\ &= \left(\frac{4\pi}{\chi}\right)^N (v_+\vec{e}_+ + v_-\vec{e}_-)\cdot\left[v_+\lambda_+^{N-1}\vec{e}_+ + v_-\lambda_-^{N-1}\vec{e}_-\right], \end{aligned} \tag{A.30}$$

where λ_+ and λ_- are the eigenvalues corresponding to eigenvectors $\vec{e}_+$ and $\vec{e}_-$ respectively. By definition, λ_+ is the largest of the two eigenvalues. Finally, we use the fact that a symmetric $n \times n$ matrix has an orthogonal set of n eigenvectors (section 7.3 in Anton and Rorres [107]), and $\underline{\underline{T}}$ is symmetric, hence $\vec{e}_+ \cdot \vec{e}_- = 0$. This gives as a result for the partition function,

$$Z = \left(\frac{4\pi}{\chi}\right)^N \left[v_+^2\left(\vec{e}_+\cdot\vec{e}_+\right)\lambda_+^{N-1} + v_-^2\left(\vec{e}_-\cdot\vec{e}_-\right)\lambda_-^{N-1}\right] \tag{A.31}$$

At this point we seek to simplify A.31 by assuming that we have a very large number of Kuhn segments. We therefore now assume the thermodynamic limit, or ground-state approximation, to hold: $N \to \infty$. In Appendix B we give the complete calculation without this assumption, and show that the thermodynamic limit is a very reasonable assumption for the number of Kuhn segments, N, that we are dealing with in this thesis. This allows us to simplify equation A.31,

$$\begin{aligned} \lim_{N\to\infty} Z &= \lim_{N\to\infty}\left(\frac{4\pi}{\chi}\right)^N \lambda_+^{N-1}\left[v_+^2\left(\vec{e}_+\cdot\vec{e}_+\right) + v_-^2\left(\vec{e}_-\cdot\vec{e}_-\right)\left(\frac{\lambda_-}{\lambda_+}\right)^{N-1}\right] \\ &= \lim_{N\to\infty}\left(\frac{4\pi}{\chi}\right)^N \lambda_+^{N-1}\, v_+^2\left(\vec{e}_+\cdot\vec{e}_+\right), \end{aligned} \tag{A.32}$$

where in the last step we used the fact that one of our eigenvalues (λ_+) is larger than the other (λ_-). However, the calculation is robust and includes the case that the two eigenvalues are equal, because this leads effectively to a renormalization of $v_+^2\left(\vec{e}_+\cdot\vec{e}_+\right)$. As we shall see, in the thermodynamic limit $v_+^2\left(\vec{e}_+\cdot\vec{e}_+\right)$ will drop out anyway.

From here on we can follow the same steps as in section A.1 for the 1-state Kuhn model. First, we calculate the free energy F and then we calculate the expectation value of the end-to-end length z. For the former we get

$$\lim_{N\to\infty} F = -k_BT\,\ln\left(Z\right) = -k_BT\left[N\ln\left(\frac{4\pi}{\chi}\right) + (N-1)\log\left(\lambda_+\right) + 2\log\left(v_+\right)\right]. \tag{A.33}$$

Finally, we calculate z, the end-to-end length of the chain. Following our calculation for the 1-state Kuhn model in Appendix A.1, we normalize the end-to-end length by $L_0 = Nl_0$. We stress that while L_0 is the contour length of the 1-state Kuhn model, it is not the contour length of the 2-state Kuhn model as it does not take into account elongation of individual Kuhn segments to *state 1*, the overstretched state. This allows for a relative extension to be larger than 1. The

calculation is given by

$$\begin{aligned}\lim_{N\to\infty}\left\langle\frac{z}{L_0}\right\rangle &= \lim_{N\to\infty} -\frac{1}{Nl_0}\frac{\partial F}{\partial f}\\ &= \lim_{N\to\infty}\frac{k_BT}{l_0}\frac{\partial}{\partial f}\left[\ln\left(\frac{4\pi}{\chi}\right)+\frac{N-1}{N}\ln\left(\lambda_+\right)+\frac{2}{N}\ln\left(v_+\right)\right]\\ &\approx \frac{k_BT}{l_0}\frac{\partial}{\partial f}\left[\ln\left(\frac{4\pi}{\chi}\right)+\ln\left(\lambda_+\right)\right]+O\left(\frac{1}{N}\right)\\ &= \frac{\partial}{\partial\chi}\ln\left(\lambda_+\right)-\frac{1}{\chi}\end{aligned} \tag{A.34}$$

The only step left is the calculation of the largest eigenvalue of the transfer matrix $\underline{\underline{T}}$ (equation A.20). Calculating the eigenvalues is straightforward, so we will omit the intermediate steps, and immediately present the result,

$$\begin{aligned}\lambda_\pm &= \frac{\exp\left(-\varepsilon_1\right)}{2\gamma_1}\Bigg[\exp\left(\varepsilon_1\right)\gamma_1\sinh\left(\chi\right)+\sinh\left(\gamma_1\chi\right)\\ &\pm\sqrt{4\exp\left(\varepsilon_1\right)\gamma_1\sinh\left(\chi\right)\sinh\left(\gamma_1\chi\right)\exp\left(-2\lambda\right)+\Big(-\exp\left(\varepsilon_1\right)\gamma_1\sinh\left(\chi\right)+\sinh\left(\gamma_1\chi\right)\Big)^2}\Bigg].\end{aligned} \tag{A.35}$$

Note that $\lambda_\pm$ gives the two eigenvalues of transfer matrix $\underline{\underline{T}}$, while λ is the cooperativity parameter that penalizes an interface between Kuhn segments in different states.

In the final step, the expression for λ_+ in equation A.35 is substituted in equation A.34. The differentiation is straightforward, so the intermediate steps are not given here. Performing the calculations and rearranging terms gives the final result of our calculation,

$$\begin{aligned}\lim_{N\to\infty}\left\langle\frac{z}{L_0}\right\rangle &= \frac{1}{2}\left(-\frac{2}{\chi}+\coth\left(\chi\right)+\gamma_1\coth(\gamma_1\chi)\right)\\ &+\frac{\gamma_1\left[\cosh\left(\gamma_1\chi\right)+\exp(\varepsilon_1)\left(\cosh(\chi)-\gamma_1\coth(\gamma_1\chi)\sinh(\chi)\right)\right]-\coth(\chi)\sinh(\gamma_1\chi)}{2\sqrt{4\exp\left(\varepsilon_1\right)\gamma_1\sinh\left(\chi\right)\sinh\left(\gamma_1\chi\right)\exp\left(-2\lambda\right)+\Big(-\exp\left(\varepsilon_1\right)\gamma_1\sinh\left(\chi\right)+\sinh\left(\gamma_1\chi\right)\Big)^2}}.\end{aligned} \tag{A.36}$$

A.3. The 3-state Kuhn model

The derivation of the force-extension curve of the 3-state Kuhn model follows exactly the same steps as the 2-state derivation in Appendix A.2, including the use of the transfer matrix method. However, this time we deal with three different states of the Kuhn segments instead of two. Also, instead of one cooperativity parameter (λ), we now have three cooperativity parameters (λ, δ and η). This causes the intermediate and final results to be much more complicated expressions than the corresponding expressions for the 2-state model. In other words, the derivation of the 3-state force-extension relation is conceptually equally difficult as the 2-state derivation, but algebraically much more cumbersome. For this reason we do not present the derivation in the same detail as we did in Appendix A.2. Instead, we present the most important intermediate results. In line with this, we do not present the final expression for the force-extension relation of the 3-state Kuhn model, because the expression is quite unwieldy. The plots of the 3-state Kuhn model that are presented in chapter 4, however, are produced with the exact expression.

The free energy of our 3-state model reads

$$\frac{\varepsilon^{3-\text{state}}[\{\hat{t}_i\},\{S_i\}]}{k_BT} = \sum_{i=1}^{N}\left[-\frac{fl_0\left(\delta_{S_i,0}+\gamma_1\delta_{S_i,1}+\gamma_2\delta_{S_i,2}\right)}{k_BT}\,\hat{t}_i\cdot\hat{z}+\varepsilon_1\delta_{S_i,1}+\left(\varepsilon_2-\mu\right)\delta_{S_i,2}\right] + \sum_{i=1}^{N-1}\left[\lambda\left(\delta_{S_i,0}\delta_{S_{i+1},1}+\delta_{S_i,1}\delta_{S_{i+1},0}\right)+\eta\left(\delta_{S_i,1}\delta_{S_{i+1},2}+\delta_{S_i,2}\delta_{S_{i+1},1}\right)+\delta\left(\delta_{S_i,2}\delta_{S_{i+1},2}\right)\right]. \tag{A.37}$$

We now repeat the steps of Appendix A.2. First, we calculate the partition function according to equation A.10, which leads to an equation analogous to equation A.11 but with the 2-state energy replaced by the 3-state energy and with the 2-state summations $\sum_{S_i=0,1}$ replaced by summations over the three possible states: $\sum_{S_i=0,1,2}$. We then proceed completely analogously to the treatment of 2-state model: we integrate over the unit vectors and use the transfer matrix method to solve the partition function that is left after integration. We end up with the same expression that we saw before in equation A.34, for the relative extension as a function of the largest eigenvalue of the transfer matrix,

$$\lim_{N\to\infty}\left\langle\frac{z}{L_0}\right\rangle = \frac{\partial}{\partial\chi}\ln\left(\lambda_+\right)-\frac{1}{\chi}. \tag{A.38}$$

However, this time λ_+ is the largest eigenvalue of a 3 x 3 matrix. This 3-state transfer matrix is given by

$$\underline{\underline{T}} = \begin{bmatrix} T_{00} & T_{01} & T_{02} \\ T_{10} & T_{11} & T_{12} \\ T_{20} & T_{21} & T_{22} \end{bmatrix}, \tag{A.39}$$

where the matrix elements are given by

$$\begin{aligned}
T_{00} &= \sinh(\chi),\\
T_{01} &= T_{10} = \sqrt{\frac{1}{\gamma_1}}\sqrt{\sinh(\chi)\sinh(\gamma_1\chi)}\exp\left(-\frac{1}{2}\varepsilon_1-\lambda\right),\\
T_{02} &= T_{20} = \sqrt{\frac{1}{\gamma_2}}\sqrt{\sinh(\chi)\sinh(\gamma_2\chi)}\exp\left(-\frac{1}{2}\left(\varepsilon_2-\mu\right)\right),\\
T_{11} &= \frac{1}{\gamma_1}\sinh(\gamma_1\chi)\exp(-\varepsilon_1),\\
T_{12} &= T_{21} = \sqrt{\frac{1}{\gamma_1\gamma_2}}\sqrt{\sinh(\gamma_1\chi)\sinh(\gamma_2\chi)}\exp\left(-\frac{1}{2}(\varepsilon_1+\varepsilon_2-\mu)-\eta\right),\\
T_{22} &= \frac{1}{\gamma_2}\sinh\left(\gamma_2\chi\right)\exp(-(\varepsilon_2-\mu)-\delta).
\end{aligned} \tag{A.40}$$

Now calculating the force-extension relation is just a matter of calculating the eigenvalues of this 3-state transfer matrix and substituting the result in equation A.38. This is the point where the calculations become cumbersome. In Appendix A.2 we calculated the eigenvalues of a 2 x 2 matrix with symbolic elements, which is equivalent to solving a quadratic equation with symbolic coefficients. Now we deal with a 3 x 3 matrix, so calculating the eigenvalues is equivalent to solving a cubic equation with symbolic coefficients. This cubic equation is solved with Cardano's formula which generates an unwieldy solution for the eigenvalues, in contrast to the compact solutions of the quadratic formula. The expression for the force-extension curve, obtained by equation A.38 from this eigenvalue, is even more unwieldy. Therefore, we do not present it here, but the interested reader can easily obtain it by using equations A.40 and A.38. In our calculations we assume the thermodynamic limit to hold, as we did for the 2-state model.

Appendix B

A justification of the thermodynamic limit

In our derivations of the force-extension relations of the 2-state (Appendix A.2) and 3-state (Appendix A.3) Kuhn models, we assumed the thermodynamic limit or ground-state approximation to hold. In other words, we assumed the number of Kuhn segments to be infinite, $N \to \infty$. This appendix justifies this approximation. First we outline the necessary steps for calculating the force-extension relation of the 2-state Kuhn model for arbitrary N in section B.1. In section B.2 the obtained result is shown graphically for several values of N and compared with the thermodynamic limit result. We show that the difference between those curves and the thermodynamic limit curve is only significant at small N ($\lesssim 50$).

B.1. Calculating the 2-state force-extension relation for arbitrary N

We start this section at the point in the derivation of the 2-state force-extension relation (Appendix A.2) where we introduced the thermodynamic limit. This point is equation A.31, that expresses the partition function in terms of the eigenvalues and eigenvectors of the transfer matrix, λ_+, λ_-, $\vec{e}_+$ and $\vec{e}_-$, and the coefficients v_+ and v_-,

$$Z \;=\; \left(\frac{4\pi}{\chi}\right)^N \left[v_+^2\,(\vec{e}_+\cdot\vec{e}_+)\,\lambda_+^{N-1} + v_-^2\,(\vec{e}_-\cdot\vec{e}_-)\,\lambda_-^{N-1}\right]. \tag{B.1}$$

The coefficients v_+ and v_- were defined in equation A.28,

$$\vec{V} \;=\; v_+\vec{e}_+ + v_-\vec{e}_-. \tag{B.2}$$

The transfer matrix is defined in equation A.20, while the vector $\vec{V}$ is defined in equation A.18. In the derivation in Appendix A.2 we took the limit $N \to \infty$ at this point, which enabled us to neglect the λ_--term and the factor $v_+^2\,(\vec{e}_+\cdot\vec{e}_+)$. So for calculating the exact expression for arbitrary N we need to calculate v_+, v_-, $\vec{e}_+$ and $\vec{e}_-$. Note that λ_- was already given in equation A.35 together with λ_+. The coefficients v_+ and v_- can be calculated according to equation B.3, while the eigenvectors $\vec{e}_+$ and $\vec{e}_-$ can be obtained from the transfer matrix by standard linear algebra [107],

$$v_+ \;=\; \frac{\vec{V}\cdot\vec{e}_+}{\vec{e}_+\cdot\vec{e}_+}, \qquad v_- \;=\; \frac{\vec{V}\cdot\vec{e}_-}{\vec{e}_-\cdot\vec{e}_-}. \tag{B.3}$$

After calculating the eigenvectors and using equation B.3, obtaining the force-extension relation is just a matter of calculating the free energy and the relative extension according to equations 3.11 and 3.12. We will not present a detailed derivation of this calculation, but the interested

reader can perform the derivation by following the steps described above.

Also, we do not present the final result of the calculation in the from of an equation. We will, however, present it in graphical form: we plot the exact expression for several N and compare those curves to the thermodynamic limit curve. We do so because the force-extension relation becomes unwieldy for arbitrary N and showing it is therefore little instructive. Moreover, we will see in the next section that the plots show that the thermodynamic limit is a very decent approximation for all $N \gtrsim 50$, so the exact force-extension relation for arbitrary N is of little interest for our research.

Finally, note that the calculation of the 3-state Kuhn model for arbitrary N goes completely analogous to this derivation, only in that case we deal with three eigenvalues, three eigenvectors and three coefficients instead of two.

B.2. The force-extension relation for arbitrary N in graphical form

For analyzing the influence of the number of Kuhn segments N on the force-extension curve, we distinguish three cases depending on the value of the cooperativity parameter λ: the cooperative transition ($\lambda > 0$), the anti-cooperative transition ($\lambda < 0$) and the non-cooperative transition ($\lambda = 0$). The latter is the most simple, since the thermodynamic limit is exact in that case. For $\lambda = 0$ there is no cooperativity between neighboring Kuhn segments, so the partition function factorizes. This leads to a result independent of N. In the other two cases the thermodynamic limit is not exact, so we will consider them here.

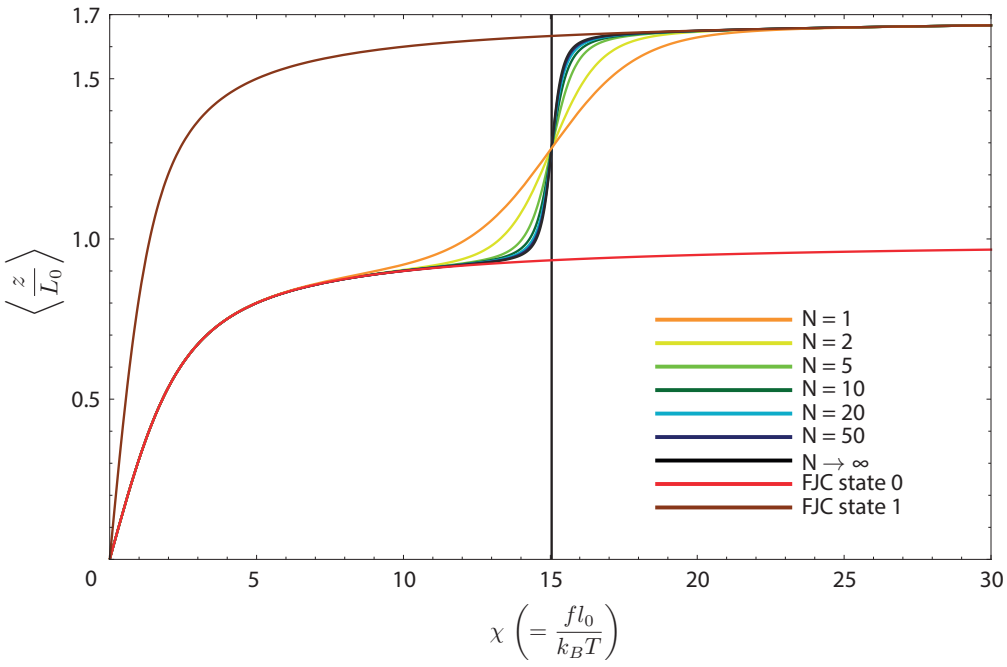

Figure B.1: Cooperative ($\lambda = 2$) 2-state force-extension curves for varying number of particles N from 1 to 50, with $\varepsilon_1 = 10$ and $\gamma_1 = 1.7$. The thermodynamic limit result (black) and freely jointed chains with all segments in state 0 and state 1 respectively are plotted as well. The exact curves converge quickly towards the thermodynamic limit approximation, and the $N = 50$ is hardly distinguishable from the thermodynamic limit curve. This shows that the thermodynamic limit is a good approximation if $N \gtrsim 50$. The dsDNA used in this data is bacteriophage lambda DNA, which contains about 48.500 base pairs. Since we take the segment length to be the distance between two base pairs, this means that we deal with 48.500 Kuhn segments. We conclude that this justifies the use of the thermodynamic limit.

Figure B.1 shows a number of cooperative ($\lambda > 0$) 2-state force-extension curves for a varying number of N Kuhn segments, from $N = 1$ to $N = 50$, as well as the thermodynamic limit result (equations 3.13 and A.36). The figure also shows force-extension curves of two freely jointed chains, where all segments are in state 0 and state 1 respectively. All curves were obtained with $\lambda = 2$, $\varepsilon_1 = 10$ and $\gamma_1 = 1.7$. The values of λ and ε_1 are not representative for dsDNA, but they are chosen because they show a clear force-extension curve.

Figure B.1 shows that the curves converge very quickly towards the thermodynamic limit curve (black). The curve with $N = 1$ is equal to the non-cooperative case ($\lambda = 0$), and deviates most from the thermodynamic limit. The $N = 10$ curve (dark green) already closely resembles the thermodynamic limit curve and the $N = 50$ curve (purple) is hardly distinguishable from the thermodynamic limit. This shows that the thermodynamic limit, as anticipated in section 3.3, is indeed a very decent approximation for $N \gtrsim 50$ in the cooperative case. Recall that the dsDNA that we are studying contains about 48.500 base pairs (section 2.1), and that we take the segment length to be the distance between two base pairs (section 3.2), and therefore our chain amply satisfies this condition. We now need to check whether the same conclusion applies for the anticooperative case $\lambda < 0$. Figure B.2 shows anti-cooperative force-extension curves for the same values of N as figure B.1.

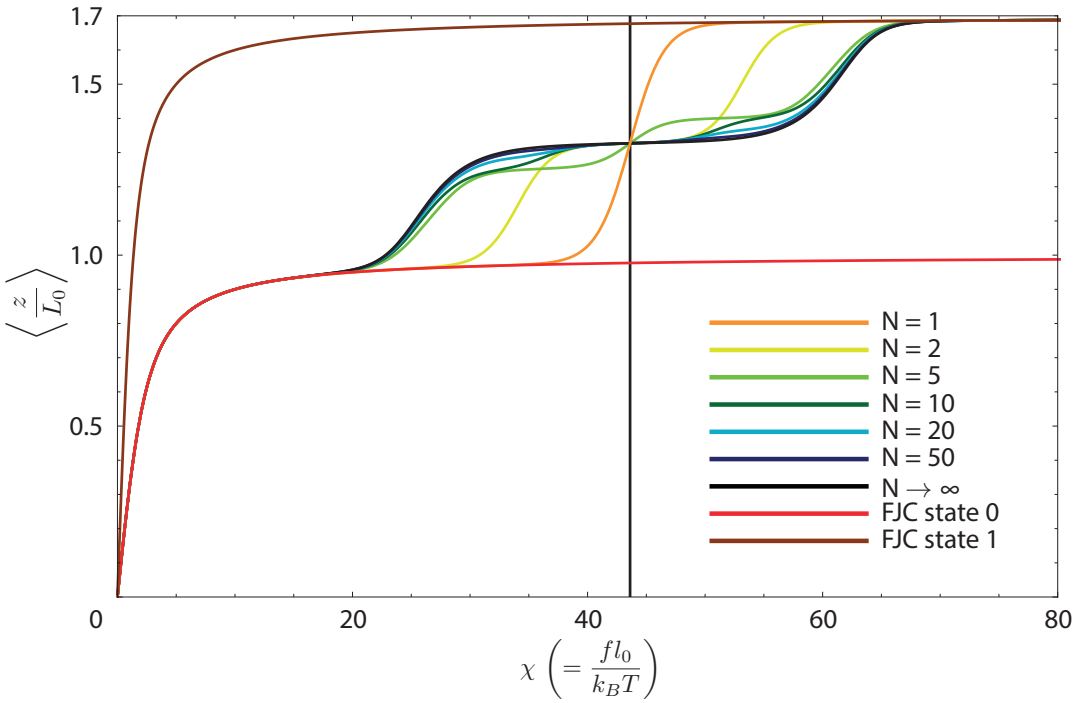

Figure B.2: Anti-cooperative ($\lambda = -6$) 2-state force-extension curves for varying number of particles N from 1 to 50, with $\varepsilon_1 = 30$ and $\gamma_1 = 1.7$. The thermodynamic limit result (black) and freely jointed chains with all segments in state 0 and state 1 respectively are plotted as well. The exact curves differ substantially from the thermodynamic limit approximation for small N, but the $N = 50$ is hardly distinguishable from the thermodynamic limit curve. This shows that the thermodynamic limit is a good approximation if $N \gtrsim 50$ for the anti-cooperative case as well.

Figure B.2 again shows the force-extension curves of freely jointed chains where all segments are in state 0 or in state 1. The other curves are plotted with $\lambda = -6$, $\varepsilon_1 = 30$ and $\gamma_1 = 1.7$, which are again chosen because they clearly illustrate the anti-cooperative transition. The $N = 1$ curve is, as it is in figure B.1, identical to the non-cooperative case. An important difference with figure B.1, however, is the change in qualitative behavior for the curves with low values of N. In the cooperative case a small number of Kuhn segments simply leads to an effective cooperativity λ that is smaller than the actual value (figure B.1). It is clear from figure B.2

that for $\lambda < 0$ the qualitative behavior changes as well. The reason for this can probably be found in the fact that the average number of neighbors is smaller than two, which changes the force at which Kuhn segments are excited towards state 1. Regardless of the reason, the $N = 50$ curve (purple) is hard to distinguish from the thermodynamic limit curve (black), as it was for positive λ. This means that for any λ the thermodynamic limit is a valid approximation for $N \gtrsim 50$, so we can safely use the results obtained with the thermodynamic limit in this thesis.